T H E U N I V E R S I T Y O F M I C H I G A N

COLLEGE OF LITERATURE, SCIENCE, AND THE ARTS
Department of Physics

Technical Report No. 23

THE POLARIZATION PARAMETER IN ELASTIC PROTON-PROTON SCATTERING FROM .75 TO 2.84 GeV

Homer A. Neal, Jr.

ORA Project 03106

under contract with:

DEPARTMENT OF THE NAVY
OFFICE OF NAVAL RESEARCH
WASHINGTON, D. C.

CONTRACT NO. Nonr-1224(23)
NR-022-274
Chairman: Lawrence W. Jones

administered through:

OFFICE OF RESEARCH ADMINISTRATION ANN ARBOR

April 1966

This report was also a dissertation submitted in partial fulfillment of the requirements for the degree of Doctor of Philosophy in The University of Michigan, 1966.

TABLE OF CONTENTS

LIST OF TABLES

LIST OF FIGURES

LIST OF FIGURES (Continued)

LIST OF FIGURES (Concluded)

ABSTRACT

A double-scattering technique has been employed to measure the polarization parameter in elastic proton-proton scattering at .75, 1.03, 1.32, 1.63, 2.24, and 2.84 GeV. An external proton beam from the Brookhaven Cosmotron was focussed on a three inch long liquid hydrogen target and the elastic recoil and scattered protons were detected in coincidence by scintillation counters. The polarization produced in the scattering process was inferred from the azimuthal asymmetry exhibited in the scattering of the recoil beam from a carbon target. This asymmetry was measured by a set of two scintillation counter telescopes which symmetrically viewed the carbon target. The analyzing power of this arrangement was previously determined in an independent experiment employing a 40% polarized proton beam at the Carnegie Institute of Technology synchrocyclotron. The range of calibration energies, 103 to 415 MeV, corresponds to the basic range of recoil energies analyzed in the primary experiment. The analyzing power was extended to 1000 MeV by utilizing the antisymmetry of the polarization parameter about 90° in the center-of-mass system. Checks were frequently made to insure that the external proton beam was unpolarized. False asymmetries were cancelled to a high order by periodically rotating the analyzer 180° about the recoil beam line. Spark chambers were employed to obtain the spatial distribution of the beam as it entered the analyzer. This information allowed an accurate determination of the corrections necessary to compensate for any misalignment of the axis of the analyzer relative to the incident

beam. The corrected values of the polarization parameter are exhibited as a function of the center-of-mass scattering angle for each incident beam energy. The prediction of the Regge theory that the polarization parameter in elastic proton-proton scattering is related to the total p-p and p-$\bar{p}$ cross sections has been found to be consistent with the experimental results.

ACKNOWLEDGMENTS

I would like to thank Professor Michael J. Longo for his invaluable assistance in all phases of this work. I also wish to express my gratitude to Professor Oliver E. Overseth and Professor Martin L. Perl for their numerous contributions to the success of this experiment. For several discussions regarding theoretical interpretation of the experimental results, I am very grateful to Professor Marc H. Ross and Professor Gordon L. Kane.

I am indebted to my colleagues David E. Pellett, Smith T. Powell III, Stephen W. Kormanyos, and Billy W. Loo for their valuable help during the data accumulation stage of the experiment. I wish to thank Mr. Orman Haas for the construction of much of the experimental apparatus. I am also grateful to the members of the Cosmotron staff, particularly Mr. Malcom McCrum, for their generous technical assistance during the rigging and performance of the experiment.

I wish to express my gratitude to the Detroit Evening News Association and the John Hay Whitney Foundation for fellowships awarded during my graduate studies.

I. INTRODUCTION

The nature of the interaction between nucleons is of fundamental importance. A complete theory of nucleon-nucleon interactions must predict not only the angular distributions in scattering experiments but also correlations between the initial and final nucleon spin states. The first successful experimental investigation of the spin dependence of the nucleon-nucleon interaction was reported by Oxley, Cartwright and Rouvina[1] in 1954. Relatively large proton-proton polarization effects were observed in their studies near 225 MeV, as had been to some extent suggested by the appreciable non-central terms in the existing models of Christian and Noyes,[2] Case and Pais,[3] and Jastrow.[4] There have since been many proton-proton polarization experiments below 1 GeV. Proton-proton polarization data have also been reported by Bareyre et al.[5] at 1.7 GeV, and recently by Chamberlain et al.,[6] who employed a polarized target, at 1.7, 2.85, 3.50, 4.00, 5.05, and 6.15 GeV, and by Kanavets et al.[7] at 8.5 GeV.

At the present there exists no theory that successfully explains the proton-proton interaction in the region 1 to 3 GeV. This region is of considerable interest since here neither high nor low-energy approximations are expected to be valid. The polarization data in this range is, however, sparse. Comparison of the results from the two previous experiments at 1.7 GeV furthermore reveals the existence of a significant discrepancy.

In the present experiment, a definitive study of the polarization parameter in elastic proton-proton scattering from .75 to 2.84 GeV has been

made. The experimental results can be interpreted in terms of the Regge theory prediction that, for fixed small four-momentum transfer, the polarization varies as $(\sigma(p\bar{p})-\sigma(pp))/\sigma(pp)$ (where $\sigma(p\bar{p})$ and $\sigma(pp)$ are the total cross sections for p-$\bar{p}$ and p-p scattering) if only the Pomeranchuck, second-Pomeranchuck, ρ and ω poles are considered and certain assumptions are made regarding the functional behavior of the poles and pole-residues.[8]

II. THEORY

The density matrix formalism is the basis for practically all contemporary analyses of polarization phenomena. Using this formalism we will outline the derivation of the relationship between polarization, asymmetry, and analyzing power for a scattering process. The possibility of calculating the phase shifts for the proton-proton system in the region 1 to 3 GeV is briefly considered. Finally, Regge pole predictions for the polarization in proton-proton scattering are examined.

A. DENSITY MATRIX FORMALISM

The polarization of a beam of particles is defined as the expectation value of the Pauli spin vector, $\vec{\sigma}$, averaged over all particles in the beam. In general, the goal of polarization experiments is to determine the scattering characteristics of individual spin states. Experimentally, however, we must deal with a mixture of spin states. In order to study the connection between the scattering properties of the "beam averaged" quantum state and individual quantum states, it is convenient to utilize the Von Neumann density matrix. The density matrix formalism was introduced in the analysis of polarization phenomena by Wolfenstein and Ashkin,[9] and Dalitz.[10] Our presentation here parallels that given by Stapp.[11]

Let us consider a complete set of quantum states $|i\rangle$. If one defines the density matrix as

$$\rho = \sum_i f_i P_i \quad , \tag{1}$$

where f_i is the fractional number of particles in the i^{th} state, and

$$P_j \,|i\rangle = \delta_{ij} \quad , \tag{2}$$

then the expectation value of any operator, Θ, is

$$\langle\Theta\rangle = \mathrm{Tr}(\rho\Theta) = \sum_j f_j \langle j|\Theta|j\rangle \quad . \tag{3}$$

Consider now a scattering process with initial and final states specified by ϕ_i and ϕ_f. If S is the scattering matrix for the process, i.e., $\phi_f = S\phi_i$, and R = S-1, then the density matrix, ρ_s, describing the scattered wave is related to the initial state density matrix ρ_i by

$$\rho_s = R\,\rho_i\,R^+ \quad . \tag{4}$$

We are here primarily interested in the expectation value of spin-space operators in a particular momentum state $\vec{k}$. Let Θ_s be a spin-space operator, then its expectation value in momentum state $\vec{k}$ is

$$\langle\Theta_s\rangle_{\vec{k}} = \frac{\langle\Theta_s\mathcal{P}(\vec{k})\rangle}{\langle\mathcal{P}(\vec{k})\rangle} = \frac{\mathrm{Tr}(\rho\mathcal{P}(\vec{k})\Theta_s)}{\mathrm{Tr}(\rho\mathcal{P}(\vec{k}))} \quad , \tag{5}$$

where $\mathcal{P}(\vec{k})$ is a projection operator for momentum state $\vec{k}$, and

$$\begin{aligned}\mathrm{Tr}(\rho\mathcal{P}(\vec{k})\Theta_s) &= \sum_i \langle i|\rho\mathcal{P}(\vec{k})\Theta_s|i\rangle \\ &= \sum_i {}_{\vec{k}}\langle i|\rho\Theta_s|i\rangle_{\vec{k}} \\ &= \mathrm{Tr}(\rho(\vec{k})\Theta_s) \quad ,\end{aligned} \tag{6}$$

where $\rho(\vec{k})$ is the spin-space density matrix for momentum state $\vec{k}$. Note that

$$\mathrm{Tr}(\rho\mathcal{P}(\vec{k})) = \mathrm{Tr}\ \rho(\vec{k})$$

and therefore

$$\langle\Theta_s\rangle_{\vec{k}} = \mathrm{Tr}(\rho(\vec{k})\Theta_s)/\mathrm{Tr}(\rho(\vec{k})) \quad . \tag{7}$$

Consider now the elastic scattering of two (Pauli) protons. If we take for our representation the sixteen base vectors $\vec{\sigma}^1_\nu\,\vec{\sigma}^2_\lambda$ (where $\vec{\sigma}^\ell_m$ is the m^{th} com-

ponent of the Pauli spin vector for particle ℓ = 1 or 2, with $\sigma_0^1 = 1$) it is seen that

$$\rho(\vec{k}) = \frac{1}{4} \mathrm{Tr}(\rho(\vec{k})) \sum_{\beta\alpha} \langle \sigma_\beta^1 \sigma_\alpha^2 \rangle_{\vec{k}} \sigma_\beta^1 \sigma_\alpha^2 \quad , \tag{8}$$

since $\rho(\vec{k})$ is certainly expandable as

$$\rho(\vec{k}) = \sum_{\beta\alpha} a_{\beta\alpha} \sigma_\beta^1 \sigma_\alpha^2 \quad ,$$

and from (7)

$$\mathrm{Tr}\ \rho(k) \langle \sigma_\beta^1 \sigma_\alpha^2 \rangle_{\vec{k}} = \sum_{\lambda\nu} a_{\lambda\nu}\ \mathrm{Tr}(\sigma_\lambda^1 \sigma_\nu^2 \sigma_\beta^1 \sigma_\alpha^2) = 4a_{\beta\alpha}$$

(since $\mathrm{Tr}(\sigma_\lambda^1 \sigma_\nu^2 \sigma_\beta^1 \sigma_\alpha^2) = 4\delta_{\lambda\beta}\delta_{\nu\alpha}$). Thus, knowing the fifteen spin correlation parameters $\langle \sigma_\beta^1 \sigma_\alpha^2 \rangle_{\vec{k}}$ is equivalent to knowing the density matrix, and, of course, the converse is also true. It is to be noticed in the development so far that the normalization has remained arbitrary. Here we choose the normalization such that

$$\rho_s(\vec{k}) = M(\vec{k},\vec{k}')\rho_i(\vec{k}')M^+(\vec{k},\vec{k}') \quad , \tag{9}$$

where $M(\vec{k},\vec{k}')$ is the spin scattering matrix whose elements are the scattering amplitudes between the various initial and final spin states (with $\vec{k}' \to \vec{k}$). That only a change in normalization has been made is evident from the fact that

$$M(\vec{k},\vec{k}') = \text{const.}\ \langle \vec{k}|R|\vec{k}' \rangle \quad .$$

The differential cross section is then

$$\frac{d\sigma}{d\Omega}(\theta,\phi) = \frac{\mathrm{Tr}\rho_s(\vec{k})}{\mathrm{Tr}\rho_i(\vec{k}')} = \frac{\mathrm{Tr}\ M(\vec{k},\vec{k}')\rho_i(\vec{k}')M^+(\vec{k},\vec{k}')}{\mathrm{Tr}\rho_i(\vec{k}')} \quad . \tag{10}$$

It has been shown in Ref. 9 that the most general form of the spin scattering matrix for the proton-proton system consistent with invariance under time reversal, spatial reflections, rotations, and particle exchange is

$$M(\vec{k},\vec{k}') = a + b(\vec{\sigma}^1\cdot\vec{N}+\vec{\sigma}^2\cdot\vec{N}) + c(\vec{\sigma}^1\cdot\vec{N}\vec{\sigma}^2\cdot\vec{N}) + d(\vec{\sigma}^1\cdot\vec{P}\vec{\sigma}^2\cdot\vec{P}+\vec{\sigma}^1\cdot\vec{K}\vec{\sigma}^2\cdot\vec{K}) + e(\vec{\sigma}^1\cdot\vec{P}\vec{\sigma}^2\cdot\vec{P}-\vec{\sigma}^1\cdot\vec{K}\vec{\sigma}^2\cdot\vec{K}) \quad (11)$$

where a, b, c, d, and e are functions of $\vec{k}\cdot\vec{k}'$ and k, and where $\vec{N}=\vec{k}\times\vec{k}'/|\vec{k}\times\vec{k}'|$, $\vec{P} = (\vec{k}'+\vec{k})/|\vec{k}'+\vec{k}|$, and $\vec{K} = (\vec{k}-\vec{k}')/|\vec{k}-\vec{k}'|$. (The corresponding matrix for the spin 1/2 - spin 0 case is simply $M(\vec{k},\vec{k}') = a+b\vec{\sigma}\cdot\vec{N}$ and the representation reduces to that of a single Pauli particle.)

By utilizing only the assumed form of the matrix M and constructing the appropriate density matrices (using relations (7) to (10)) one can readily derive the following points which are pertinent to the present experiment:

1. If a beam of polarization $\vec{P}$ and center-of-mass momentum $\vec{k}'$ scatters from an arbitrary target at an angle $\pm\phi$ in the plane whose normal is $\vec{N}$, then

$$\epsilon(k',\phi) = \vec{P}\cdot\vec{N}A(k',\phi)$$

where

$$\epsilon(k',\phi) = \frac{I(\phi)-I(-\phi)}{I(\phi)+I(-\phi)}$$

and $I(\phi)$ is the differential cross section for scattering at angle ϕ in the plane containing $\vec{k}'$ and $\vec{k}'\times\vec{N}$. $\epsilon(k',\phi)$ is commonly called the azimuthal asymmetry. $A(k',\phi)$ depends only on k', ϕ and properties of the target and is commonly referred to as the "analyzing power" of the interaction. This relationship forms the basis for the techniques employed in this experiment. The asymmetry, $\epsilon(k',\phi)$, is easily obtained experimentally, and consequently,

so is $A(k',\phi)$ when $\vec{P}$ is known. An independent experiment was performed to measure what is essentially the quantity $A(k',\phi)$. If one knows this quantity, then measurement of the azimuthal asymmetry exhibited by a beam of known energy determines the polarization of that beam.

2. The direction of the polarization vector produced in scattering an unpolarized beam from an unpolarized target is normal to the scattering plane. This can also be inferred directly from the requirement that the interaction be invariant under spatial reflections and the fact that the only axial vectors that can be formed from the physical vectors $\vec{k}$ and $\vec{k}'$ are $\sim\vec{k}\times\vec{k}'$.

The treatment of this topic has been non-relativistic. It should be pointed out that a relativistic treatment, though somewhat more involved, yields exactly the same results. This arises because the required Lorentz rotation is about an axis normal to the scattering plane, and thus parallel with the polarization vector.[12,13]

B. PHASE SHIFT ANALYSIS

The possibility of analyzing data from this experiment in terms of phase shifts is briefly considered in this section.

Phase shifts provide the most complete description of a scattering process and a convenient connection between theory and experiment. However, phase shift analyses become quite complicated at energies above 400 MeV, where absorption processes can not be neglected. For example, in order to carry out such an analysis for $l_{max} = 4$, there exists one mixing parameter,

three singlet and six triplet complex phase shifts to be determined. At present, only cross section and polarization data are available in the region 1 to 3 GeV and, consequently, one must deal with eleven free parameters (i.e., an expansion of I and IP in Legendre polynomials determines only 8 parameters). With this freedom, a multiplicity of phase shift solutions which satisfactorily reproduce the existing data would be obtained. Future experimental data on the proton-proton spin correlation parameters would, of course, limit the number of possible solutions. It should be remarked that $l_{max} = 4$ is somewhat conservative for the energy region of interest, and therefore a proper analysis would lead to even more ambiguities than indicated above.

Now consider the possibility of theoretically predicting some of the phase shifts and calculating the remainder from the experimental data. In the two existing p-p phase shift analyses above 400 MeV (at 660 and 970 MeV) the resonance model has been employed in this manner.[16] It has been assumed that the principal inelastic process is single pion production (Fig. 1b) in a (3/2, 3/2) state, with the remaining nucleon in a S or P-state (at 660 MeV) or S, P, or D- state (at 970 MeV). The imaginary part of each phase shift considered is then related to cross sections of processes allowed by the above assumptions. Low energy phase shift solutions were extrapolated to the energy of interest and used to limit the "search" region of the free parameters. Notwithstanding the additional complications due to a larger l_{max}, a phase shift analysis of our data could be carried out along these lines if a reasonable model could be constructed to supplant

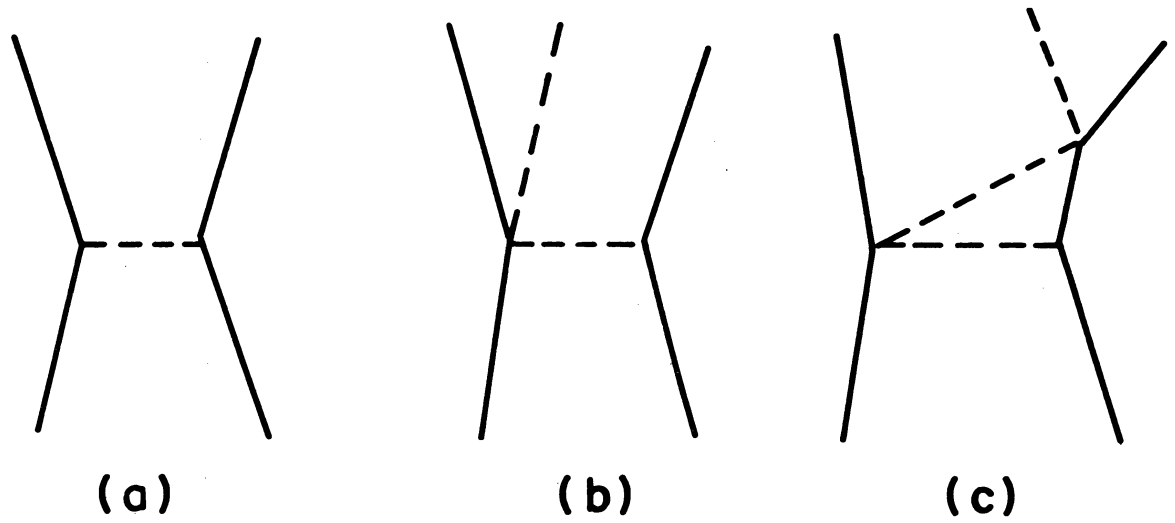

Fig. 1. One-pion exchange diagrams for computation of phase shifts. (a) One-pion exchange diagram for the process N+N → N+N. In the energy region below 400 MeV, higher real phase shifts have been successfully predicted from this model (Ref. 14). (b) Inelastic one-pion exchange diagram for the process N+N → N+N+π. This interaction has been assumed to be the dominant inelastic process in all existing phase shift analyses above 400 MeV. Phillips (Ref. 15) has pointed out that while a process as shown in (c) can give singularities near those from (b), the integrated cross section appears to still be dominated by (b) since the other processes can occur only over restricted energy and angular regions.

the above usage of the resonance model, whose range of applicability is ≈ 400 to 1000 MeV.[16]

C. REGGE POLE PREDICTIONS

The hypothesis of Regge poles in high energy nucleon-nucleon scattering leads to simple predictions for the proton-proton polarization parameter when certain assumptions are made. We will briefly indicate here how these predictions are derived and in Section V compare the predictions with the experimental results. The details of the derivations are to be found in Refs. 17, 18, and 19.

Let the proton-proton scattering process be characterized by a spin-space matrix ϕ, chosen so the differential cross section for the process

$$p_{\lambda_1} + p_{\lambda_2} \rightarrow p_{\lambda_1'} + p_{\lambda_2'}$$

is

$$\frac{d\sigma}{d\Omega} = |\langle \lambda_1'\lambda_2'|\phi|\lambda_1\lambda_2\rangle|^2$$

where $\lambda_1\lambda_2$ and $\lambda_1'\lambda_2'$ represent the helicities of the initial and final state protons, respectively. The matrix ϕ depends only on the scattering angle, θ, and the total center-of-mass energy, E_t, and is related to the Feynman amplitudde for the process by the equation

$$M = (2\pi E_t/m^2) \langle \lambda_1'\lambda_2'|\phi|\lambda_1\lambda_2\rangle \quad , \tag{12}$$

where m is the proton mass. Symmetry requirements limit the number of independent matrix elements to five. In order to derive the relations between the various ϕ matrix elements, it is convenient to utilize the known properties of the helicity amplitudes introduced by Jacob and Wick.[20] In terms

of these amplitudes, the elements of ϕ are

$$\langle\lambda_1'\lambda_2'|\phi|\lambda_1\lambda_2\rangle = \left(\frac{1}{P}\right)\sum_J (2J+1)\,\langle\lambda_1'\lambda_2'|T^J(E_t)|\lambda_1\lambda_2\rangle\, d^J_{\lambda\lambda'}(\theta) \quad , \tag{13}$$

where

$$\langle\lambda_1'\lambda_2'|T^J(E_t)|\lambda_1\lambda_2\rangle = \left(\frac{1}{2i}\right)\left(\langle\lambda_1'\lambda_2'|S^J|\lambda_1\lambda_2\rangle - \delta_{\lambda_1\lambda_1'}\delta_{\lambda_2\lambda_2'}\right) \quad ,$$

p is the center-of-mass momentum and $d^J_{\lambda\lambda'}$ are reduced rotation matrices with $\lambda = \lambda_1-\lambda_2$ and $\lambda' = \lambda_1'-\lambda_2'$, and S^J is the angular momentum (J) submatrix of the S- matrix. The rotation matrices have the property that

$$d^J_{\alpha\beta}(\theta) = (-1)^{\alpha-\beta}\, d^J_{\beta\alpha}(\theta) = d^J_{-\alpha-\beta}(\theta) \tag{14}$$

Conservation of parity and isotopic spin require that

$$\langle\lambda_1'\lambda_2'|T^J(E_t)|\lambda_1\lambda_2\rangle = \langle-\lambda_1'-\lambda_2'|T^J(E_t)|-\lambda_1-\lambda_2\rangle \tag{15}$$

and

$$\langle\lambda_1'\lambda_2'|T^J(E_t)|\lambda_1\lambda_2\rangle = \langle\lambda_2'\lambda_1'|T^J(E_t)|\lambda_2\lambda_1\rangle \quad .$$

In addition, time reversal invariance implies

$$\langle\lambda_1'\lambda_2'|T^J(E_t)|\lambda_1\lambda_2\rangle = \langle\lambda_1\lambda_2|T^J(E_t)|\lambda_1'\lambda_2'\rangle \quad . \tag{16}$$

The symmetry relations for the elements $\langle\lambda_1'\lambda_2'|\phi|\lambda_1\lambda_2\rangle$ are now easily obtained. Here we desire only to find a complete set of independent amplitudes. A suitable choice is found to be

$$\begin{aligned}
\phi_1 &\equiv \langle{+}{+}|\phi|{+}{+}\rangle \\
\phi_2 &\equiv \langle{+}{+}|\phi|{-}{-}\rangle \\
\phi_3 &\equiv \langle{+}{-}|\phi|{+}{-}\rangle \\
\phi_4 &\equiv \langle{+}{-}|\phi|{-}{+}\rangle \\
\phi_5 &\equiv \langle{+}{+}|\phi|{+}{-}\rangle
\end{aligned} \tag{17}$$

where the quantity 1/2 in the helicity specification has been suppressed.

Each ϕ_j is related to a Feynman amplitude through Eq. (14). Recall now that in a scattering process with pseudoscalar exchange, as shown in

Fig. 2, the Feynman amplitude is given by

$$M_{ac-bd} = \text{const.}\ \bar{u}_b \gamma_5 u_a \frac{1}{\mu^2 - t} \bar{u}_d \gamma_5 u_c \qquad (18)$$

where u_j is a spinor describing particle j, μ is the mass of the exchanged particle, and t is the square of the four-momentum transfer. In the Regge theory, it is assumed that the amplitude for the s channel scattering process can be represented as an expansion of contributions from poles in the complex angular momentum (J) plane in the t channel. The position of each pole in the complex J plane changes with energy and, in the t channel, the trajectory corresponding to each pole is specified in the following by $\alpha(t)$ and the residue of each pole by $\beta(t)$. The exchange of a particle in the diagram in Fig. 2 is analogous to the exchange of a Regge trajectory. Formally, the Regge amplitude corresponding to the exchange of a trajectory is obtained from Eq. (18) by the substitution

$$\frac{1}{\mu^2 - t} \longrightarrow \frac{2\alpha(t)+1}{\sin \pi\alpha(t)} \left[P_{\alpha(t)}(\cos \theta_t) + P_{\alpha(t)}(-\cos \theta_t) \right] \beta(t) ,$$

where P_i is the i^{th} Legendre polynomial and θ_t is the center-of-mass scattering angle in the t reaction. The relation (12) is still true, where M now represents the Regge amplitude. Thus, each ϕ_j may be expressed as an expansion in Regge poles. It should be remarked that, as in Fig. 2 where the exchanged particle must have quantum numbers consistent with the initial and final states, only those trajectories whose associated quantum numbers are appropriate need be considered.

In the following, the matrix R will represent the relativistic generalization of the density matrix introduced in Section A(ϕ corresponds to the spin-space matrix M in that context). The optical theorem for proton-proton

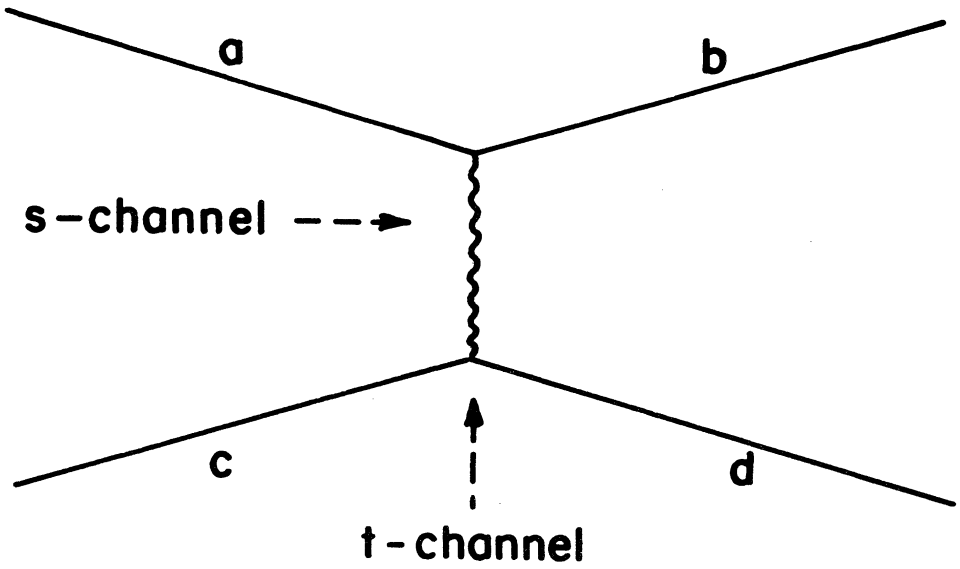

Fig. 2. Diagram for scattering process in which a pseudoscalar particle is exchanged.

scattering in terms of the density matrix, center-of-mass momentum p, and ϕ becomes

$$\sigma(pp) = \frac{4\pi}{p} \mathrm{Im}(\mathrm{Tr}\ R_i\ \phi)_{t=0} \ ,$$

where R_i is the density matrix for an unpolarized beam and can be written as

$$R_i = \delta_{\lambda_1\lambda_1'}\delta_{\lambda_2\lambda_2'}/4 \qquad \text{(see Eq. (8))}$$

The total cross section then reduces to

$$\sigma(pp) = \frac{2\pi}{p} \mathrm{Im}(\phi_1+\phi_3)_{t=0}$$

From Eq. (7), we note that the polarization parameter can be expressed as

$$\mathcal{P} = \mathrm{Tr}(\phi R_i \phi^+ S)/\mathrm{Tr}(\phi R_i \phi^+)$$

where S is the relativistic generalization of $(\vec{\sigma}_3)$ and R_i is again the density matrix corresponding to an incident unpolarized beam. Performing the indicated operation and utilizing the relations between the various ϕ matrix elements leads to

$$\mathcal{P} = \frac{\mathrm{Im}\{(\phi_1+\phi_2+\phi_3-\phi_4)\phi_5^*\}}{\frac{1}{2}\{|\phi_1|^2+|\phi_2|^2+|\phi_3|^2+|\phi_4|^2+4|\phi_5|^2\}}$$

The principle of crossing symmetry relates the scattering amplitudes for the s and t- channel processes. That is, knowledge of the ϕ_j's allows the construction of the $\bar{\phi}_j$'s, where for our case $\bar{\phi}$ describes the process $p+\bar{p} \to p+\bar{p}$. We may write the total cross section for $p\bar{p}$ scattering as

$$\sigma(p\bar{p}) = \frac{2\pi}{p} \mathrm{Im}(\bar{\phi}_1+\bar{\phi}_3)_{s=0}$$

Now if one evaluates the above expression for $\mathcal{P}$ in the limit $s \to \infty$ and

assumes the only contributing Regge poles are the Pomeranchuck P, and its nearest neighbor N, it is found that

$$\rho \sim \sqrt{-t}\, f(t)(s/s_o)^{\alpha_p(t)-\alpha_N(t)} \quad ,$$

where f is some function of t, and s_o is a constant generally taken to be $2m^2$, where m is the nucleon mass.[17]

On the other hand, by considering the contributions from the second-Pomeranchuck P', P, ρ, and ω poles, Hara has shown that the polarization parameter may be related to the total pp and $p\bar{p}$ cross sections as

$$\rho \sim \sqrt{-t}\, A(t)(\sigma(p\bar{p})-\sigma(pp))/\sigma(pp) \quad ,$$

where $\sigma(p\bar{p})$ and $\sigma(pp)$ represent the total cross sections for $p\bar{p}$ and pp scattering, and A(t) is a sum of pole residue terms that is expected to be a slowly varying function of t.[18] The π and η trajectories have been shown not to contribute in forward nucleon-nucleon scattering in Ref. 21. Even if these trajectories did contribute to the forward amplitude, the magnitude of the contribution would be expected to decrease relatively fast with increasing energy due to the negative α parameters involved.

The principal physical difference in the two predictions lies in the assumptions made about the participating poles, and therefore the relative success of the two predictions is of considerable interest. Our results at $t = -.3\ (\mathrm{GeV/c})^2$ have been independently fitted with the following functional forms:

a. $P(s) = a\, s^b$, a and b constants

b. $P(s) = c((\sigma(p\bar{p})-\sigma(pp))/\sigma(pp))$, c constant

The resulting fitting curves are presented and discussed in Section V.

III. EXPERIMENTAL APPARATUS AND TECHNIQUES

A. GENERAL DISCUSSION

The polarization parameter in elastic proton-proton scattering has been measured in the energy region .75 to 2.84 GeV by employing a double-scattering technique. An external proton beam from the Cosmotron accelerator was extracted at the desired energy and focused on a 3" long liquid hydrogen target. The elastic scattered and recoil protons were detected by scintillation counter telescopes S_1S_1' and $S_0(S_2S_2')$ at the appropriate kinematic angles (Fig. 3). The geometry was such that counts from inelastic processes were negligible.

The polarization of the recoil beam was determined from the left-right asymmetry exhibited in its scattering from a carbon target. This asymmetry was measured by scintillation counter telescopes T_1T_2 and U_1U_2. In order to cancel any instrumental asymmetries, these telescopes were periodically interchanged by rotating the analyzer 180° about the recoil beam line. The amount of carbon in the second target depended on the recoil beam energy. Typically .5% to 3% of the protons incident on the carbon target scattered into the telescopes. A beam pulse of 4×10^9 protons incident on the hydrogen target resulted in about 20 analyzed recoil protons. The analyzing power for the geometry used in the second scattering was determined in an independent calibration experiment utilizing a 40% polarized proton beam at the Carnegie Institute of Technology synchrocyclotron (see Appendix I). The range of calibration energies, 103-415 MeV, corresponds to the principal

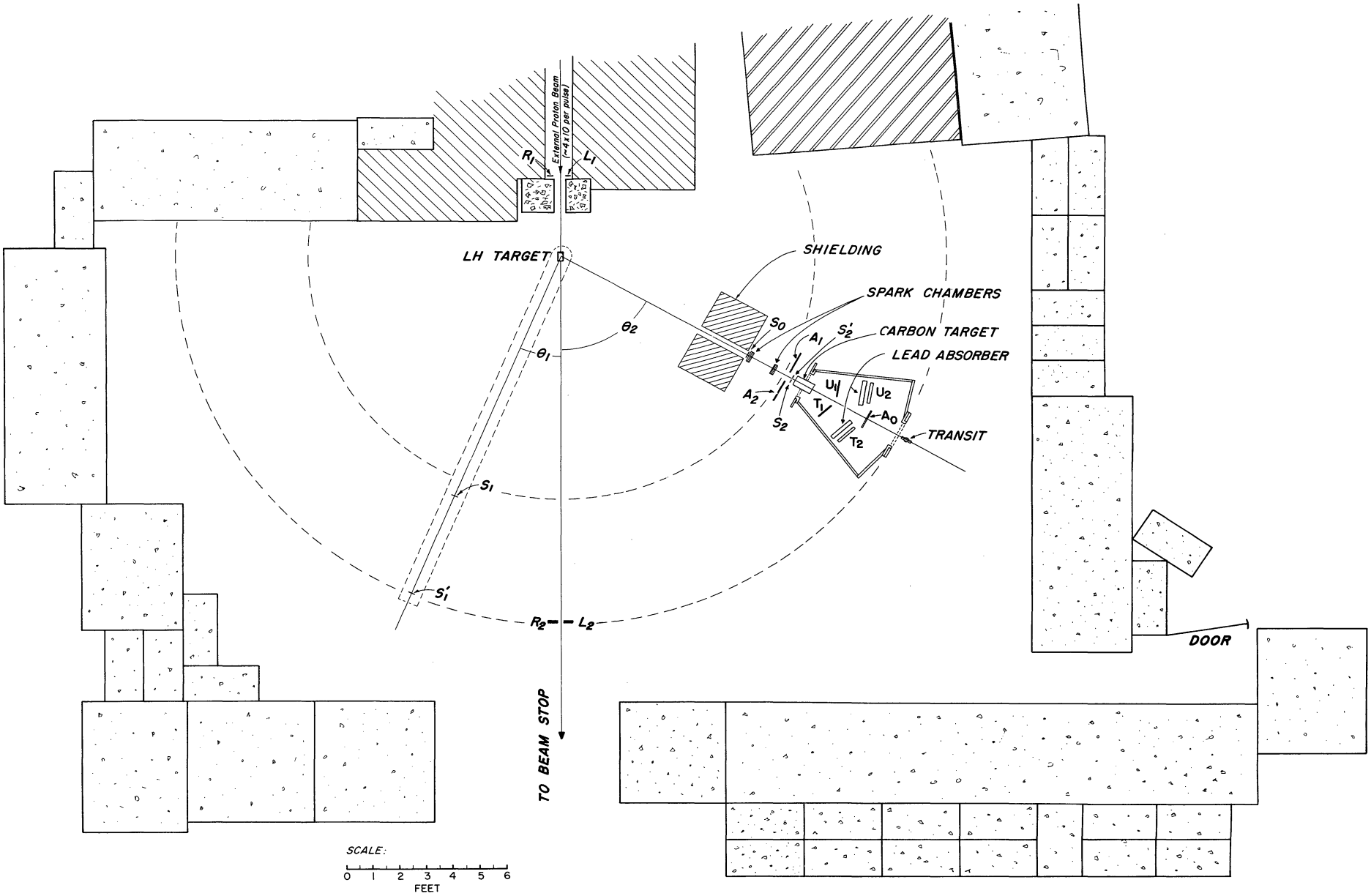

Fig. 3. The experimental layout.

range of recoil proton energies analyzed in the primary experiment. The analyzing power was determined also at several energies above 415 MeV by utilizing the antisymmetry of the pp polarization parameter about 90° in the center-of-mass system. For example, at the incident proton beam energy of 1.35 GeV the scattered protons of energy 350 MeV and 1000 MeV have the same polarization in magnitude; we can directly determine the asymmetry exhibited by the 1000 MeV protons and the polarization of the 350 MeV protons (since this energy lies in the calibration range), and can consequently determine the analyzing power at 1000 MeV. The argument, of course, assumes that the incident beam is unpolarized. Frequent checks were made to insure that the incident beam was unpolarized by separately analyzing recoil protons on each side of the incident beam line. In all cases, the incident polarization determined in this manner was consistent with zero.

Important accidental rates were constantly monitored and were found to be negligibly small. Also, contamination due to scattering from the hydrogen target assembly was found to be completely negligible.

The left-right asymmetry in scattering from the carbon target is quite sensitive to the relative alignment of the average incident beam trajectory and the axis of the analyzer. In order to make corrections for any such misalignment, spark chambers were employed upstream of the analyzer in both the analysis and calibration experiments to obtain the spatial and angular distribution of the incident beam with respect to the analyzer. In the calibration experiment, the dependence of the asymmetry on the relative orientation of the analyzer and the average beam trajectory was studied in

detail. Results from this study furnished the derivatives necessary in making the required corrections in the primary experiment.

B. BEAM

The beam layout is shown in Fig. 4. External proton beam III from the Cosmotron was extracted at the energies .75, 1.03, 1.32, 1.63, 2.24, and 2.84 GeV and focused on the hydrogen target by means of three bending magnets, M300, M304 and M305, and two pairs of quadrupole magnets, Q302-Q303 and Q306-Q307.

First, the beam is corrected in angle by magnet M300; this is necessary because the virtual beam source in the Cosmotron varies laterally with energy. Quadrupoles Q302-Q303 then focus the beam at F_1. This intermediate focus in included in the beam design to optimize transmission and therefore minimize background contamination. Magnets M304 and M305 bend the beam through a total angle of 15°. Finally, quadrupoles Q306-Q307 are used to achieve a second focus at the hydrogen target. The width of the beam spot at the hydrogen target varied from ≈ 3/16" at 2.84 GeV to ≈1-1/4" at .75 GeV. The angular spread was typically ±.5°. Polaroid exposures in the beam at .75 and 2.84 GeV are shown in Fig. 5.

Initial values for the magnet gradients were computed utilizing the 7090 computer program OPTIK.[22] The corresponding currents were determined from existing gradient-current graphs. Final operating currents were determined by studying properties of the beam spots at the two foci (by means of television cameras which viewed scintillating screens placed in the beam)

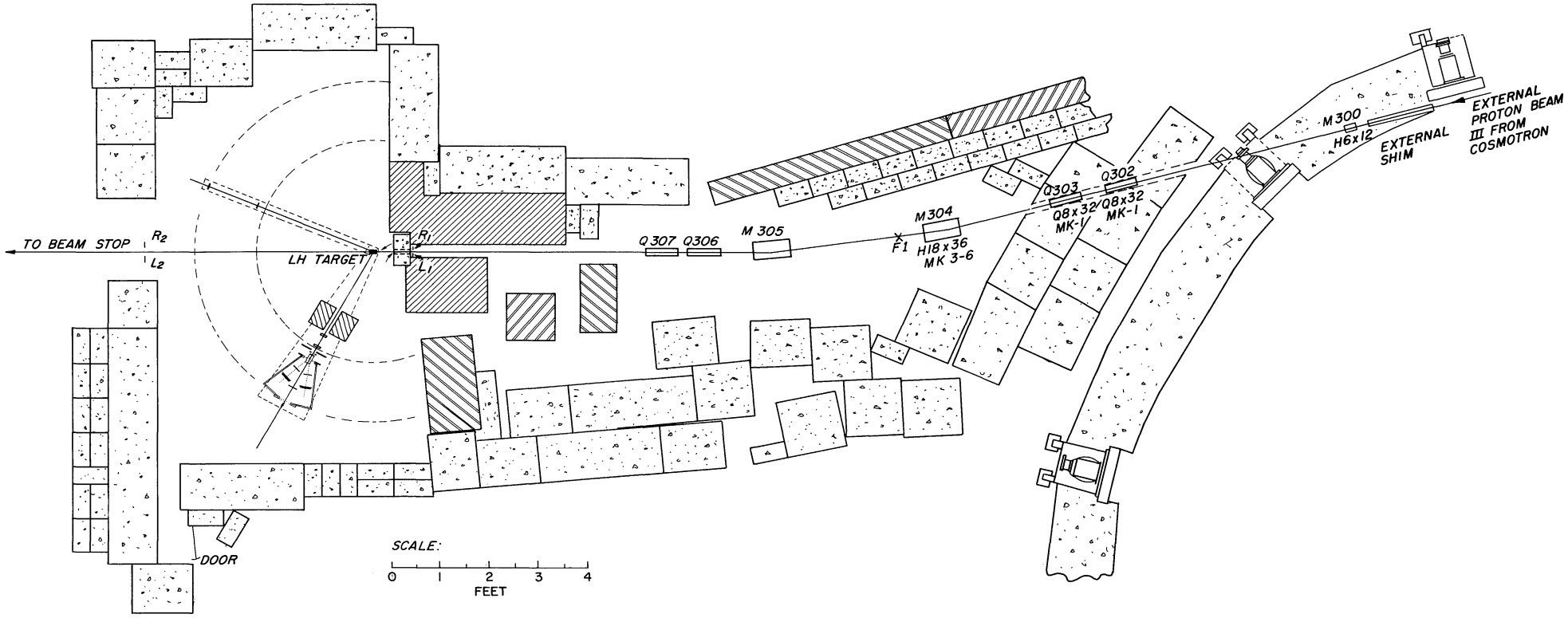

Fig. 4. The beam layout.

(a) Polaroid exposure at first focus at .75 GeV.

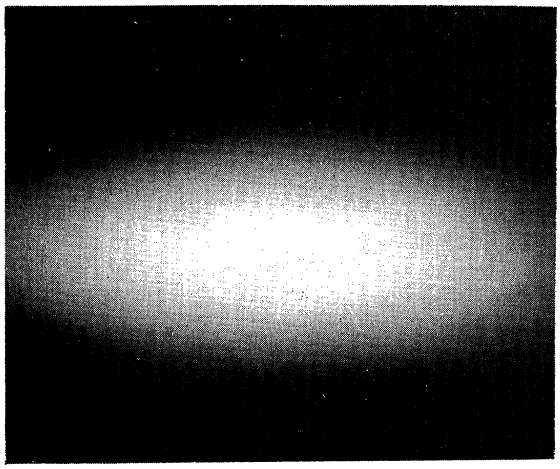

(b) Polaroid exposure at hydrogen target at .75 GeV.

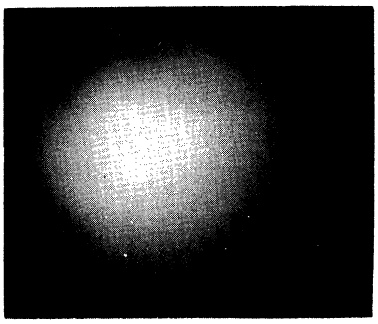

(c) Polaroid exposure at first focus at 2.84 GeV.

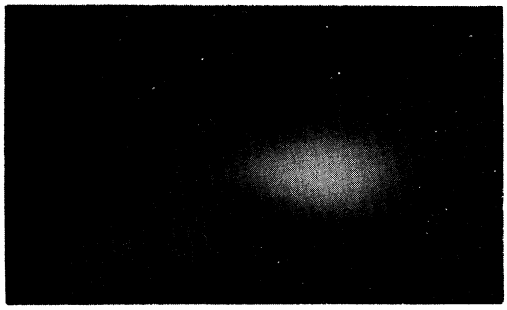

(d) Polaroid exposure at hydrogen target at 2.84 GeV.

Fig. 5. Polaroid exposures at the extreme energies. Beam spot size is generally exaggerated due to overexposure.

as the magnet currents were varied about their initial values. In most cases the final and initial currents differed by less than 1%.

Intensities up to 1 x 10^{11} protons per pulse were obtainable in this beam. However, our requirement that the important accidental rates in the analyzer be less than 2% generally limited the maximum usable intensity to $\approx 4 \times 10^9$ protons per pulse. The beam spill was approximately 150 ms with an effective duty cycle of 50%.

The energy of the incident beam was determined initially by the usual field and frequency methods as described in a Cosmotron internal report.[23] A somewhat more reliable determination results from the analysis of the experimental kinematic parameters. As will be described in a later section, spark chambers were used to sample the recoil beam. By projecting each track in the sample to the hydrogen target and requiring that the conjugate proton scatter, at a point in the hydrogen target along this trajectory, at the average angle allowed by the geometry, one is able to calculate an incident proton energy value for each such event. The average of these values taken over several hundred events at each of many angular settings is expected to provide an accurate determination of the beam energy. This scheme is somewhat insensitive to small lateral and angular changes in the incident beam trajectory, since for these changes the sum of the scattered and recoil proton angles remains practically constant. The values of the energies used throughout this work were obtained in this manner and differ from the field-frequency values by less than 3.5% in all cases.

The two pairs of scintillation counters R_1-L_1 and R_2-L_2 were placed in the tails of the incident beam, as shown in Fig. 3, to provide constant monitoring of the beam position and angle. Also, a television camera viewed a .005" scintillator which was centered on the beam line at the hydrogen target. Corrections were easily made for any deviation of the beam from the design trajectory by varying the currents in magnets M304 and M305.

In order to reduce the halo around the focal spot, a 24" deep lead collimator with a 2" x 2" opening was placed upstream of the hydrogen target. The beam was also collimated in magnet M300 to reduce the beam phase space volume. The width of this collimator was varied with beam energy.

Beam vacuum pipes were employed between magnets M300 and M304, and between magnet M305 and the hydrogen target. Helium bags were used over that portion of the beam path where beam pipes could not conveniently be used. Since helium has a much lower density than air, it effectively reduces the multiple coulomb scattering of the beam.

C. HYDROGEN TARGET

The exterior features of the hydrogen target assembly are shown in Fig. 6. Liquid hydrogen is contained in the inner vessel A, which is a 1.5" long, .01" thick, mylar cylinder of radius 1.25", with a .005" thick mylar hemispherical cup attached at each end. The overall length of the target in the median plane is 3".

The target vessel is located in a vacuum produced by evacuating outer vessel C. To reduce heat transfer further, the hydrogen target was wrapped with .002" of superinsulation (aluminized mylar). The incident beam enters

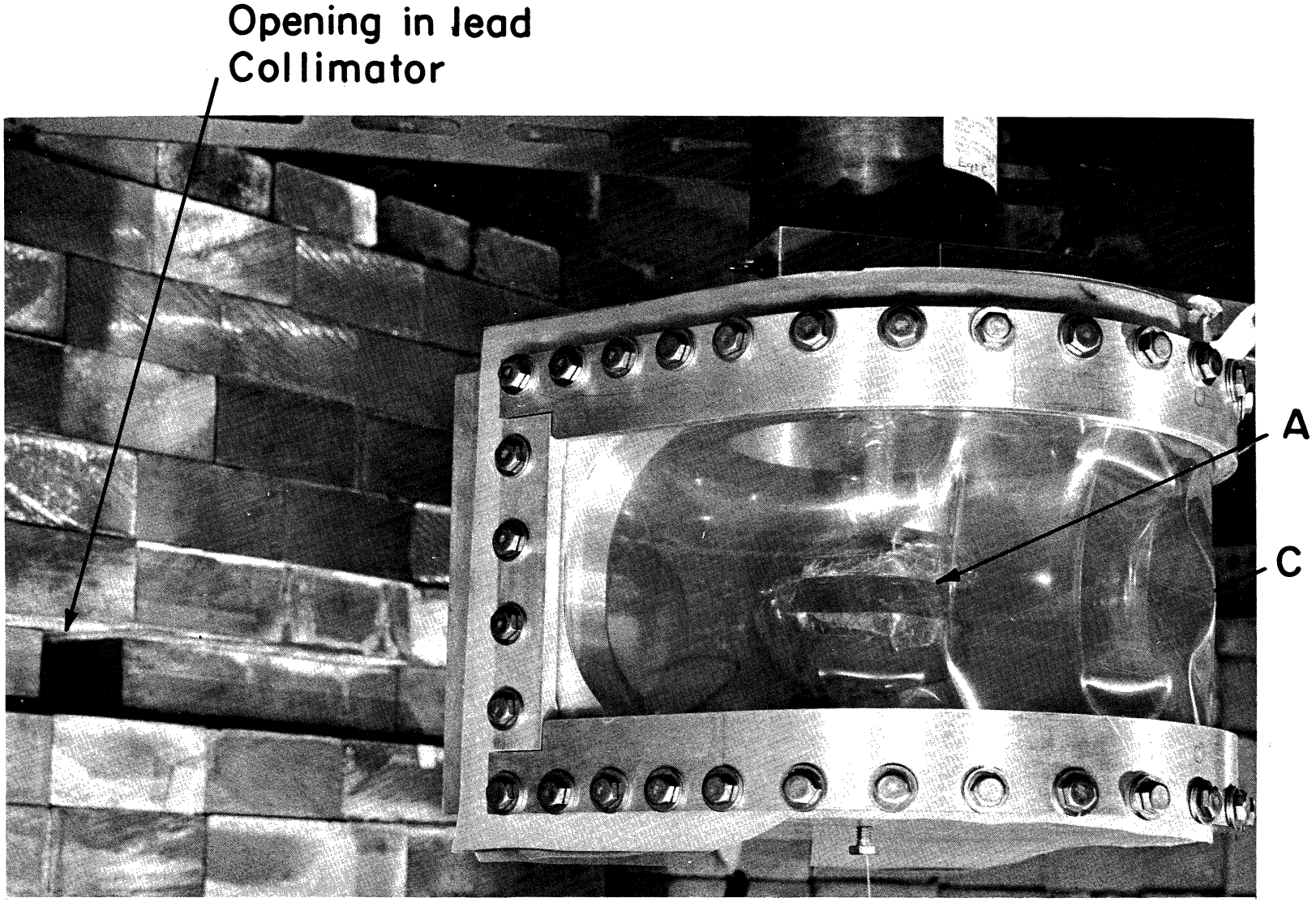

Fig. 6. The hydrogen target assembly.

vessel C through a .005" thick, circular mylar window, and the scattered protons emerge through two .005" mylar wrap-around windows (only the inner window supports the vacuum).

The center of the target vessel was marked with a vertical crosshair. The superinsulation described above was wrapped in such a way that the crosshair was externally visible. This crosshair was used to position the target in the designed location and to also provide a reference for aligning the various counters relative to the hydrogen target.

The effect of background events due to scattering from the mylar associated with the target assembly was frequently investigated by accumulating data with the target empty. It was found that this effect was completely negligible.

D. DETECTION APPARATUS AND LOGIC

The deployment of the various counters is shown in Fig. 3. All counters are plastic scintillators viewed by RCA 6810-A photomultipliers through lucite light pipes. Counter dimensions are given in Table I. In order to facilitate the alignment of the axis of the analyzer with the hydrogen target by means of a transit at the downstream end of the analyzer, counters A_0, and S_2-S_2' were designed with $\approx$ 1" diameter holes through their centers.

Counters R_1-L_1 and R_2-L_2 are beam position monitoring counters. The high voltages on these counters were adjusted so that R_1 and R_2 produced the same output at L_1 and L_2, respectively, when exposed to identical beams. These counters were employed in the tails of the incident beam. The signals from these four counters were displayed on an oscilloscope; a change

TABLE I

COUNTER DIMENSIONS

Counter	Width x Height x Thickness
S_2	1-1/2" x 9" x 1/4"*
S_2'	1-1/2" x 9" x 1/4"*
A_0	9" x 21" x 1/2" (1-1/8" dia. hole through center)
A_1	10-1/4" x 22" x 1/2"
A_2	10-1/4" x 22" x 1/2"
T_1	8" x 18" x 1/2"
T_2	10-1/4" x 22" x 1/2"
U_1	8" x 18" x 1/2"
U_2	10-1/4" x 22" x 1/2"
S_0	3-1/4" x 9-3/8" x 1/8"
S_1	see Table II
S_1'	see Table II

*Counters S_2 and S_2' are identical and are mounted as shown below:

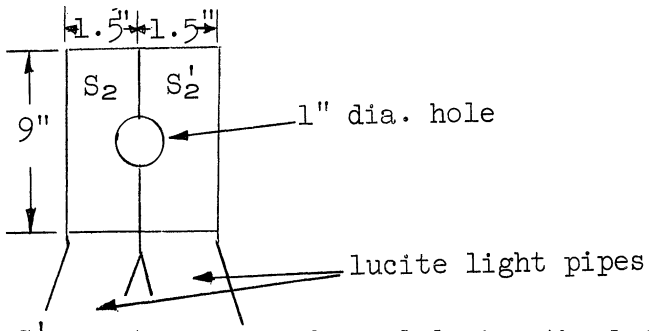

The dimensions of the S_2-S_2' counters were changed during the latter part of the experiment, after it was realized that the angular resolution could be appreciably improved without significantly sacrificing analyzing rate. Agreement of the polarization measured in the two situations was good and hence no distinction is made in the presentation of the results. The new dimensions of S_2 and S_2' were 1-1/8" x 9" (wxh), with all other parameters as shown above.

in the relative amplitude of the R_1-L_1 signals and/or the R_2-L_2 signals indicated a shift in the beam position.

In order to prevent the accidental rates in the various counters from becoming prohibitively large when the spill length or intensity of the external beam fluctuated, the output from an auxillary lucite cerenkov counter (not shown), which was located directly in the external beam, was used to gate off the electronics while the beam intensity was in excess of some preset level. This technique proved effective since most "spikes" in the beam spill had a width of a few milliseconds, while the reaction time of the monitor counter and the associated logic was a few nanoseconds.

Scattered protons were detected by the "S_1" arm, which consists of two counters, S_1 and S_1'. The dimensions of the counters used as S_1 and S_1' changed with energy. Design studies showed that the most reasonable compromise between high counting rates and low accidental rates would be obtained by choosing S_2-S_2', S_1 and S_1' such that they subtended approximately the same center of mass solid angle. The dimensions of the S_2-S_2' counters were taken fixed (see Table I) and those of S_1 and S_1' variable. Each S_1 and S_1' scintillator was mounted on identical threaded fittings that allowed rapid changeover from one pair to another. See Table II for the dimensions of the S_1 and S_1' counters used.

The recoil protons were detected and analyzed by counters on the "S_2" arm in appropriately delayed coincidence with the scattered protons (S_1S_1'). A typical recoil proton which is accepted by the geometry produces a count in S_0 and in S_2 or S_2', either scatters into one of the two telescopes

TABLE II

S_1-S_1' COUNTER DIMENSIONS*

S_1 (width x height)	S_1' (width x height)
1.35" x 1.35" 1.56" x 2.08"	2.34" x 3.12"
1.68" x 2.76" 1.90" x 3.50"	2.85" x 5.25"
2.21" x 4.58" 2.50" x 6.00"	3.75" x 9.00"

*Thickness of all counters: 1/4".

$U(=U_1U_2)$ or $T(=T_1T_2)$, or passes through anti-counter A_0. Anti-counter A_0 served to greatly reduce the accidental rates by negating any chance coincidences that occur when the proton scatters through too small an angle to be accepted by the telescopes. Anti-counters A_1 and A_2 served primarily to reduce the accidental events in which a proton directly enters telescope T or U without passing through S_2 or S_2'.

The analyzer consists of the counters S_2, S_2', T_1, T_2, U_1, U_2, A_0 and a carbon target. Each of these components is rigidly mounted in a single rotating carriage, for which a rotation of 180° effectively interchanges the two telescopes T and U. As is shown in Section IV-A, the average of the azimuthal asymmetries measured with the analyzer in the two orientations is essentially independent of any instrumental differences between the two telescopes. Counters S_2 and S_2' are also effectively interchanged by a 180° rotation of the carriage. When the quantity $\left((S_2-S_2')/(S_2+S_2')_I+(S_2'-S_2)/(S_2'+S_2)_{II}\right)$

is zero, where the subscripts refer to the carriage orientation, the median of the beam at S_2-S_2' is very nearly centered on the axis of rotation of S_2-S_2'. This fact was utilized in the experiment to guarantee that the separation of the axis of the analyzer and the recoil beam at the analyzer would be small. As a matter of experimental procedure, prior to accumulating data at each point the angular setting of the S_1 arm was slightly varied until the above expression was less than .02 in magnitude.

Spark chambers (see Fig. 3) were employed to determine the relative orientation of the average recoil beam trajectory and the axis of the analyzer. Deviation from colinearity was generally small ($\lesssim$ .07" at carbon target and $\lesssim$ .07°, in horizontal plane). The measured corrections were applied to the data in the manner discussed in Section IV-A. The two spark chambers are identical thin-plate (.001" Al) chambers with four .375" gaps and a width and height of 5" and 12-1/2", respectively. The chambers were filled with a mixture of 85% helium and 15% neon gases at a pressure of 1 atmosphere. During the course of the experiment both hydrogen thyratrons and spark gaps were used to "fire" the chambers. The chambers were triggered by every Nth analyzed recoil proton, where N was typically in the range 10 to 20. The scaler unit initiating the trigger was not reset between beam pulses, and consequently there existed no correlation between the triggering and the beam spill; this insured that the sample of events photographed was unbiased. Typically, one or two events were photographed per frame of film. The film was advanced between beam pulses. A diagram of the electronic logic is shown in Fig. 7. Most logic units were commercially available modules

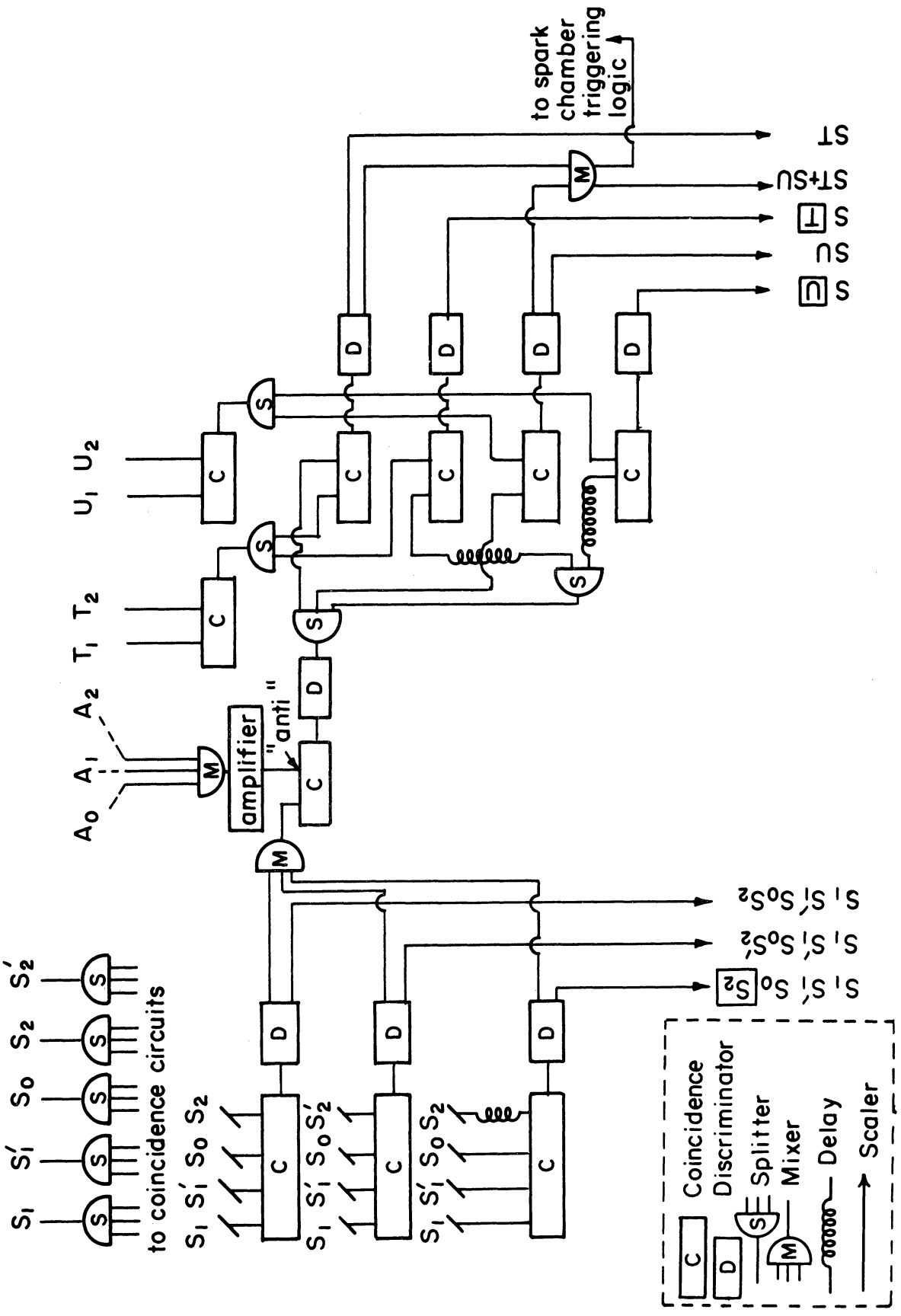

Fig. 7. Block diagram of electronics.

described in Ref. 24.

In order to accurately determine the position of the axis of rotation of the analyzer in the spark chamber pictures, fiducial strips which rotated with the analyzer were viewed by the camera. A typical spark chamber photograph is shown in Fig. 8. Fiducials F_1 and F_2 are fixed and F_3 to F_6 rotate. Directly underneath $F_3 \ldots F_6$ are fiducials $F_3' \ldots F_6'$ which appear on the spark chamber film when the analyzer is in the alternate orientation. The axis of rotation is determined, for example, as the average of the line F_3F_4 (measured with the analyzer in the orientation shown) and the line $F_3'F_4'$ (measured with the analyzer rotated by 180° from the orientation shown). All fiducials were Sylvania luminescent panels with a mask of the desired dimensions superimposed (see Fig. 9). These panels were continuously powered by 70 v.a.c. A Beattie- Coleman camera and 35mm Linagraph Shellburst film were employed for the photography.

The nominal angular acceptance of the telescopes T and U is 9°-26°. This range represents a compromise between high analyzing power and high counting rate. Different configurations of the analyzer were used depending on the recoil proton energy; a configuration is specified by the thickness of the carbon target and the amount of lead absorber between T_1 and T_2 (and U_1U_2). The absorber served to discriminate against low energy background. These parameters, for each configuration (see Table III), were chosen to optimize the analyzing rate and minimize background contamination over each respective range of energies. The maximum amount of carbon in the target was limited by the requirement that the recoil protons, after scattering

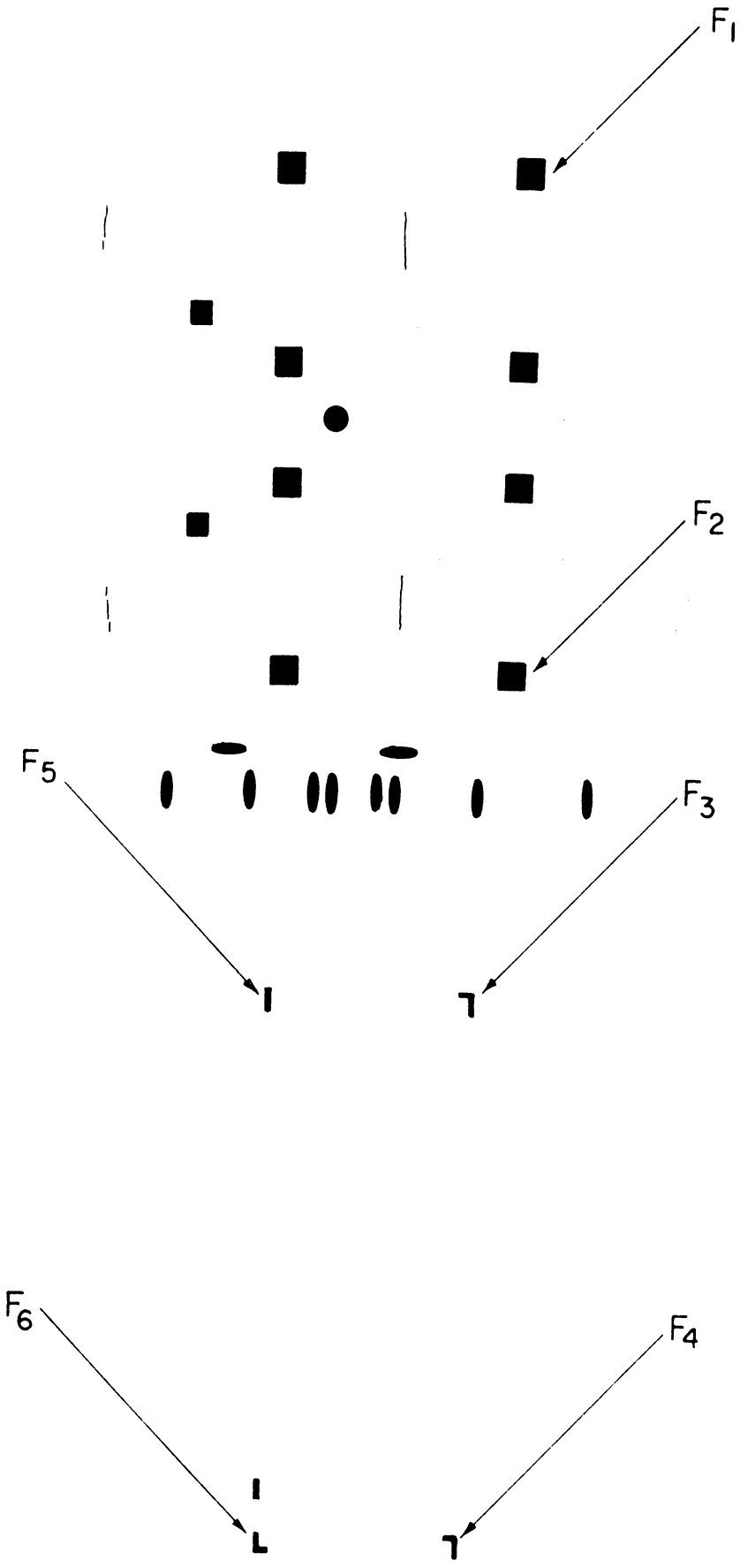

Fig. 8. Typical spark chamber photograph.

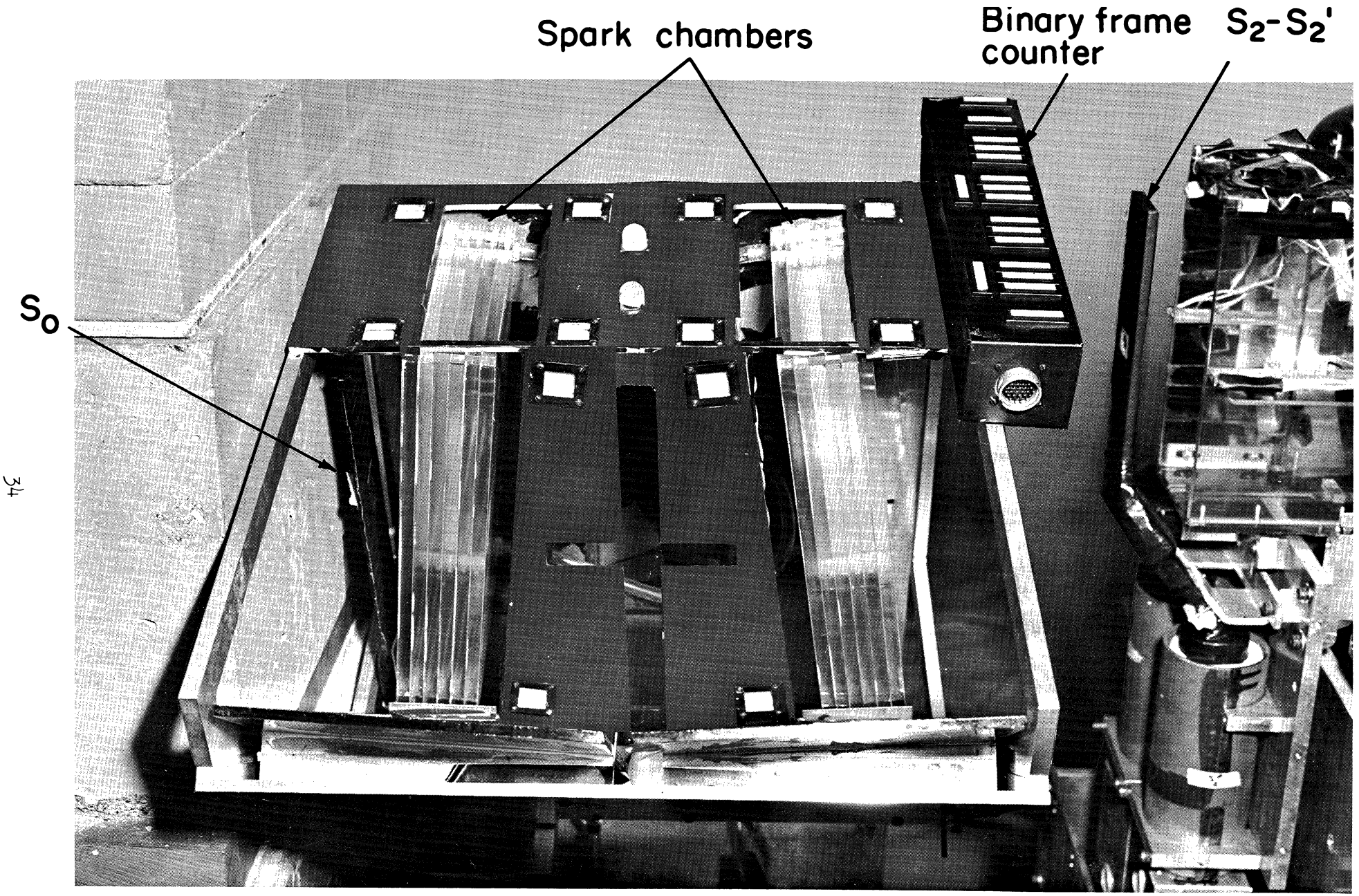

Fig. 9. Photograph of spark chambers and associated fiducials.

from the carbon, have sufficient energy to be efficiently detected by the telescopes T and U. The additional carbon at the higher recoil energy points often entirely compensates for the effect of the drop in the differential cross section in the first scatter; the analyzing rates were therefore approximately constant at all angles.

The asymmetry is the fractional difference of the events $S_1S_1'S_0(S_2$ or $S_2')$ $T_1T_2\bar{A}_0\bar{A}_1\bar{A}_2$ and $S_1S_1'S_0(S_2$ or $S_2')$ $U_1U_2\bar{A}_0\bar{A}_1\bar{A}_2$, where bars denote anti-coincidence, and the appropriate sign is chosen (depending on the orientation of the carriage). For the case of the incident protons scattering to the right, the recoil protons generally scattered preferentially to the right at the carbon target.

The procedure used in making a typical "run" will now be described. First, with the appropriate counters installed for S_1 and S_1', the "S_1" arm was surveyed to the desired kinematic angle utilizing a transit mounted directly beneath the center of the hydrogen target. The "S_1" arm was mounted on rails so its angular position could be easily changed; in aligning the arm, checks were made to insure that <u>both</u> S_1 and S_1' were at the appropriate kinematic angle. Each of the counters shown in Fig. 3, with the exception of S_2-S_2' and A_0, had a .015" diameter pin mounted through its exact center. These pins were externally visible and were used in aligning the counters. Next, the "S_2" arm was aligned. This arm was mounted on the same rail system as the "S_1" arm and its angular position was also easily varied. A vertical crosshair marked the center of the S_2-S_2' counter pair and the "S_2" arm was positioned such that this crosshair appeared at the desired kinematic

recoil angle as measured by the transit mentioned above. A transit at the downstream end of the analyzer, and which was centered on the axis of rotation of the analyzer, was used in "pointing" the axis at the center of the hydrogen target. The "pointing" procedure did not change the angular setting of S_2-S_2' since the analyzer was pivoted directly underneath S_2-S_2'. The spark chambers were easily moved in and out of the beam line for the alignment process. Next, the appropriate amount of carbon was installed in the second target. If required for the particular recoil energy being studied, the lead absorber between T_1 and T_2 (and U_1 and U_2) was changed. Also, film for the spark chamber photography was changed at this time. Now, with the beam on, all counters were timed and then the angular setting of the "S_1" arm was varied slightly (by a remotely controlled motor) until the median of the recoil beam was centered on the axis of rotation of the analyzer at the carbon target, as discussed earlier in this section. At this point accumulation of data was begun. After approximately 10,000 protons had been analyzed, the readings of all scalers were printed out by an on-line typewriter. The process was then repeated with all parameters the same. Then the analyzer was rotated 180° about the recoil beam line by a remotely controlled motor and a set of four measurements of the above type were made. The analyzer was then rotated to its original position and two final measurements were made. This particular sequence of carriage orientations minimizes the amount of time used in rotating the analyzer, while allowing a high degree of cancellation of false asymmetries, even if these asymmetries drift in time. Spark chamber photographs were taken in uniformly

spaced intervals throughout the above sequence. Important accidental rates were constantly monitored by scaling coincidences between the pertinent counters with their signals delayed in such a manner that only chance coincidences could occur.

IV. ANALYSIS AND RESULTS

A. DATA CORRECTIONS

The relative alignment of the axis of the analyzer and the mean recoil beam trajectory is quite crucial, as, for example, a misalignment of .1" at the carbon target (or a divergence of .1°) would result in an error of approximately .08 in the polarization parameter. Spark chambers were employed to determine the corrections necessary to refer the measured asymmetries to the asymmetries that would have been observed if there were no misalignment. In this section the manner in which these corrections were applied to the data will be discussed.

In the calibration experiment (see Appendix I) the asymmetry produced by scattering a 40% polarized proton beam from carbon target C (Fig. 28) was measured at several beam energies, with the same geometry used in the primary experiment, for various orientations of the beam relative to the axis of the analyzer. Analysis of these data yielded an asymmetry function $E(y,\theta,p)$, where y is the separation of the axis of rotation of the analyzer and the centroid of the recoil beam at the carbon target, θ is the angle between the beam and the axis of the analyzer, p is the beam momentum, and E is the asymmetry produced by scattering a 40% polarized proton beam with these parameters (see Fig. 10).

In the primary experiment the problem is the following: Knowing the asymmetry ϵ_m observed in scattering an arbitrarily polarized proton beam,

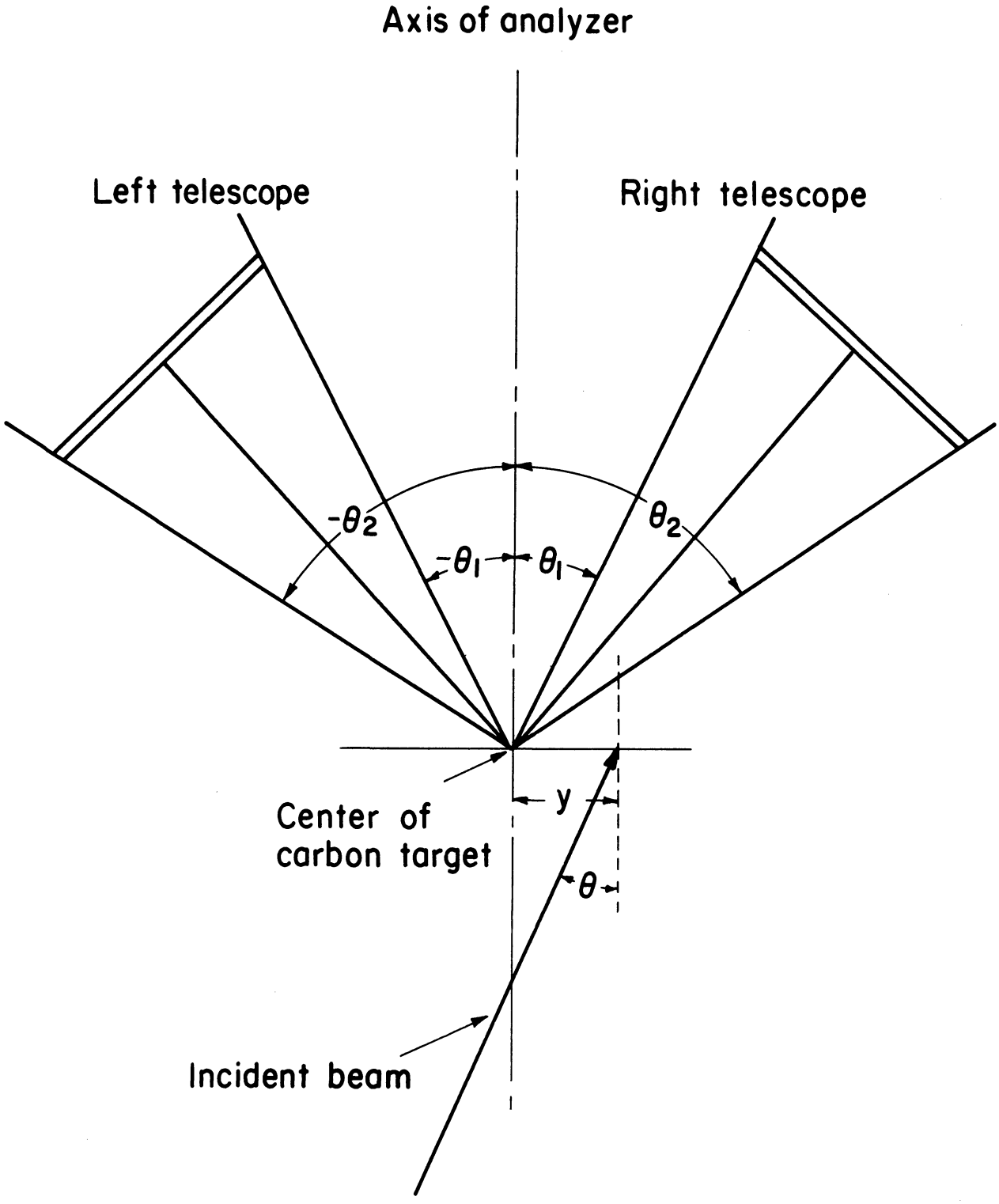

Fig. 10. Parameterization of incident beam trajectory relative to axis of analyzer.

and y, θ, and p, what is the polarization, P, of this beam. In Appendix II it is shown that the asymmetry, ϵ_o, which would have been observed if the centroid of the recoil beam were coincident with the axis of rotation of the analyzer, is related to the measured asymmetry, ϵ_m, by

$$\epsilon_o = \epsilon_m - \alpha(y,\theta,p) \quad ,$$

where

$$\alpha(y,\theta,p) = E(y,\theta,p) - E(0,0,p) \quad .$$

Each experimental point was corrected in this manner by calculating $\bar{\alpha}$ from the sample of events photographed. The analyzing powers, A, for our geometry and the y and θ slopes of α (at $y = 0$, $\theta = 0$), together with other parameters of the analyzer are presented in Table III. From the true asymmetry, ϵ_o, the polarization parameter is given by ϵ_o/A.

A linear function approximates α to the desired accuracy, and therefore $\bar{\alpha}$ can be evaluated from $\bar{y}$ and $\bar{\theta}$ (i.e., higher moments are not necessary). Both $\bar{y}$ and $\bar{\theta}$ were determined from analysis of the spark chamber photographs. Each accepted event was required to have originated from the hydrogen target (appropriately enlarged to account for multiple coulomb scattering) and to have passed through the counter pair S_2S_2'. This restriction greatly reduces the effect of any asymmetrical background contributions on the measured average beam trajectory. A scatter plot of the beam distribution at counters S_2S_2' at a typical data point is exhibited in Fig. 11. Due to the plotting routine used in making this plot, each asterisk represents one or more protons and, consequently, the distribution presented is not the true density distribution. The relative accidental contributions are somewhat exaggerated

TABLE III

ANALYZER PARAMETERS

Configuration	Recoil Energy (MeV)	Thickness of Graphite Target	Lead Between T_1-T_2 (and U_1-U_2)	$\left.\frac{\partial\alpha}{\partial y}\right\|_{\substack{y=0\\ \theta=0}}$	$\left.\frac{\partial\alpha}{\partial\theta}\right\|_{\substack{y=0\\ \theta=0}}$	A
1	1000	9.0"	1.358"	.221	.104	.236
	710			.221	.104	.264
	650			.221	.104	.263
	615			.221	.104	.262
	580			.221	.104	.260
	520			.221	.104	.259
	500			.221	.104	.259
	450			.221	.104	.259
	425			.221	.104	.259
	415			.221	.104	.259
	400			.243	.110	.257
	375			.301	.130	.341
	350			.360	.151	.425
2	350	7.0"	0.0"	.156	.078	.238
	325			.179	.088	.307
	300			.202	.099	.378
	270			.246	.118	.428
	260			.261	.125	.445
3	240	2.5"	0.0"	.151	.082	.288
	210			.184	.105	.301
	200			.196	.113	.310
4	185	.75"	0.0"	.165	.102	.335
	150			.214	.127	.330
	120			.224	.144	.230
5	150	.25"	0.0"	.162	.122	.317
	135			.159	.129	.277
	125			.157	.136	.238
	103			.110	.151	.222

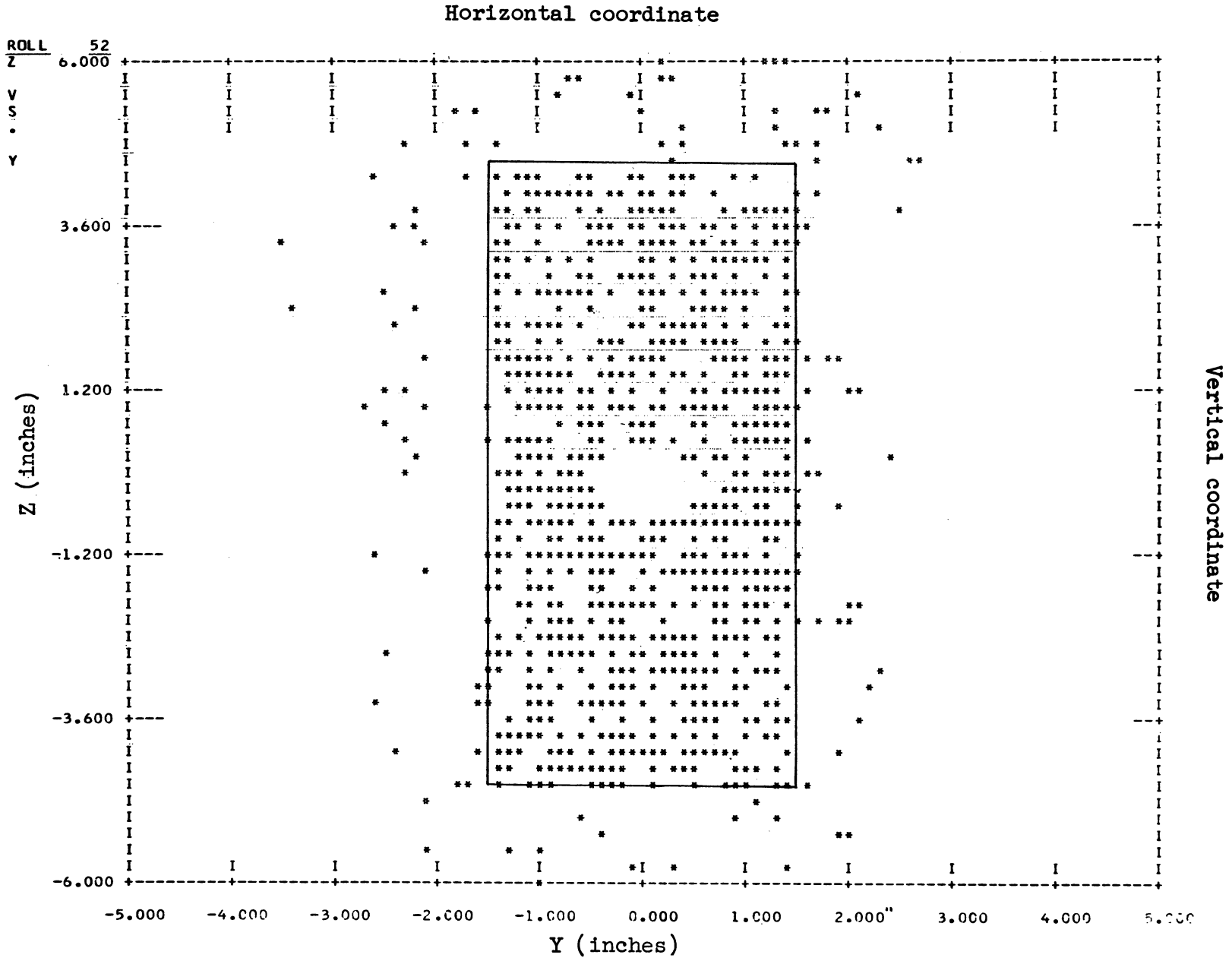

Fig. 11. Scatter plot or recoil beam at S_2S_2.

in this method of plotting. It should also be remarked that the coordinates of each event are rounded to the nearest grid intersection before plotting. The solid lines enclose the region occupied by counters S_2S_2'. The profile of the S_2S_2' counter pair is prominent; the hole in the center of the plot is the image of the 1" circular hole in S_2S_2' (see Table I). Typical histograms of the recoil beam distribution are shown in Figs. 12-14. As was discussed in Section III-D, the axis of rotation of the analyzer was referred to the fixed fiducial system by fiducial strips which rotated with the analyzer and appeared on the spark chamber film. The distribution in measured horizontal angle and displacement of these strips relative to the fixed fiducial coordinate system, at a data point where the total number of measurements was 1050, is shown in Fig. 15.

As a check on the accuracy of the beam centroid determinations from the spark chamber photographs, the median of the recoil beam at S_2S_2', as calculated from the number of counts in S_2S_2', was compared with the median of the y distribution obtained from the spark chamber photographs. In most cases the agreement was quite good. The discrepancies found were attributed to accidentals in the spark chamber photographs and corrections were made utilizing the median determined by S_2S_2'. We will explicitly show how the position of the median of the recoil beam at S_2S_2', relative to the axis of the analyzer, can be found from the knowledge of the number of counts in S_2 and S_2' in each of the two supplementary carriage orientations. Before dealing with this problem, however, the importance of the relative efficiencies of the counters S_2S_2' and their alignment with respect to the axis of the analyzer will be investigated. It should be pointed out that this analysis applies not only

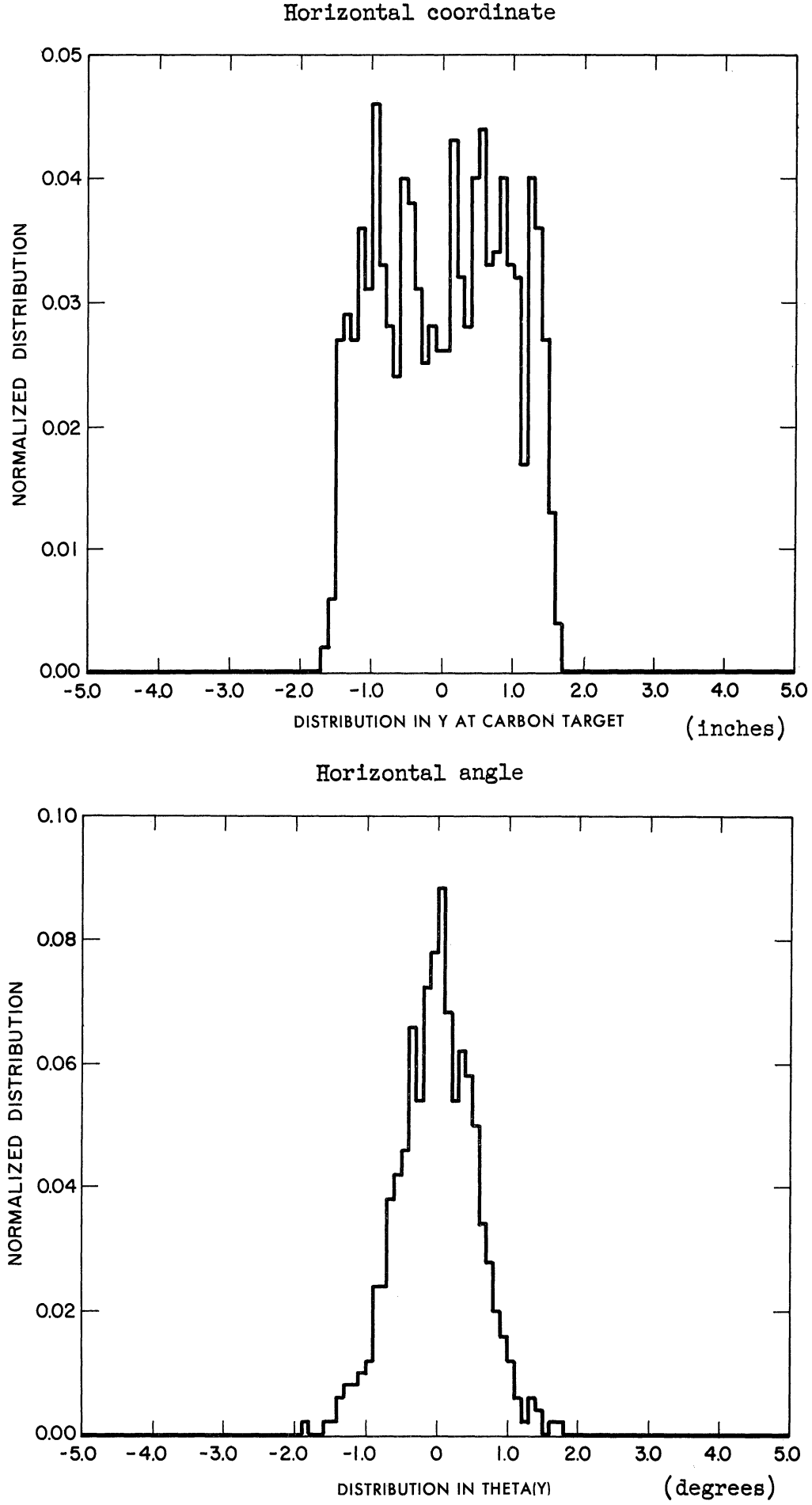

Fig. 12. Histograms of recoil beam distribution in horizontal displacement and angle at carbon target.

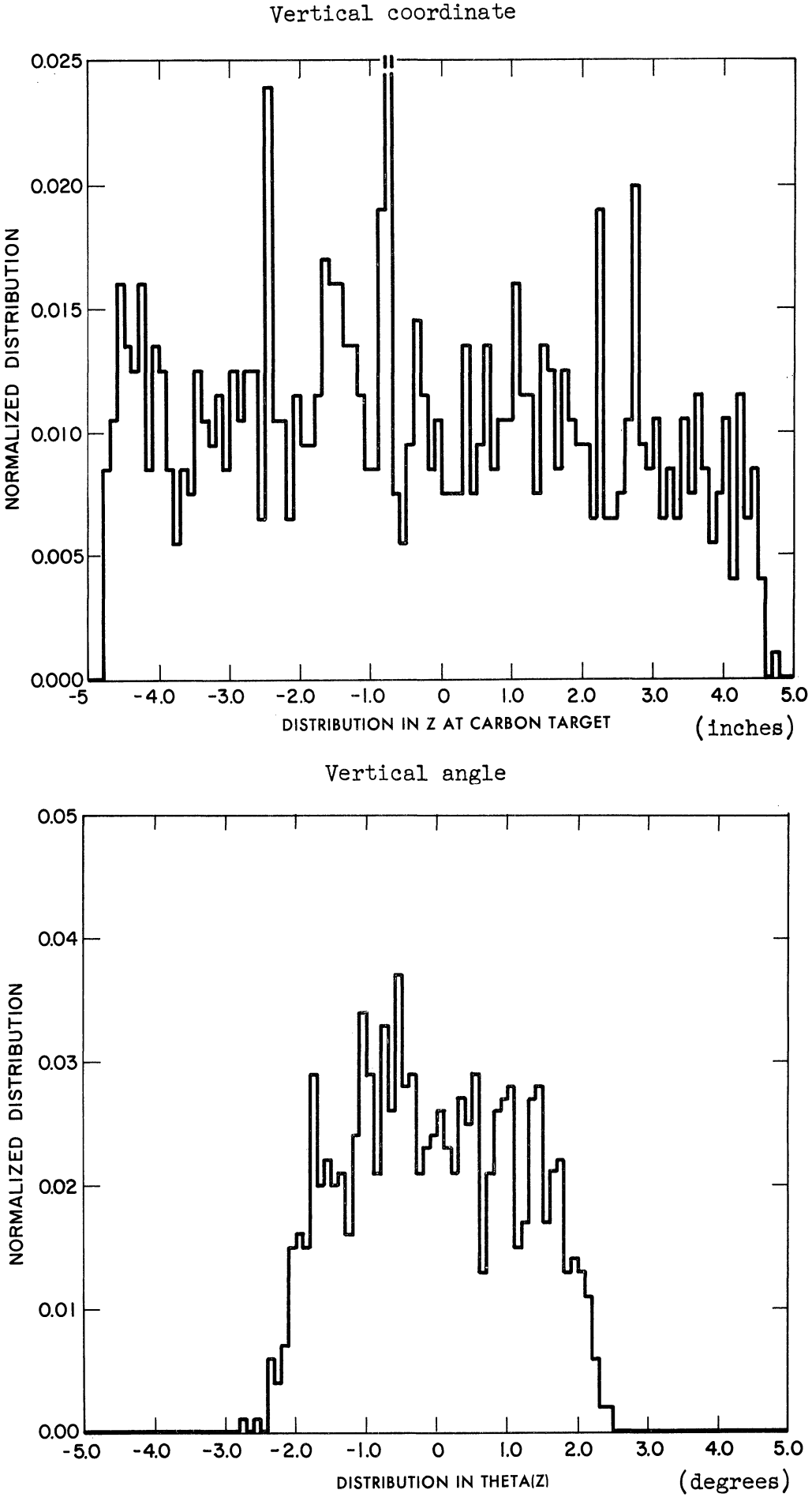

Fig. 13. Histograms of recoil beam distribution in vertical displacement and angle at carbon target.

Horizontal coordinate

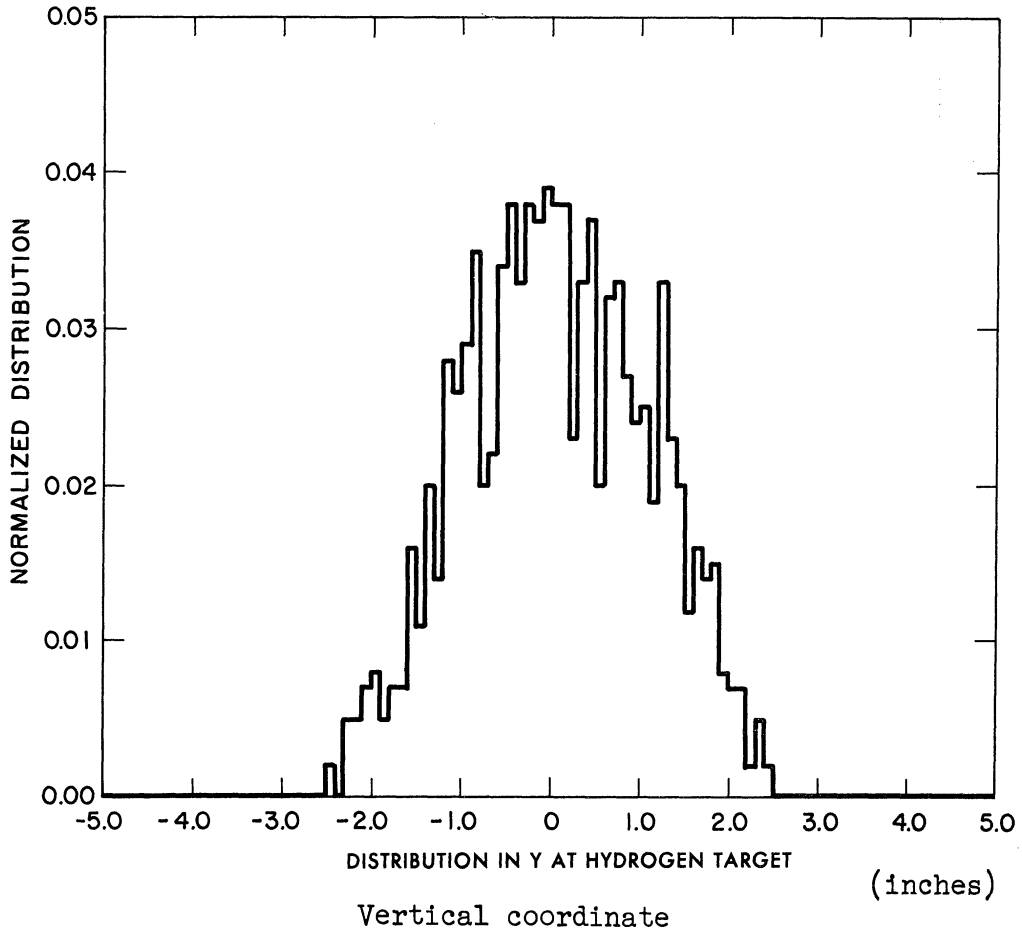

Vertical coordinate

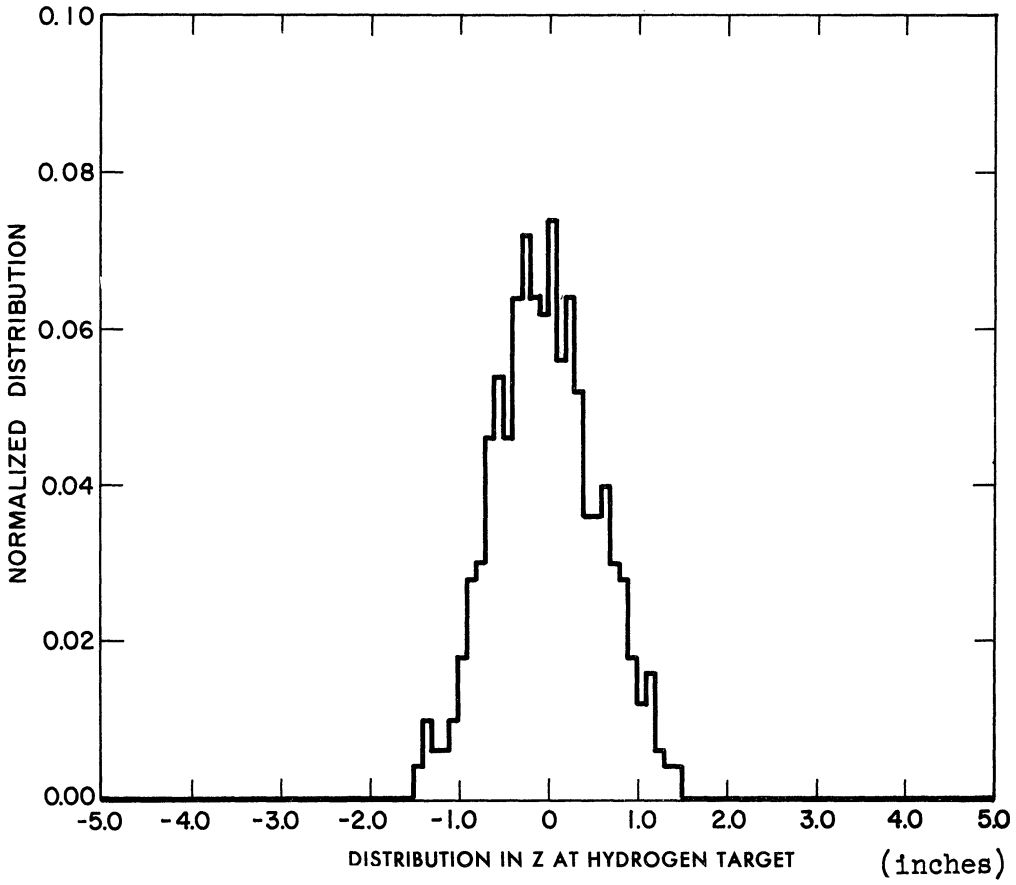

Fig. 14. Histograms of recoil beam distribution in horizontal and vertical displacement at hydrogen target.

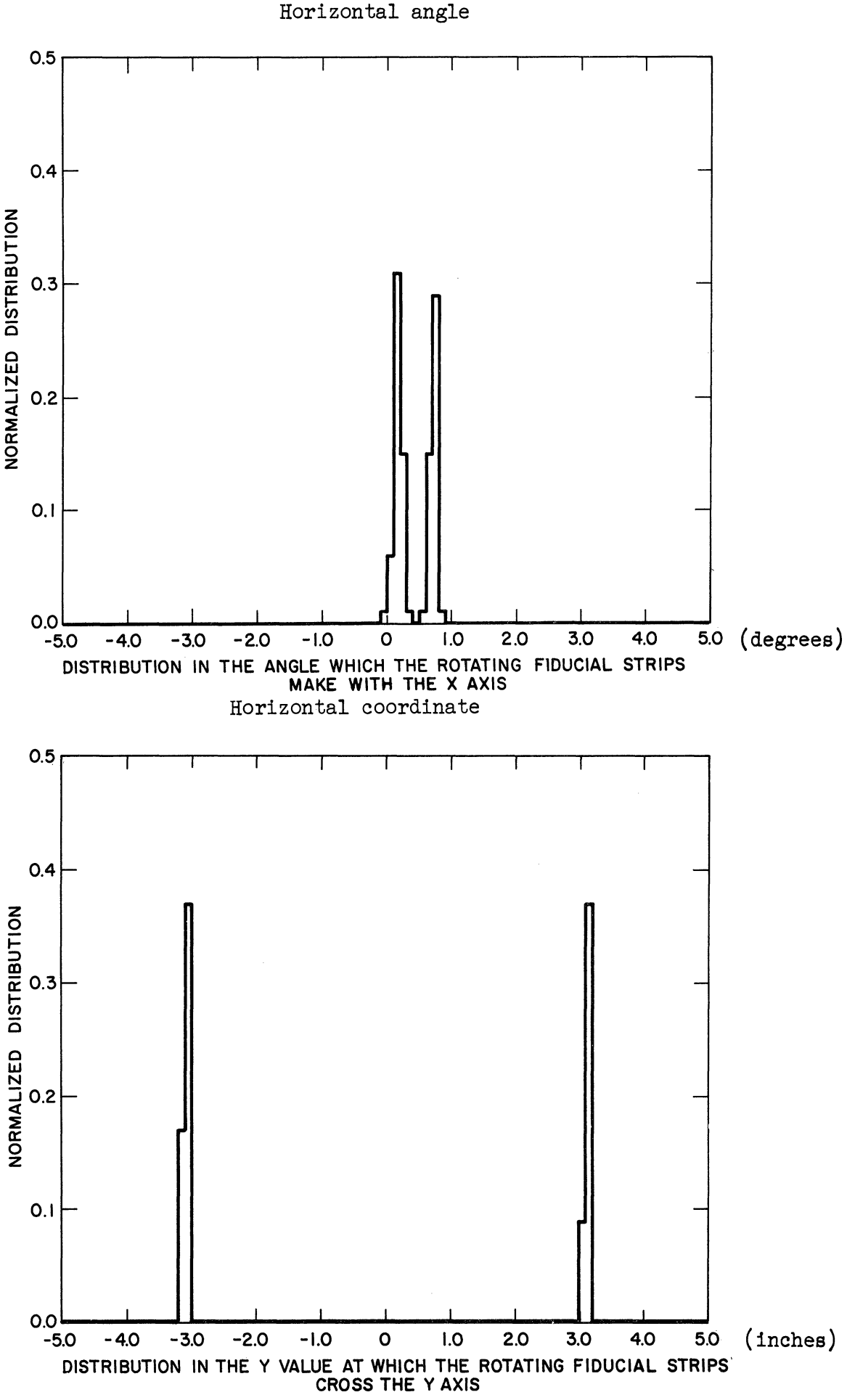

Fig. 15. Histograms for the distribution in horizontal angle and horizontal displacement for the rotating fiducial strips.

to S_2S_2' but also, with the obvious modifications, to the telescopes T and U. Let L_1 and R_1 represent the number of counts in S_2 and S_2', respectively, for the carriage in position I, and L_2 and R_2 the number of counts in S_2' and S_2, respectively, for the carriage in position II. We will allow the following possibilities and independently examine their consequences: 1. the actual number of protons passing through counter $S_2(S_2')$ differs from the measured number by a constant, $\Delta_2(\Delta_2')$, times the actual number, and 2. the center of the S_2-S_2' counter pair does not lie exactly on the axis of rotation. For part 1 assume

$$L_1 = L_1^\circ + \Delta_2 L_1^\circ \quad ,$$

where L_1° is the true number of protons scattered to the left of the axis of rotation in carriage orientation I (see Fig. 16a). Similarly,

$$R_1 = R_1^\circ + \Delta_2' R_1^\circ$$

$$L_2 = L_2^\circ + \Delta_2' L_2^\circ$$

$$R_2 = R_2^\circ + \Delta_2 R_2^\circ$$

Define

$$\beta = 1/2((L_1-R_1)/(L_1+R_1) + (L_2-R_2)/(L_2+R_2))$$

$$= (L_1L_2-R_1R_2)/N_1N_2 \quad ,$$

where

$$N_1 = L_1 + R_1$$

$$N_2 = L_2 + R_2 \quad .$$

Therefore,

$$\beta = \left(L_1^\circ L_2^\circ(1+\Delta_2)(1+\Delta_2') - R_1^\circ R_2^\circ(1+\Delta_2)(1+\Delta_2')\right) \Big/ \left(\left(L_1^\circ(1+\Delta_2)+R_1^\circ(1+\Delta_2')\right)\left(L_2^\circ(1+\Delta_2')+R_2^\circ(1+\Delta_2)\right)\right)$$

$\beta = \beta_0(1+\Delta_2+\Delta_2')$ to first order in Δ_2 and Δ_2', where β_0 is the "true" value of β.

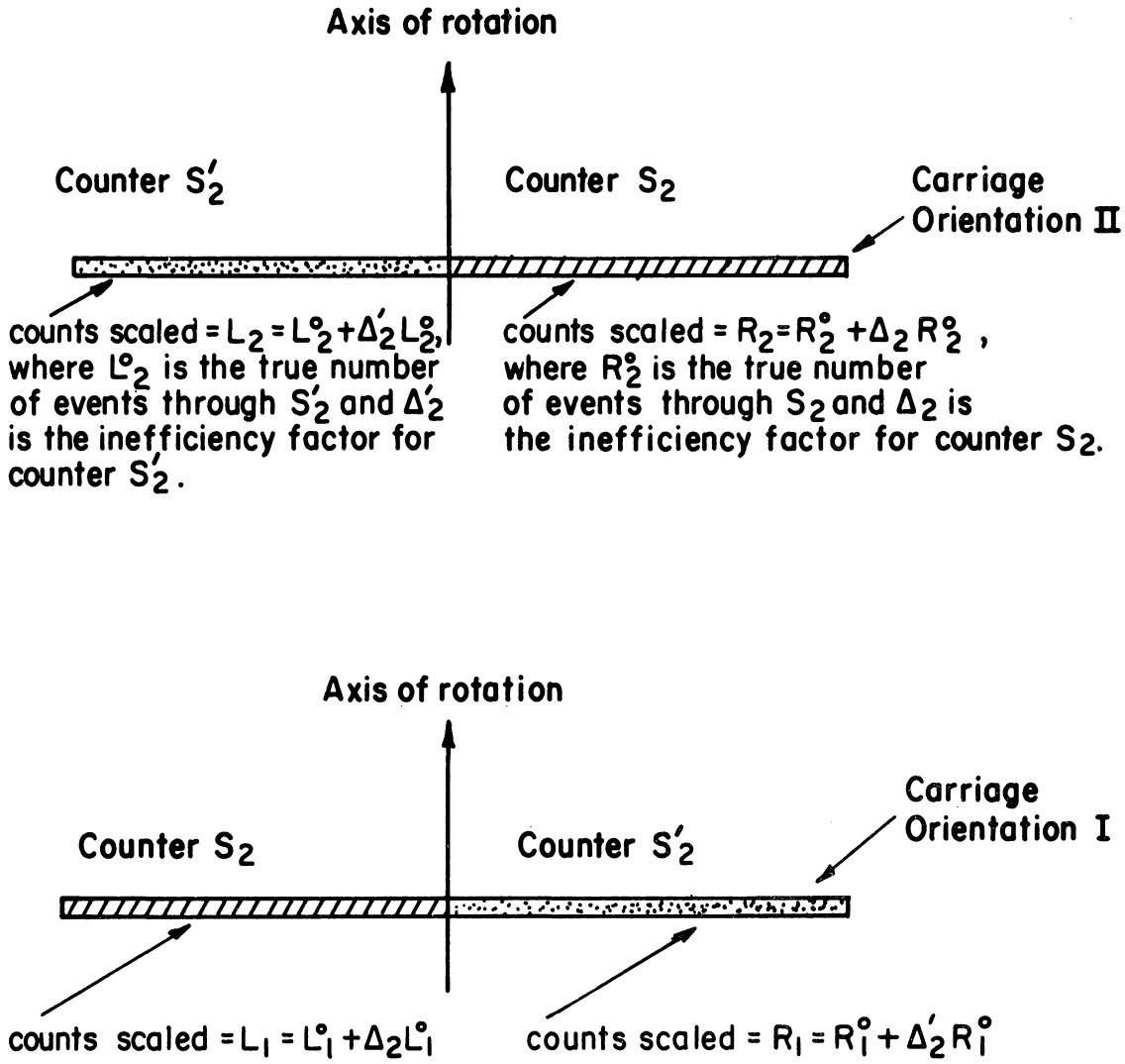

Fig. 16a. Effect of instrumental differences in counters S_2 and S_2'.

As will be shown below $2\beta \sim y_{med}$ where y_{med} is the median of the y-distribution. The maximum β value used in the experiment was .05, and the scaler data indicates a reasonable upper limit for Δ_2 and Δ_2' to be .1. Therefore, the maximum error in β due to instrumental differences between the counters is .010 ($\Delta y_{med} \sim .020"$). This error was found to be negligible for practically all cases encountered. Next, the dependence of β on the misalignment of S_2-S_2' relative to the axis of rotation is examined (Fig. 16b). The notation is the same as above. In addition define $\delta_1 L_1^\circ(\delta_2 L_2^\circ)$ to be the number of protons between the axis of rotation and the S_2-S_2' counter boundary when the carriage is in orientation I(II). The quantity $(\delta_1-\delta_2)/(\delta_1+\delta_2)$ is approximately equal in magnitude to the center of gravity of the y sub-distribution in the region y_1 to y_2, since experimentally $L_1^\circ \cong L_2^\circ$. For the entire experiment it was true that $|y_1-y_2| \lesssim .04"$. Therefore the difference $|\delta_1-\delta_2|$ is at least an order of magnitude smaller than either δ_1 or δ_2. We will take $\delta = \delta_1 = \delta_2$. Then

$$L_1 = L_1^\circ(1+\delta)$$

$$L_2 = L_2^\circ(1-\delta)$$

$$R_1 = R_1^\circ - \delta L_1^\circ$$

$$R_2 = R_2^\circ + \delta L_2^\circ$$

and

$$\beta = (L_1L_2-R_1R_2)/((L_1+R_1)(L_2+R_2))$$

$$= \beta_0 + \Delta\beta \ ,$$

where

$$|\Delta\beta| \leq 2\delta^2$$

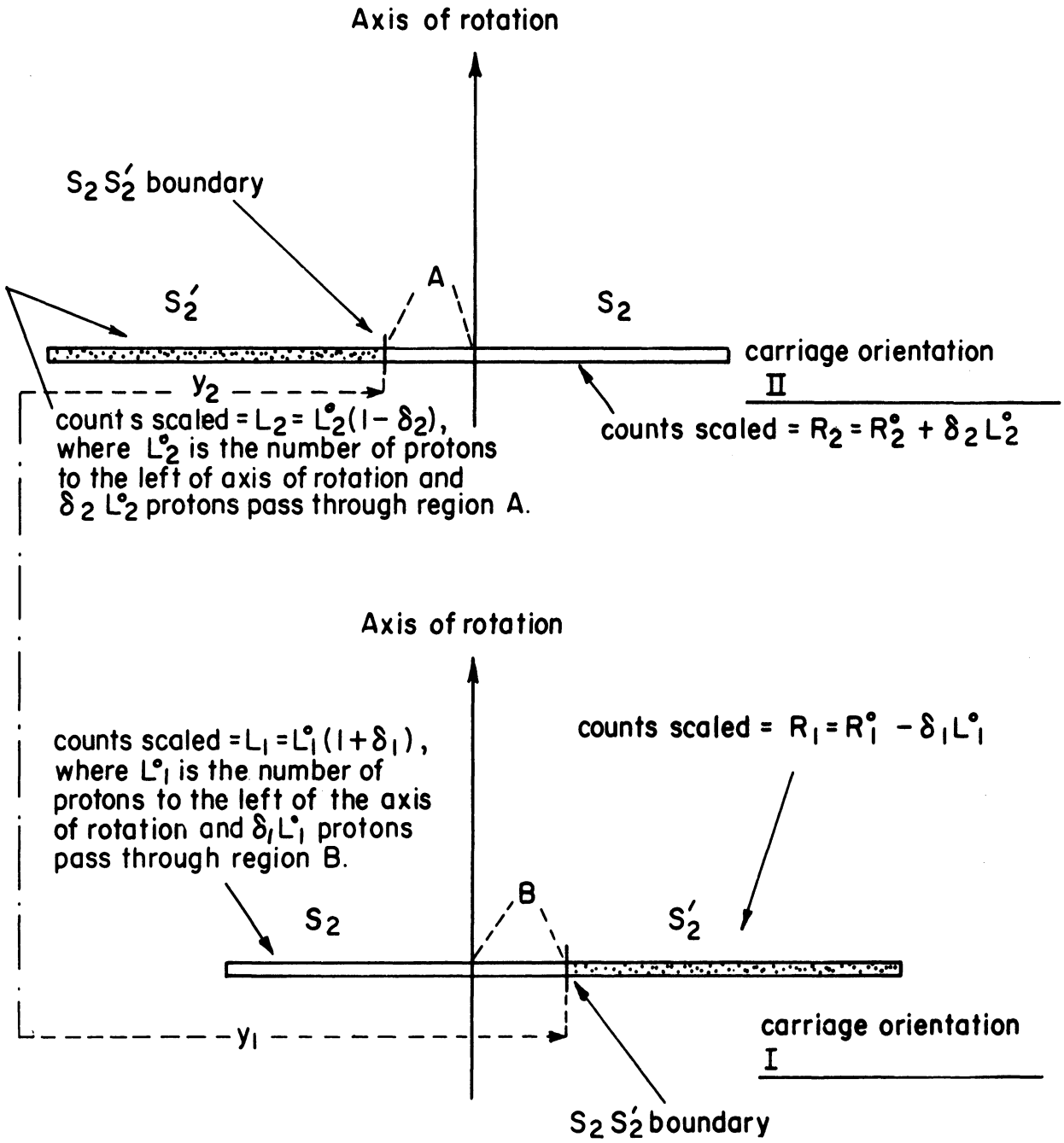

Fig. 16b. Effect of misalignment of counters S_2-S_2'.

From the spark chamber photographs it is known that the region y_1-y_2 contains less than 2% of the total number of particles in the distribution. Therefore, the maximum error is β due to misalignment of S_2-S_2' is .0032 (or $\Delta y_{med} \lesssim .006"$) and can be neglected.

The relationship between β and y_{med} will now be ascertained. Figure 17 shows a hypothetical distribution in y at S_2-S_2'. If H represents the average number of events per inch in the interval (y_m, y_r), where y_m is the y-coordinate of the median and y_r is the y- coordinate of the axis of rotation, then the fractional number of particles contained in (y_m, y_r) is $H\gamma/N$, where N is the total number of events in the distribution and $\gamma = y_m - y_r$. If we designate the number of particles in the shaded region by L, then the fractional number of particles in (y_m, y_r) is also seen to be $1/2 - L/N$. Equating these two expressions leads to

$$\gamma = -\beta/((2H/N)) \quad ,$$

since

$$\beta = 2L/N - 1 \quad .$$

Therefore

$$\gamma = -\beta/.7$$

or

$$-\beta/.5$$

since the ratio (H/N) is approximately constant at .35 or .25 depending on the set of S_2-S_2' counters used.

Corrections due to the energy loss of the recoil beam between the first and second targets were not necessary since the corresponding energy loss in

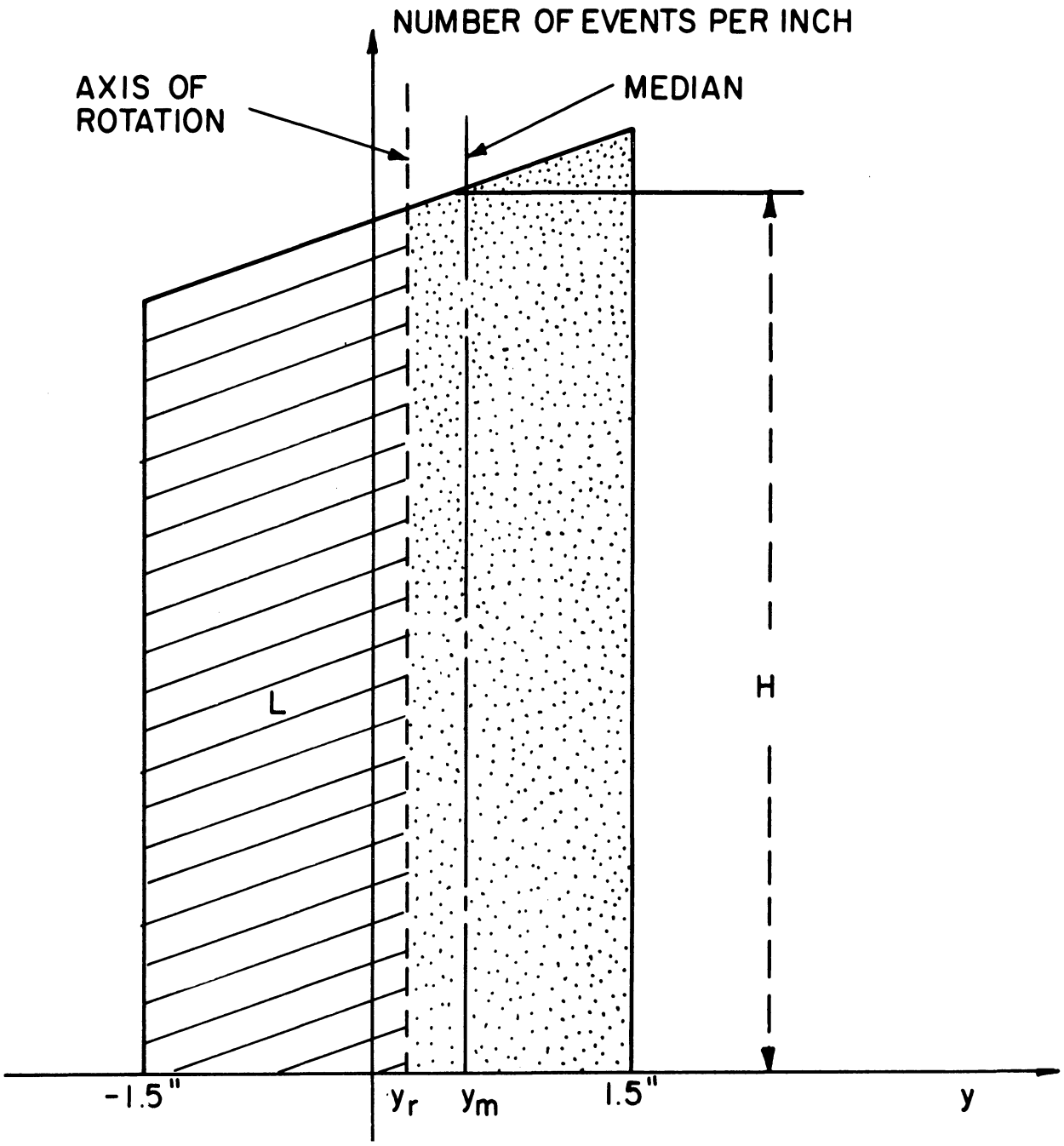

Fig. 17. Hypothetical distribution in y used in deriving the relationship between the median of the y distribution and the counts in S_2-S_2'.

the calibration experiment was very nearly the same.

If the external beam were polarized, the polarization parameter would not be equal to the negative of the recoil polarization, as has been tacitly assumed so far. From a study of the mechanisms involved in accelerating and extracting the incident beam, it appears unlikely that an incident polarization would be present. Nevertheless, a systematic search for an incident polarization was made employing techniques which will now be discussed. Suppose the internal beam (of $2N_1$ protons) is polarized by an amount P_1 by a left scattering in the accelerator (Fig. 18). Let us designate the analyzing powers for the second and third scattering by P_2 and P_3, where the second scattering occurs at the hydrogen target and the third scattering at the graphite target of the analyzer. Also, it will be assumed that the three scattering planes are parallel. Then the number of incident protons scattering to the left three times (at $\theta_1,\theta_2,\theta_3$) is

$$LLL = N_1(1+P_1)(1+P_2)(1+P_3) + N_1(1-P_1)(1-P_2)(1-P_3)$$

Similarly,

$$LLR = N_1(1+P_1)(1+P_2)(1-P_3) + N_1(1-P_1)(1-P_2)(1+P_3)$$

$$LRL = N_1(1+P_1)(1-P_2)(1+P_3) + N_1(1-P_1)(1+P_2((1-P_3)$$

$$LRR = N_1(1+P_1)(1-P_2)(1-P_3) + N_1(1-P_1)(1+P_2)(1+P_3)$$

The asymmetry observed when the second scatter is to the left is

$$\epsilon_L = (LLL-LLR)/(LLL+LLR)$$

$$= (P_2P_3+P_1P_3)/(1+P_1P_2)$$

$$\cong \epsilon_L^\circ + P_1P_3 \quad ,$$

where ϵ_L° is the asymmetry that would have been observed if there existed no

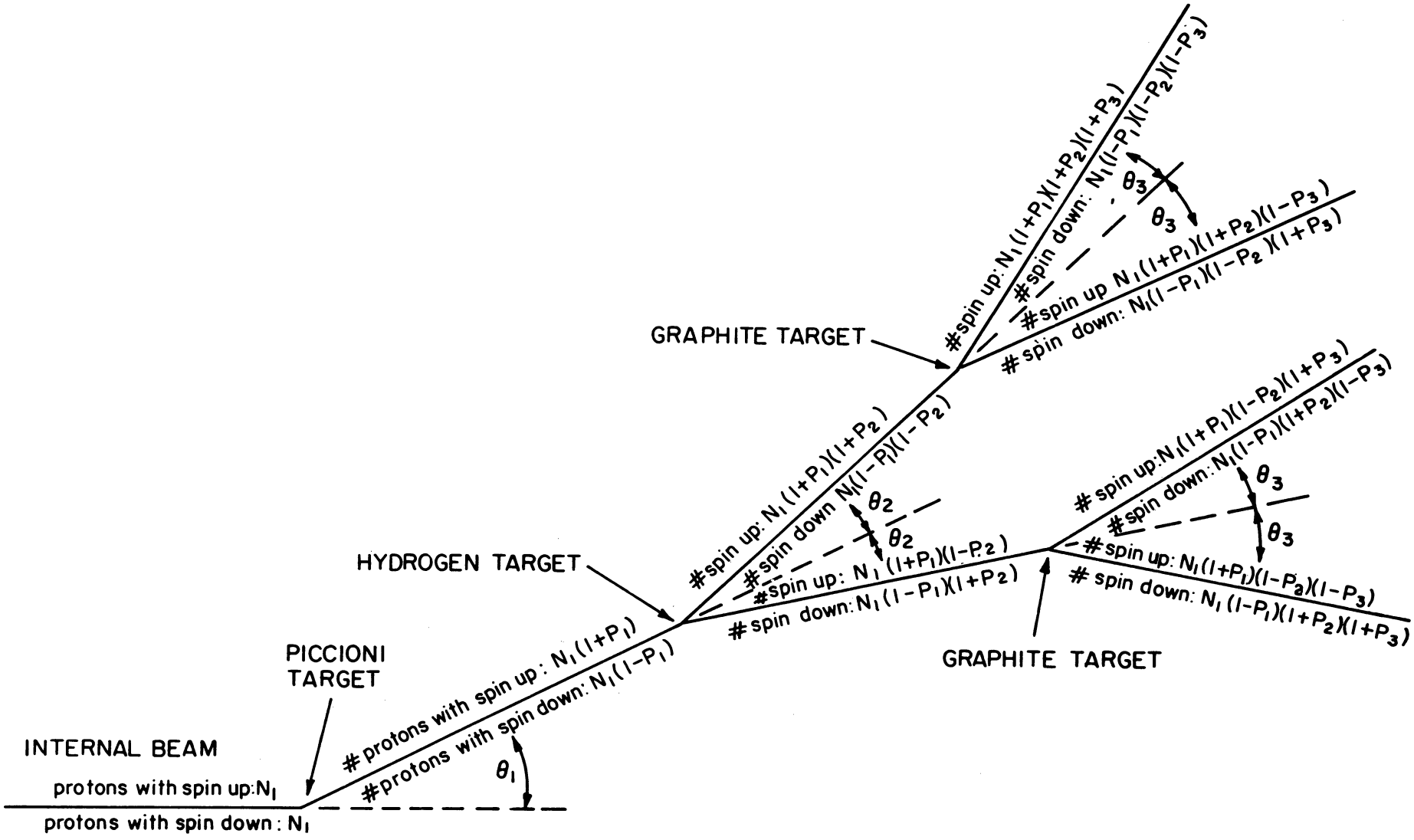

Fig. 18. Diagram illustrating dependence of final asymmetry on initial beam polarization.

initial polarization (P_1). The asymmetry observed when the second scatter is to the right is (taking into account the change in sign of the polarization of the second scattered protons)

$$\epsilon_R = -(LRL-LRR)/(LRL+LRR)$$

$$= (P_2P_3-P_1P_3)/(1-P_1P_2)$$

$$\cong \epsilon_R^\circ - P_1P_3$$

If we define

$$\bar{\epsilon} = 1/2\ (\epsilon_L+\epsilon_R)$$

then

$$\Delta\bar{\epsilon} = P_2P_3(1-P_1^2)/(1-P_1^2P_2^2) \cong -P_1^2\,\bar{\epsilon}\ ,$$

where $\Delta\bar{\epsilon}$ is the contribution to the averaged asymmetry, $\bar{\epsilon}$, due to the incident beam being polarized.

It is seen that an incident beam polarization can be detected by comparing ϵ_L and ϵ_R, which are the asymmetries measured with the analyzing system in the orientation shown in Fig. 3 and in the orientation with $\theta_1 \to -\theta_1$ and $\theta_2 \to -\theta_2$. Furthermore, all dependence of the average asymmetry $\bar{\epsilon}$ on P_1 vanishes to first order, and the necessary correction can be calculated to an even higher order. Experimentally, however, no systematic difference between ϵ_L and ϵ_R was found and no corrections for an incident polarization were necessary.

B. ERRORS

In this section the possible sources of error will be discussed and the magnitude of their effects examined. These errors include the uncertainty due to counting statistics, statistical error in the beam center of gravity,

accidentals, misalignment of counters in the analyzing telescopes, a difference in efficiencies between the telescopes, and scanning bias.

It is known from the theory of the binomial distribution that if the probability of one of two mutually exclusive results in P, then the probable error in L_p, the number of p- type successes after N trials, is $\sqrt{L_p(1-L_p/N)}$.[25] For the moment, assume that the beam has vanishing width so a common probability can be assigned to each particle. The error in the average asymmetry determined in this situation is then

$$\sqrt{(\Delta\bar{\epsilon})^2} = \sqrt{(1-\epsilon^2)/N}$$

since

$$\Delta(L/N) = \frac{1}{N}\sqrt{L(1-\frac{L}{N})}$$

and

$$\epsilon = \frac{2L}{N} - 1 \ ,$$

where L is the number of protons scattered to the left and N is the total number analyzed. The effect of a beam of finite width can now be investigated. Imagine the incident beam to be divided into n bins with $N_i (= L_i + R_i)$ being the total number of protons in the i^{th} bin. If we further require that $N_i = N/n$, the average asymmetry for the entire beam is

$$\bar{\epsilon} = (\sum_i L_i - \sum_i R_i)/N = 2\sum_i L_i/N - 1 = \frac{1}{N}\sum \epsilon_i N_i$$

If the $\Delta\epsilon_i$ are assumed uncorrelated, the probable deviation in $\bar{\epsilon}$ is given by

$$(\Delta\bar{\epsilon})^2 = \frac{1}{n^2}(\sum_i (\Delta\bar{\epsilon}_i)^2)$$

It was shown above that (for a beam of vanishing width)

$$(\Delta\bar{\epsilon}_i)^2 = (1-\epsilon_i^2)/N_i$$

Therefore,

$$(\Delta\bar{\epsilon})^2 = \frac{1}{N}\left(1 - \frac{1}{n}\sum_i \epsilon_i^2\right) .$$

The second term in this expression is always at least two orders of magnitude smaller than the first, and can be neglected. Therefore, in computing the statistical error in the asymmetry the expression $\Delta\bar{\epsilon} = \sqrt{1/N}$ was used.

The statistical errors in the beam centroid were calculated from the relations

$$\Delta y = \sqrt{\sum_i (y_i - \bar{y})^2}/\ N \ , \qquad \Delta\theta = \sqrt{\sum_i (\theta_i - \bar{\theta})^2}/\ N$$

where N is the number of events in the reconstructed distribution.

Three possible cases for accidental background contamination in the analyzer telescopes will be studied: 1. background proportional to the number of true events, with the proportionality factor being the same for both telescopes, 2.) background additive and the same for both telescopes, and 3.) background additive but different for each telescope. In the following let L and R represent the number of particles that scatter into the left and right telescopes, respectively, and B is a parameter characterizing the accidental contributions; the superscripts M and T represent "measured" and "true."

Case 1.
$$L^M = L^T(1+B)$$
$$R^M = R^T(1+B)$$
$$\Delta\epsilon^M = 0 \text{ (i.e., no error in this case)}$$

Case 2.
$$L^M = L^T + B$$
$$R^M = R^T + B$$
$$\Delta\epsilon^M = -(2B/N)\epsilon^T$$
Assume $B/N = .01$ and $\epsilon^T = .04$, then
$$\Delta\epsilon \cong .0001 \text{ and is negligible.}$$

Case 3. $L^M = L^T + B$

$R^M = R^T + B_r$

$\Delta\epsilon^M = (B-B_r)/N$

Assume $B-B_r = .01N$, then $\Delta\epsilon^M = .01$.

It is seen that accidentals of the type in Case 3 potentially pose the most serious problem. At each data point the quantities $(B-B_r)/(B+B_r)$ and $(B+B_r)/N$ were measured. For all cases it was true that $(B-B_r)/N < .002$. Therefore, even accidentals of type 3 produce no appreciable error in the measured asymmetry. Furthermore, comparison of asymmetry measurements made at high and low beam intensities experimentally established that the effect of accidentals was negligible at the beam intensity normally used.

Examination of the recoil beam distribution reconstructed from spark chamber photographs reveals in some cases a sizable number of accidental spark chamber events. The higher accidental rates in the chambers is to be expected because of the long resolving time of the chambers compared with scintillation counters. The most significant of these events, as far as their effect on the determination of the beam center of gravity is concerned, are those that appear at large distances from the axis of the analyzer. In order to eliminate events of this type, each accepted spark chamber event was required to originate from the hydrogen target and intersect the counter pair S_2-S_2'. The spark chamber accidentals that remain are thus contained in the region ± 1.5" at S_2S_2', and are not expected to produce a shift in the y center of gravity by more than $\pm .015$" (corresponding to an error in the corrected asymmetry of $\approx .003$, assuming no accidental effect on θ).

The effect of an asymmetry in the efficiency of the two analyzing telescopes, due to differences in scintillator, associated electronics, or

alignment, could be quite significant. It has been shown in Section IV-A, however, that their effect on the average of the asymmetries measured by S_2-S_2' with the carriage in each orientation is negligible. The argument and result is identical for the case of the analyzing telescopes. If the difference between the telescopes is characterized by a parameter q, and the counts in the left and right telescopes specified by L and R (with superscripts representing "measured" and "true," and subscripts specifying the carriage orientation), where

$$L_I^M = L_I^T(1-q), \quad L_{II}^M = L_{II}^T, \quad R_I^M = R_I^T, \quad \text{and} \quad R_{II}^M = R_{II}^T(1-q),$$

then $\Delta\epsilon/\epsilon \cong q$, where ϵ is the average azimuthal asymmetry. It is experimentally known that $|q| < .02$, and consequently the maximum contribution to the error in ϵ is always less than .003.

All spark chamber film was scanned utilizing a semiautomatic digitizing machine. The basic unit for this machine was .0023" (corresponding to approximately .003" in real space). Reproducibility and linearity checks were periodically made. Approximately 97% of all film was rescanned with the film reversed (i.e., left and right reversed) and the results averaged with the corresponding normally scanned results to minimize scanning bias. The unrescanned data was corrected by the average universal difference in the two scans. It is believed that no significant scanning bias remains in the averaged data.

The individual errors included in calculating the total error in the measured polarization are summarized below (where A = analyzing power, ∂_y

and ∂_θ are the derivatives of the asymmetry with respect to y and θ, at $y = 0$, $\theta = 0$, as determined in the calibration experiment):

$\frac{(\Delta\epsilon)_s}{A}$ ...statistical counting error (typically .020)

$\frac{\Delta\bar{y}\partial_y}{A}$ ...statistical error in average value of y (typically .015)

$\frac{\Delta\bar{\theta}\partial_\theta}{A}$ ...statistical error in average value of θ (typically .010)

$\frac{.015\ \partial_y}{A}$ ...error due to accidentals in spark chamber photographs (typically .01)

$\frac{.003}{A}$ ...error due to differences in analyzing telescopes (maximum of .003/A)

During the course of the experiment many measurements of the polarization parameter were repeated one or more times. In most cases, reproducibility was better than one standard deviation.

The above errors are combined in quadrature and presented in Table IV. There exists, in addition, a 5% uncertainty in the polarization due to normalization (see next section).

C. RESULTS

A summary of the final results is presented in Table IV, and the corresponding graphs, for each incident beam energy, appear in Figs. 19-24. Each entry in Table IV represents the combined data, in most cases, from two or more separate measurements.

The polarization parameter is well known at .75 GeV. Results from independent experiments by Betz,[26] Cheng,[27] and Ducros et al.[28] show good

TABLE IV

POLARIZATION PARAMETER IN ELASTIC PROTON-PROTON SCATTERING

Incident Proton Energy	θ_{cm} (deg.)	P	ΔP
.75 GeV	43.85	.541	.075
	47.19	.513	.044
	53.25	.530	.029
	63.98	.470	.067
	86.29	.097	.078
1.03 GeV	39.88	.419	.031
	42.47	.464	.040
	53.60	.481	.023
	57.81	.417	.038
	61.62	.325	.033
	65.32	.258	.073
	68.52	.245	.033
	71.37	.265	.037
	77.25	.095	.029
	88.25	-.021	.034
1.32 GeV	32.30	.361	.036
	34.77	.403	.030
	39.06	.343	.045
	46.63	.407	.025
	49.77	.339	.022
	53.13	.266	.020
	61.21	.190	.025
	68.26	.034	.030
	74.76	.062	.032
	81.81	.059	.034
	88.23	.034	.029
1.63 GeV	28.87	.228	.029
	32.80	.352	.032
	38.55	.335	.025
	44.07	.369	.020
	49.67	.177	.040
	56.03	.151	.053
	61.91	.141	.035
	67.04	.025	.028
	73.93	.025	.030
	80.57	.000	.031

TABLE IV (Concluded)

Incident Proton Energy	θ_{cm} (deg.)	P	ΔP
2.24 GeV	25.32	.227	.031
	27.09	.315	.026
	30.42	.252	.026
	36.08	.292	.030
	38.74	.229	.052
	40.41	.205	.025
	43.45	.178	.027
	47.14	.182	.033
	50.65	.163	.037
	52.25	.134	.036
	54.01	.147	.032
	57.04	.048	.075
	62.22	.020	.041
	69.30	.093	.050
	85.24	.006	.061
2.84 GeV	22.18	.193	.026
	23.78	.188	.054
	31.65	.237	.039
	35.91	.199	.057
	41.37	.175	.037
	47.15	.142	.071
	60.04	.115	.055
	72.72	.043	.059

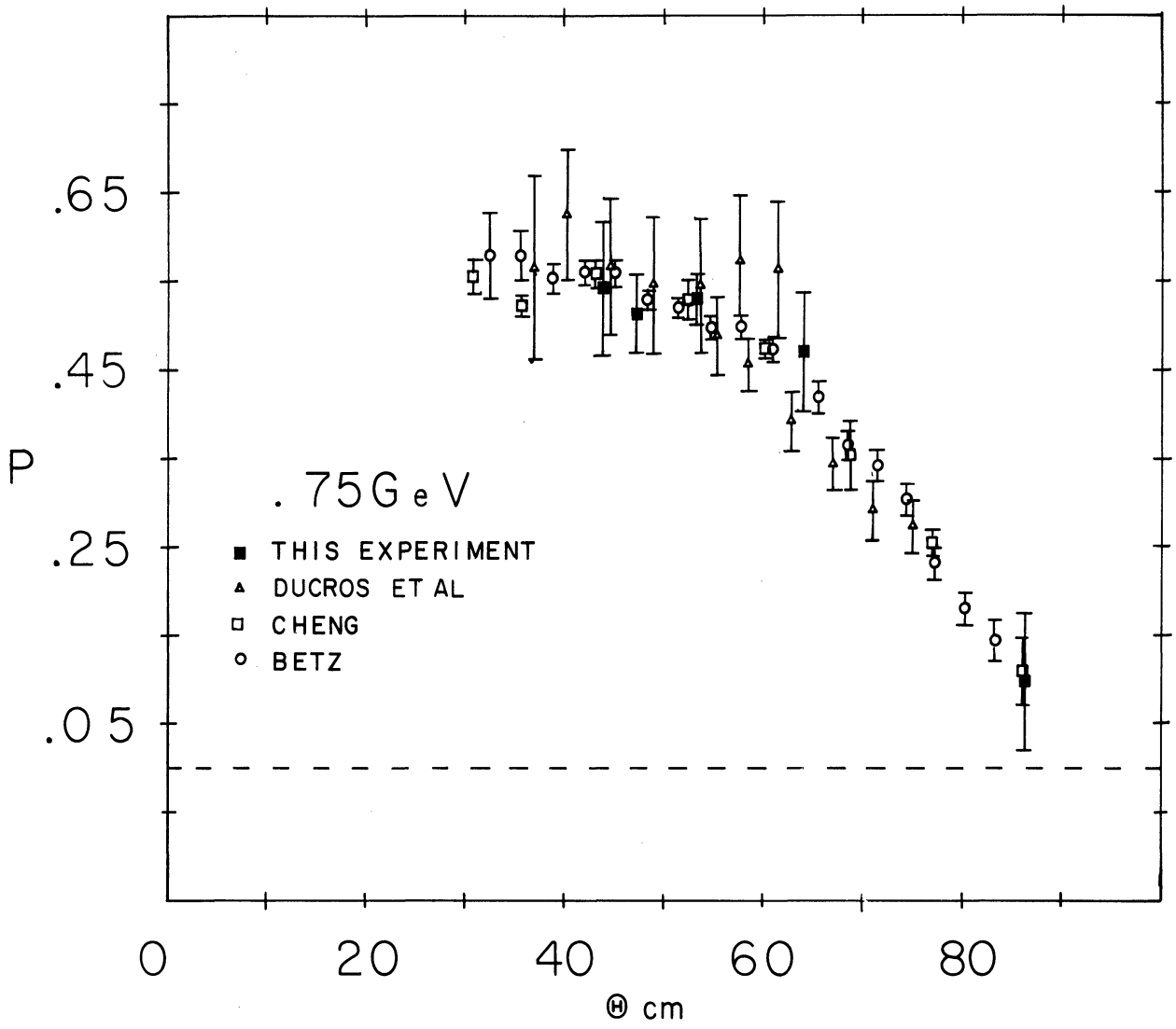

Fig. 19. Polarization parameter in elastic proton-proton scattering as a function of center-of-mass scattering angle at .75 GeV.

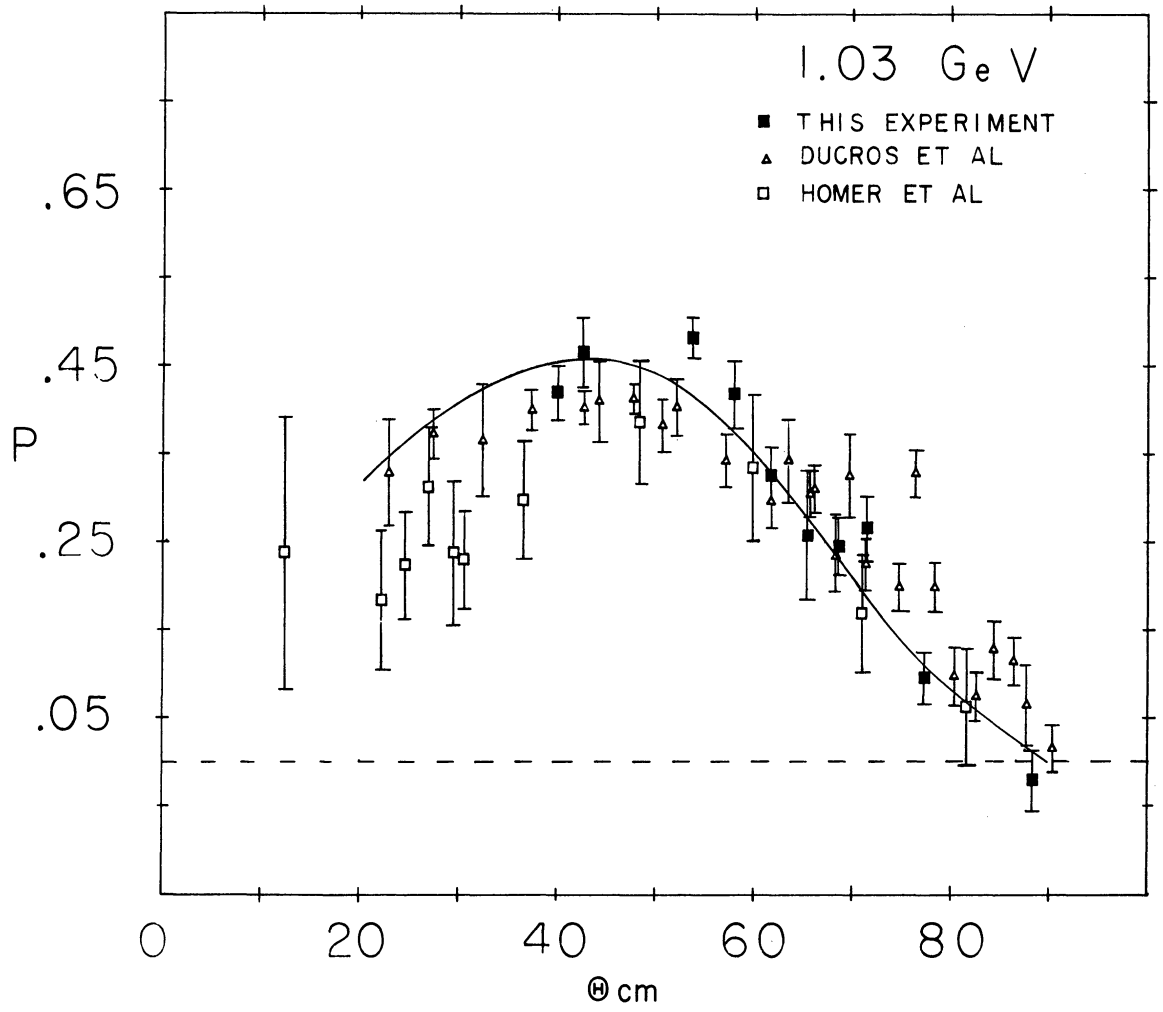

Fig. 20. Polarization parameter in elastic proton-proton scattering as a function of center-of-mass scattering angle at 1.03 GeV.

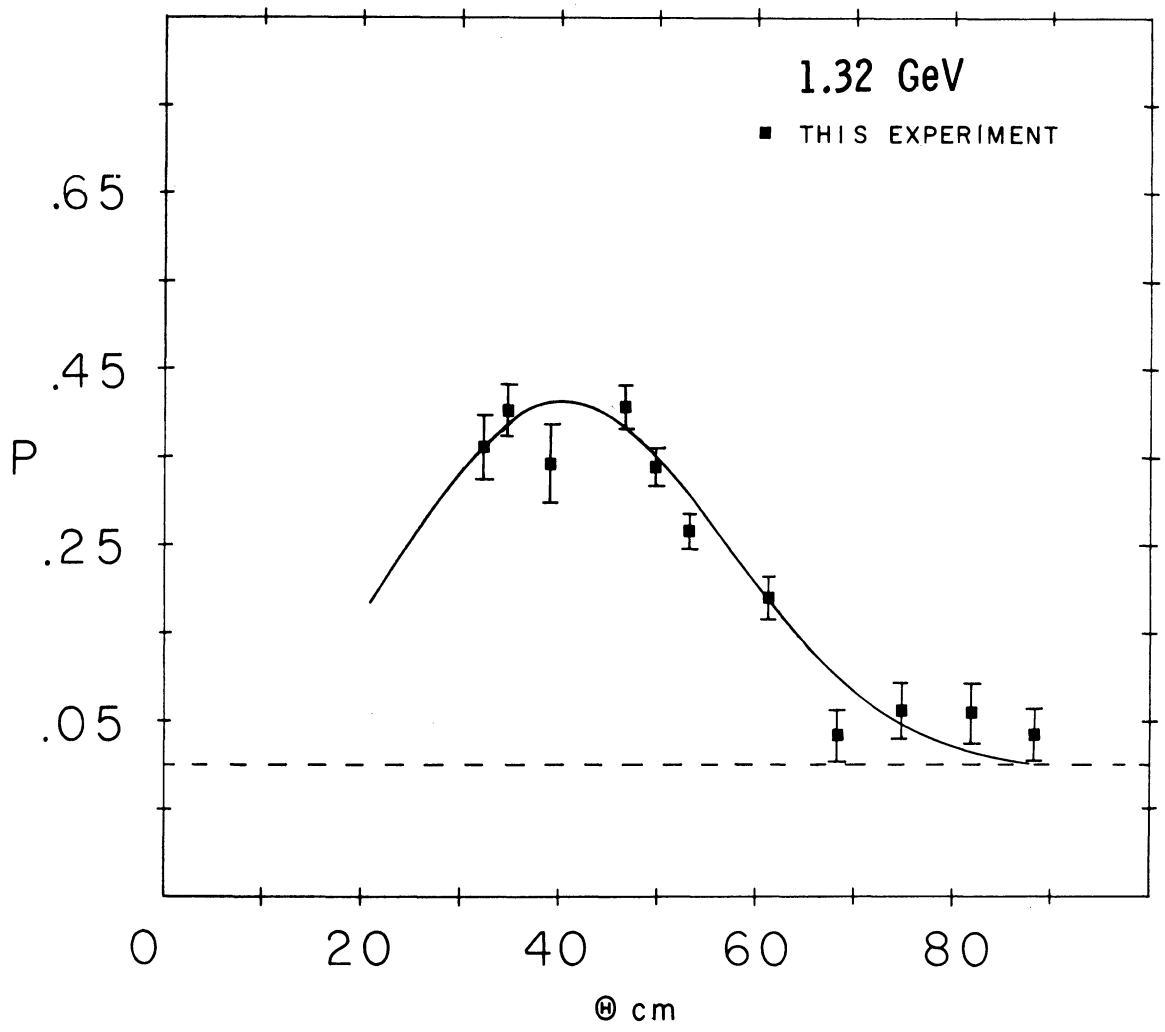

Fig. 21. Polarization parameter in elastic proton-proton scattering as a function of center-of-mass scattering angle at 1.32 GeV.

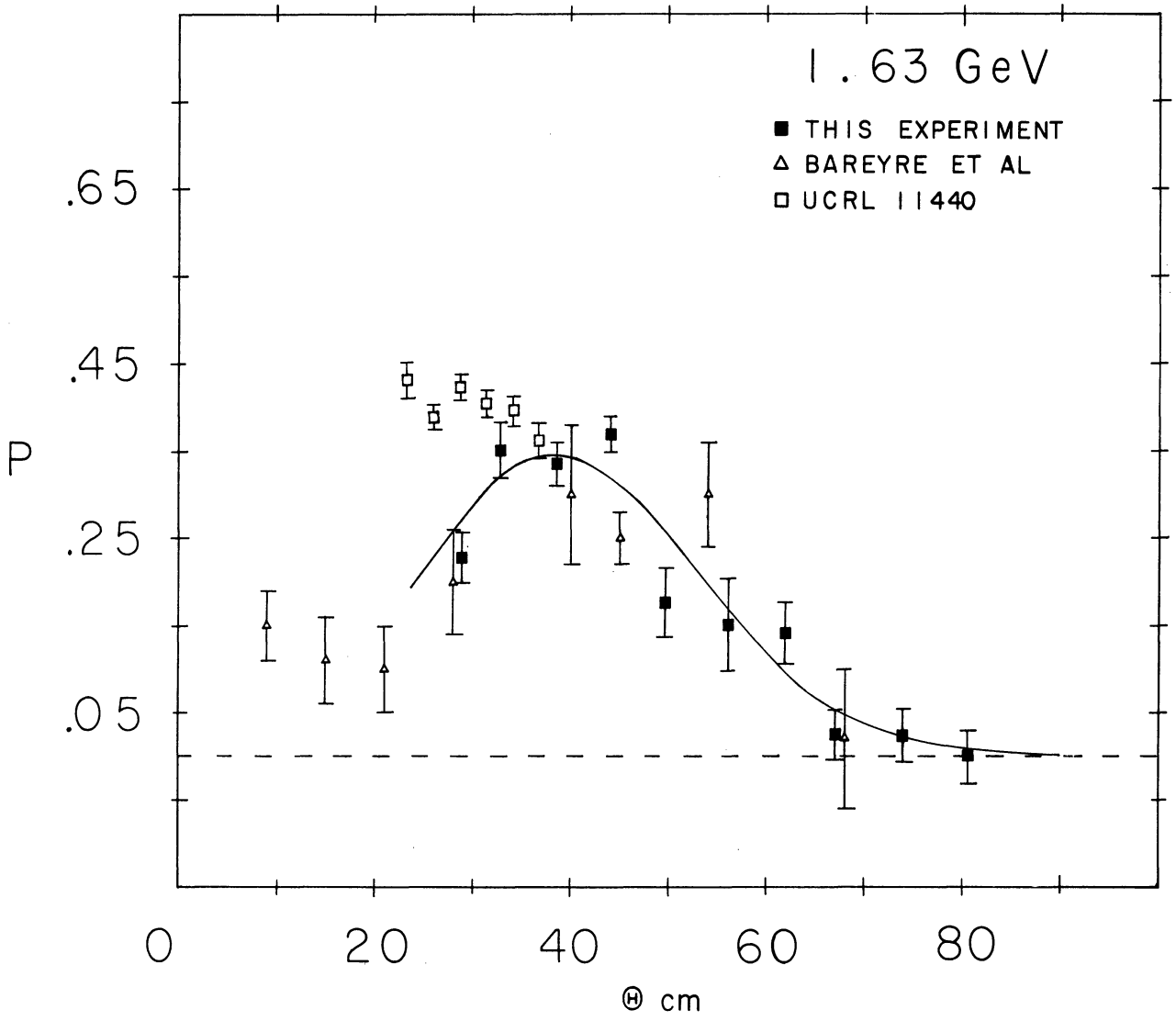

Fig. 22. Polarization parameter in elastic proton-proton scattering as a function of center-of-mass scattering angle at 1.63 GeV.

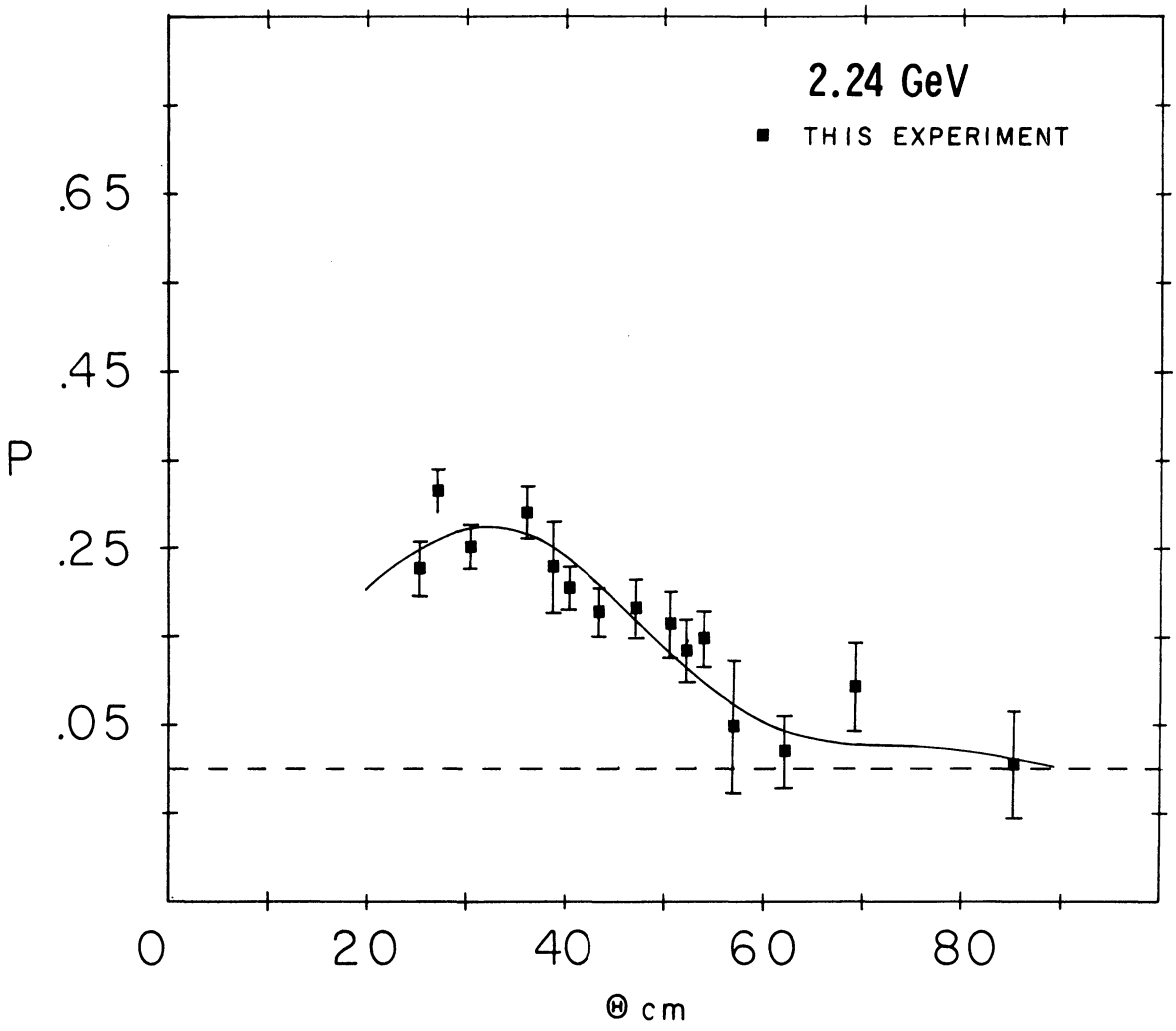

Fig. 23. Polarization parameter in elastic proton-proton scattering as a function of center-of-mass scattering angle at 2.24 GeV.

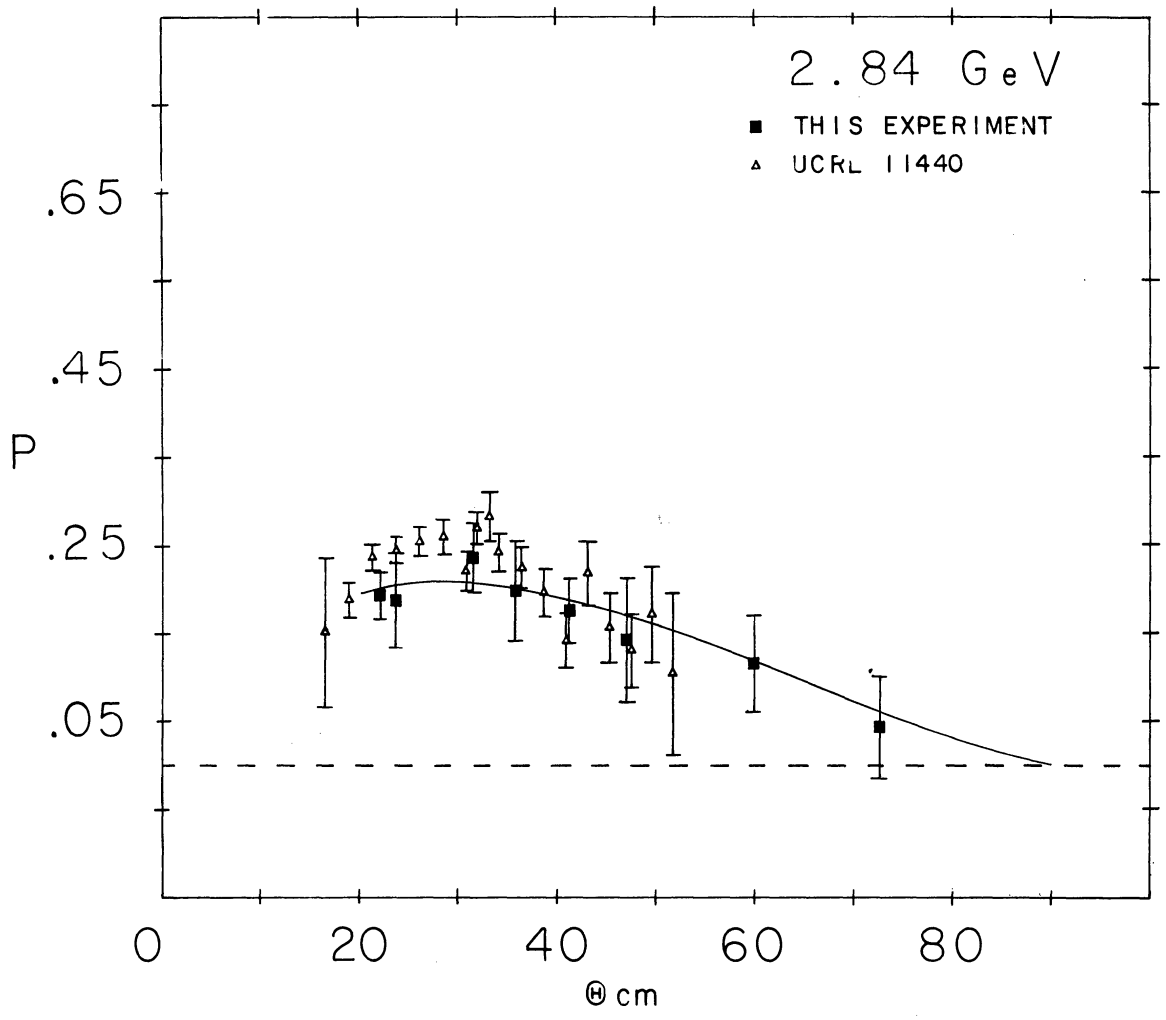

Fig. 24. Polarization parameter in elastic proton-proton scattering as a function of center-of-mass scattering angle at 2.84 GeV.

agreement. Since the polarization parameter at .75 GeV is better known than the polarization of the beam used in the calibration experiment, data from this experiment have been normalized to give good agreement with the existing mean curve at .75 GeV. The corresponding calibration beam polarization is thus predicted to have been 40% ± 5% (see Ref. 29).

Data from this experiment have been fitted with a two dimensional least squares function of the following form:

$$P(E,\theta^*) = \sum_{\ell=1,k=1}^{\ell=5,k=4} \alpha_{\ell k} E^{\ell-1} \sin\theta^* \mathcal{P}_{2k-1}(\cos\theta^*) \quad ,$$

where $P(E,\theta^*)$ is the polarization parameter for incident beam energy E and center-of-mass scattering angle θ^*, and $\mathcal{P}(\cos\theta^*)$ are Legendre polynomials. The values of the coefficients $\alpha_{\ell k}$, and their associated errors, are given in Table V. In Figs. 20-24 the smooth curve shown is the plot of the function $P(E,\theta^*)$ at the appropriate value of E.

At 1.03 GeV (Fig. 20) results from this experiment are consistent with the results of the Birmingham group[30] and the preliminary results of the Saclay group.[28] Data at 1.32 GeV are exhibited in Fig. 21. The maximum in the fitting function occurs at approximately 40° in the center-of-mass system and has the value of approximately .41. Because of the significant discrepancy in the results of the Chamberlain group[6] and Bareyre et al.[5] at 1.7 GeV, measurements have been made near this energy (Fig. 22). Our results show better agreement with the latter. New polarization data at 2.24 GeV are shown in

TABLE V

EXPANSION COEFFICIENTS FOR POLARIZATION AS A FUNCTION OF θ^* AND T

$\alpha_{\ell k}$

ℓ ↓ \ k →	1	2	3	4
1	4.0790± .6429	1.5032± .9790	5.9178±1.3195	2.3870± .9549
2	-5.4880±1.1308	-1.6258±1.200	-11.2572±2.1926	-4.2545±1.4606
3	2.9906± .6046	- .2148± .8827	6.8023± .8081	2.5720± .1890
4	- .6894± .0366	.6532± .4588	-1.5837± .4164	- .6798± .3479
5	.0555± .0191	- .1521± .0592	.1158± .0747	.0700± .0491

Fig. 23. The trend of smaller polarizations for higher energies continues to be true here. In Fig. 24 results at 2.84 GeV are shown. Agreement with the Chamberlain group[6] at this energy is quite good. A plot of the maximum polarization versus energy is given in Fig. 25.

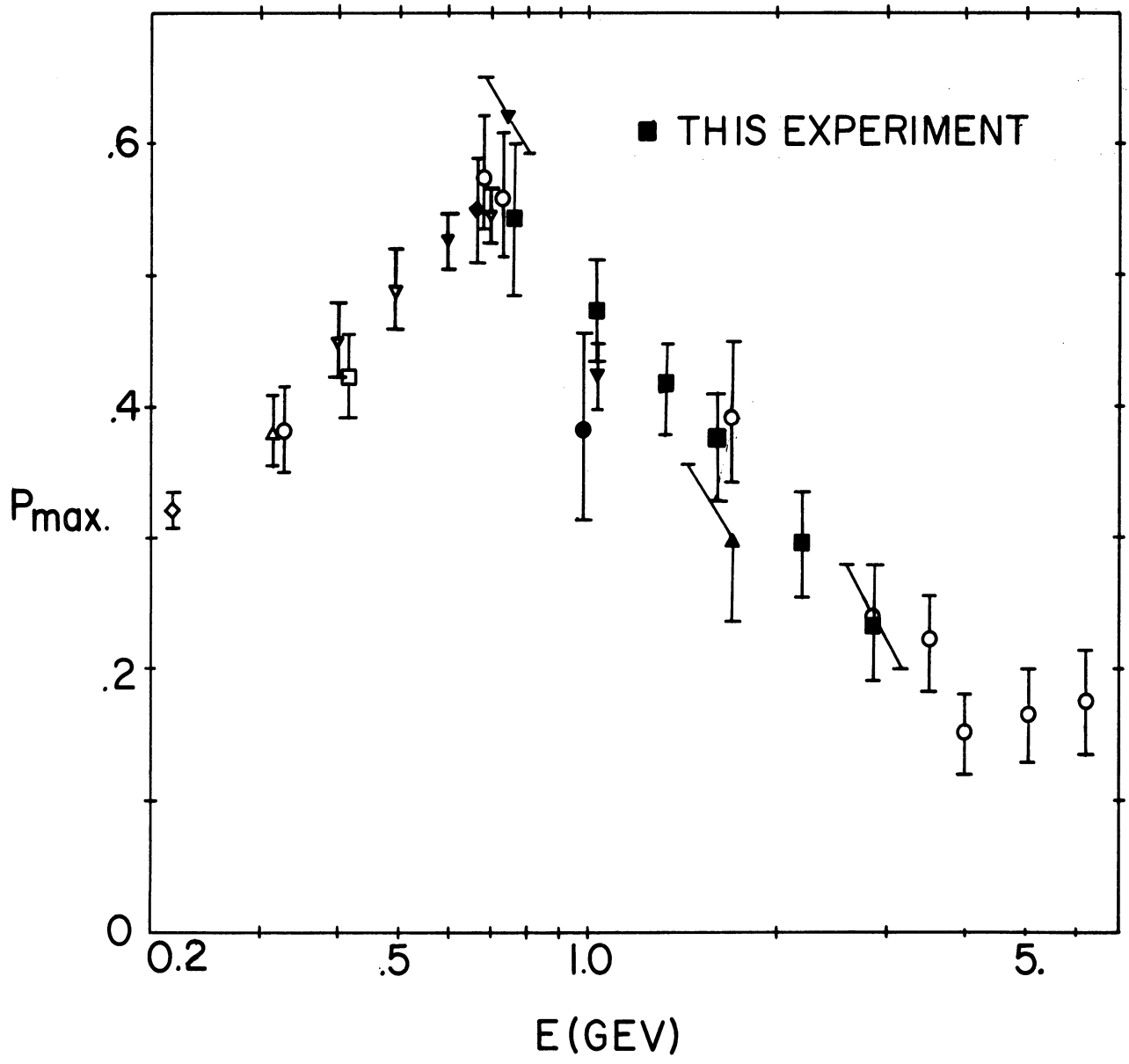

Fig. 25. Maximum polarization versus incident kinetic energy.

○ Ref. 6 ◇ Ref. 31

● Ref. 30 △ Ref. 32

▲ Ref. 5 □ Ref. 29

▼ Ref. 28 ▽ Ref. 27

◆ Ref. 33

V. DISCUSSION

The polarization parameter in elastic proton-proton scattering is seen to vary smoothly with incident beam energy and center-of-mass scattering angle. It is notable that the polarization becomes very small in the angular region 60°-70° at 1.32, 1.63, and 2.24 GeV. At present this behavior is not theoretically understood.

The peak in the maximum polarization occurs at the incident beam energy of $\approx$ 700 MeV and is quite prominent. It is interesting to note that at approximately this energy the total proton-proton cross section is approaching a relative maximum, presumably due to single pion production (Fig. 26).

Results from this experiment have been analyzed in terms of two specific predictions developed in the framework of the Regge theory, as described in Section II-C. The predictions are that, for fixed small four-momentum transfer t, the polarization should vary as

$$\text{a.} \quad P(s) = as^b$$

$$\text{b.} \quad P(s) = c(\sigma(p\bar{p})-\sigma(pp))/\sigma(pp)$$

where s is the invariant mass squared, and a, b, and c are constants, and $\sigma(pp)$ and $\sigma(p\bar{p})$ are total cross sections for proton-proton and proton-antiproton scattering. Since, as stated in Section II-C, the t dependence of the polarization is expected to be approximately $\approx \sqrt{-t}$, these predictions appear valid only for $|t| \lesssim .3(\text{GeV/c})^2$ (i.e., only for those values of t at which the polarization is increasing as a function of center-of-mass scattering angle). Now, the value of t at which the maximum value of the polariza-

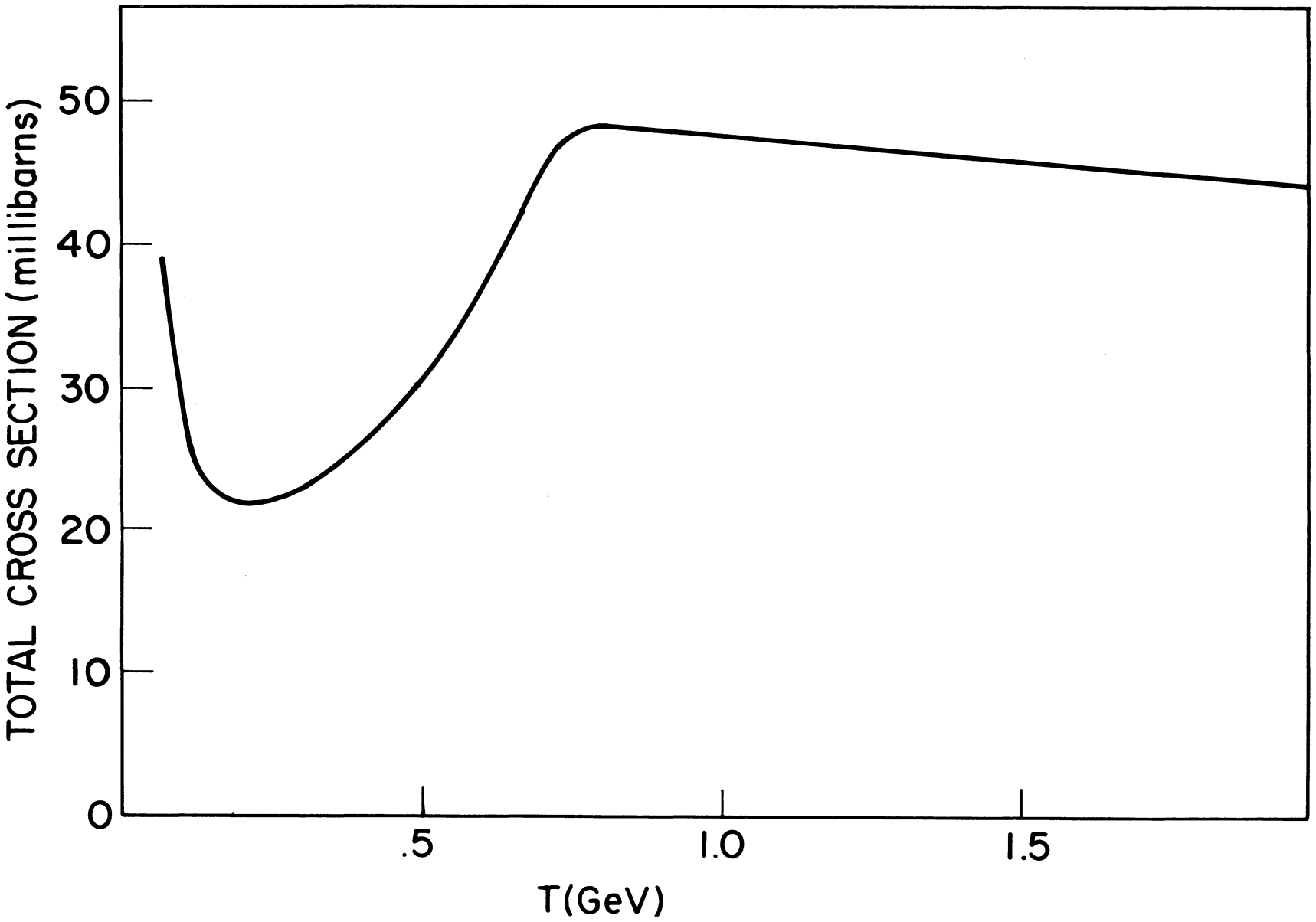

Fig. 26. Total cross section in proton-proton scattering.

tion occurs at a given energy is essentially independent of the energy and is equal approximately to $-.3(\mathrm{GeV}/c)^2$. Data on the maximum polarization from this experiment were fitted with the two above forms. The values of the parameters used in the fits shown in Fig. 27 are a = 5.915, b = -1.475, and c = .425. Data on the cross sections in b were taken from Refs. 34 and 35. It is seen that both predictions a and b agree remarkably well with the polarization data from .75 to 6 GeV. Fits to the data at other values of t notably different from $|t| = .3(\mathrm{GeV}/c)^2$ are not given since for $|t| \gg .3(\mathrm{GeV}/c)^2$ the assumptions required in making the predictions do not appear to be justified, and almost no data presently exist for $|t| \ll .3(\mathrm{GeV}/c)^2$.

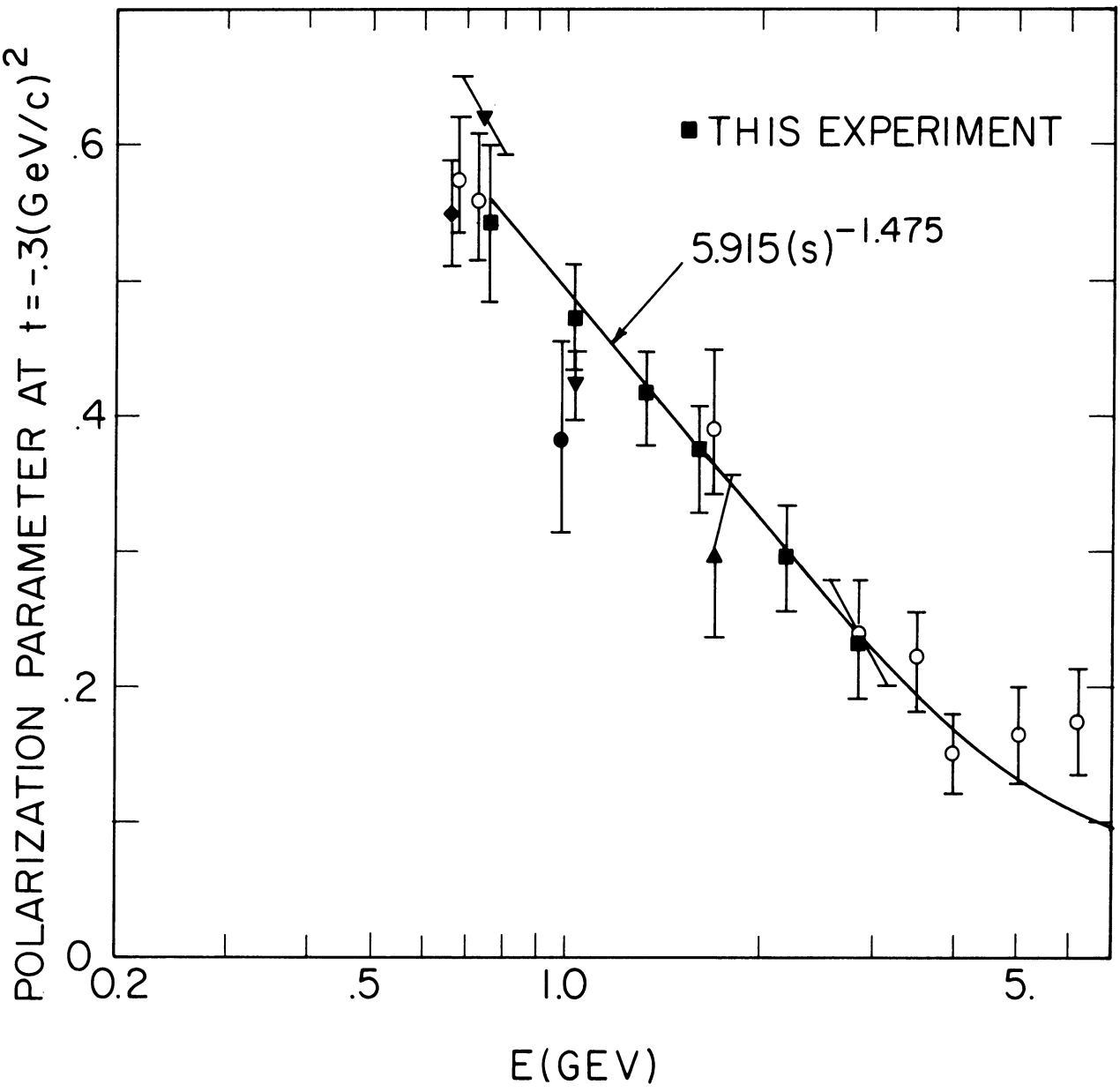

Fig. 27a. Regge theory prediction (a) for the polarization in elastic proton-proton scattering at $t = -.3(\mathrm{GeV}/c)^2$.

○ Ref. 6 ▼ Ref. 28

● Ref. 30 ◆ Ref. 33

▲ Ref. 5

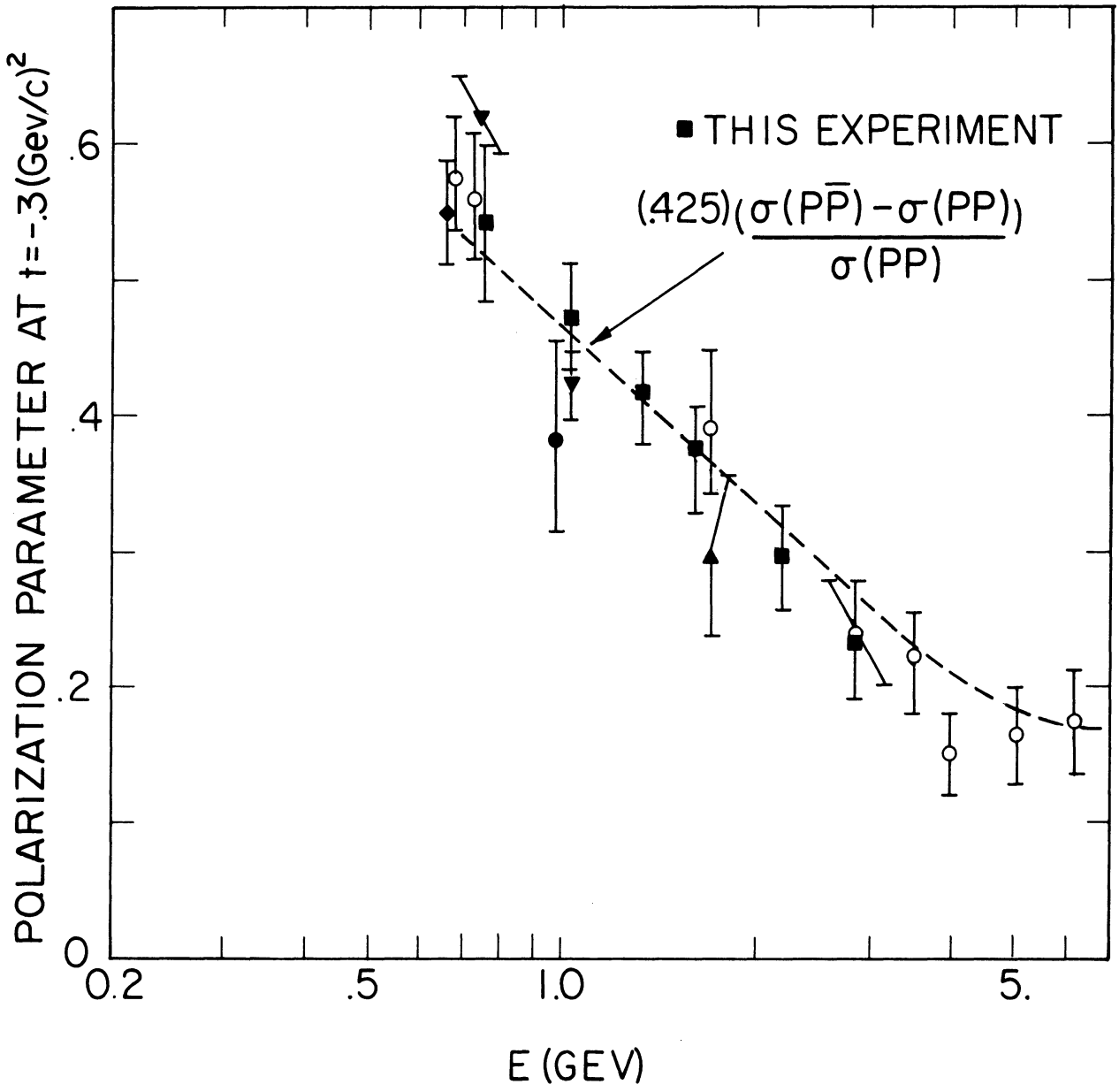

Fig. 27b. Regge theory prediction (b) for the polarization in elastic proton-proton scattering at $t = -.3(\mathrm{GeV/c})^2$.

○ Ref. 6 ▼ Ref. 28

● Ref. 30 ◆ Ref. 33

▲ Ref. 5

APPENDIX I

In this section the details of the preliminary calibration experiment will be presented. It was shown in Section II-A that in a scattering process the azimuthal scattering asymmetry, ϵ, is related to the polarization, P, of the incoming beam, and the analyzing power, A, of the interaction by the expression $\epsilon = PA$. For a given analyzer, the quantity A can depend only on the incoming beam energy. In a calibration experiment the quantity ϵ is measured, and, since the beam polarization is known, the analyzing power is determined. The above statements assume, of course, that the incident beam is coincident with the axis of symmetry of the analyzer; experimentally, this is not the case. In order to refer the measured asymmetries to the axis of the analyzer, the relative orientation of the analyzer axis and the average beam trajectory at each energy was determined from spark chamber photographs, and the dependence of the asymmetry on this relative orientation was studied. The range of energies over which the calibration measurements were made correspond to the basic spectrum of recoil protons to be analyzed in the primary experiment.

The calibration measurements were made utilizing a proton beam at the Carnegie Institute of Technology synchrocyclotron. A 40% ± 5% polarized beam was produced by an internal scattering from a carbon target. The polarization of this beam was determined by normalizing our data from the primary experiment to give good agreement with the existing mean curve at .75 GeV,

where the polarization parameter is well known. The extracted polarized beam of $\approx 10^5$ protons/cm^2 sec entered the experimental area through a 1" x 1-7/8" collimator in the shield wall of the synchrocyclotron. The beam then was bent through an angle of 20° by a magnet, collimated, and subsequently analyzed. The beam layout is shown in Fig. 28.

A differential range method, as illustrated in Fig. 29, was employed to determine the beam energy. The quantity $C = C_1C_2C_3C_4\bar{C}_5/C_1C_2$ was measured as a function of the thickness of copper between counters C_3 and C_4. For small amounts of copper, essentially all beam protons have sufficient energy to traverse the entire array of counters and thus C is small. As additional copper is added, C becomes larger since now more protons are stopping before C_5. The maximum value of C should occur when the average beam proton stops in C_4. If more copper is added, most protons fail to reach C_4, and thus C is again small. Therefore, the value of the copper thickness at which the maximum C value occurs determines the initial range of the beam and thus the initial kinetic energy.[36] In calculating the energy, account was taken of all material in the beam upstream of the stopping point, which includes air, scintillator, and a fixed amount of graphite and lead which was added to reduce the beam energy to a level that required a reasonable number of copper sheets for the differential range curve. The incident energy was determined to be 415 ± 15 MeV. This value agreed with the energy of 415 ± 10 MeV determined by Kane et al.[29] using a similar method in this beam.

The analyzer was calibrated for proton energies of 103, 125, 150, 165, 185, 200, 240, 260, 300, 350, 400, and 415 MeV. Variation of the energy was

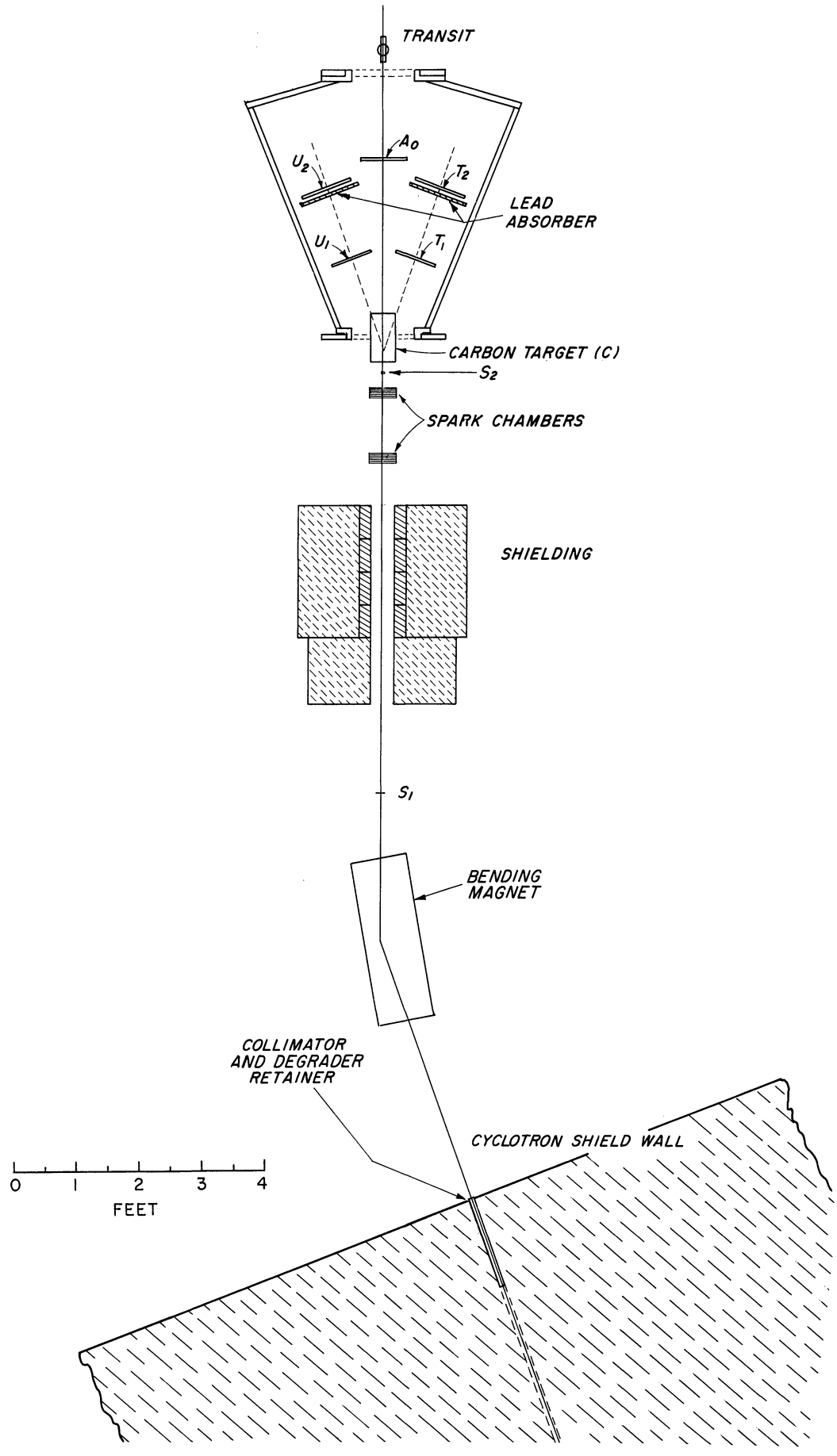

Fig. 28. Layout for calibration experiment.

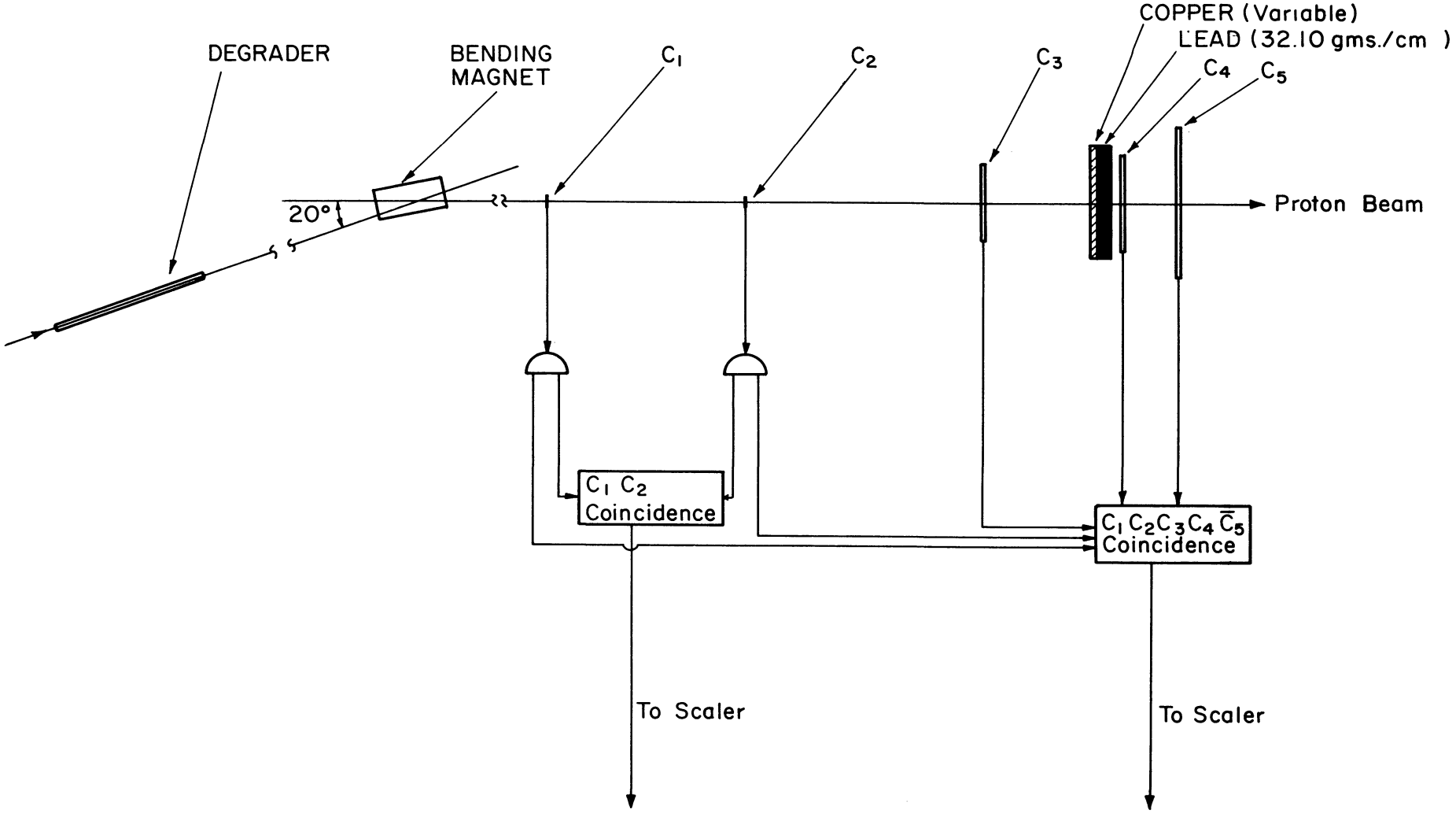

Fig. 29a. Logic used for differential range curve.

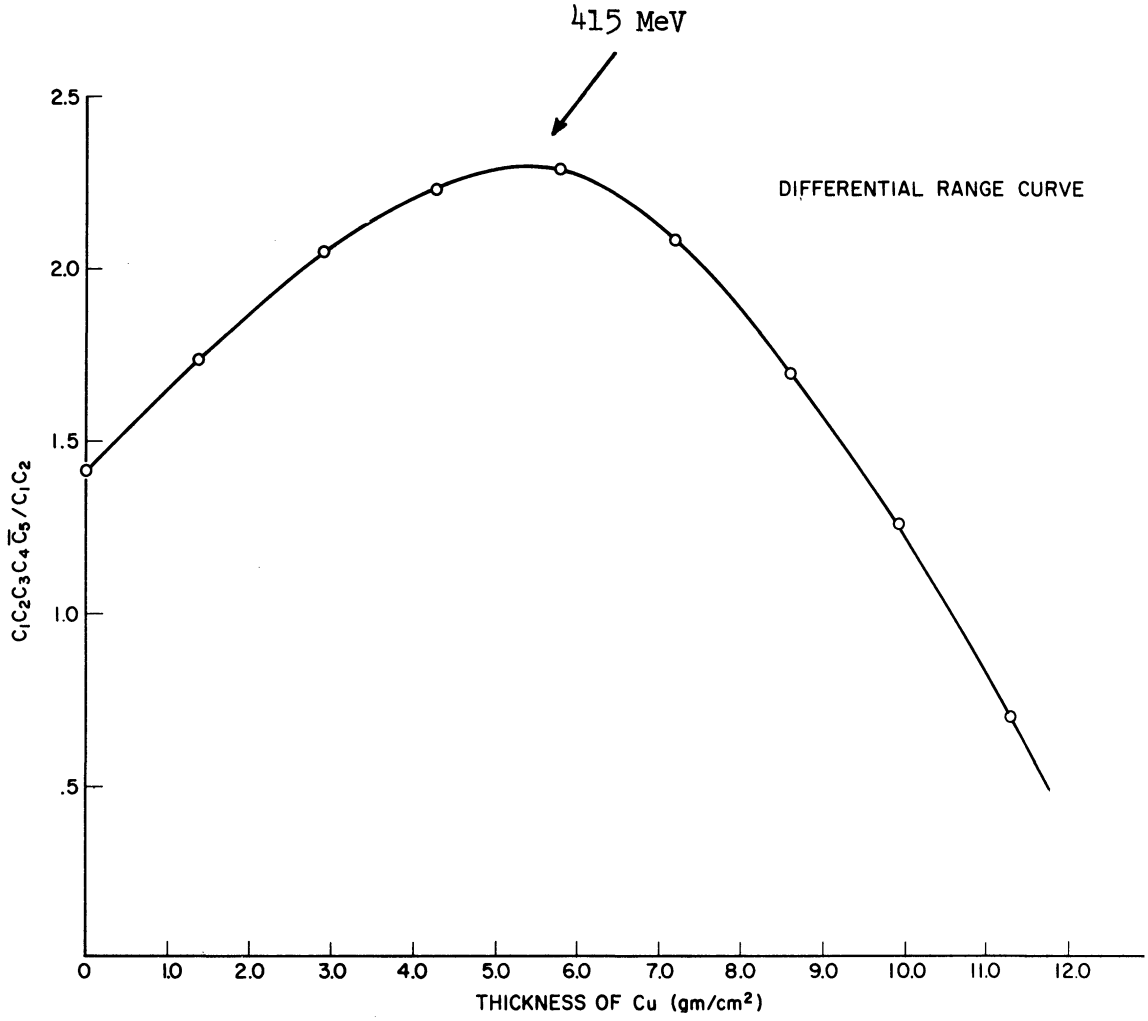

Fig. 29b. Differential range curve used in determining energy of beam in calibration experiment. The horizontal scale represents only the copper in the beam; there was, in addition, a constant amount of graphite, lead and scintillator.

accomplished by inserting appropriate amounts of graphite in the exit collimator of the synchrocyclotron. The effect of the energy degradation on the incident polarization is assumed negligible.[37]

The experimental layout is shown in Fig. 28 and the counter dimensions in Table VI. A typical event is $S_1S_2\ T_1T_2\ \bar{A}$. The analyzer has been previously described in Section III-D. With the exception of the "beam proton" selection counters, the electronic logic used in the calibration experiment is the same as used in the primary experiment and described in Section III-D.

In order to measure the dependence of the asymmetry on the relative orientation of the axis of the analyzer and the average incident beam trajectory, the analyzer was mounted on a platform that could be translated ± 1" and independently rotated ± 1° in the horizontal plane. For each energy and corresponding analyzer configuration (see Section III-D), the asymmetry was measured at each of the thirteen nominal (y,θ) points in Table VII, where y and θ are as defined in Fig. 10. Each of these (y,θ) points was corrected by $\bar{y}$, $\bar{\theta}$, the centroid of the beam relative to the analyzer as determined from the analysis of the spark chamber photographs (referral of the beam to the axis of the analyzer was made possible by the utilization of the rotating fiducial strips, as described in Section III-D). The calibration experiment therefore furnishes the function $E(y,\theta,p)$, that is, the asymmetry as a function of y, θ, and the momentum p. The analyzing power at the momentum p and analyzing configuration j is $E_j(0,0,p)/P_{in}$, where P_{in} is the calibration beam polarization. The derivation given in Appendix II shows that this information is sufficient to determine the polarization in an analysis

TABLE VI·

COUNTER DIMENSIONS FOR CALIBRATION EXPERIMENT

Counter	Width x Height x Thickness
S_1	1" x 3-1/2" x 1/8"
S_2	1/2" x 7" x 1/4"
A_o	9" x 21" x 1/2" (1-1/8" dia. hole through center)
T_1	8" x 18" x 1/2"
T_2	10-1/4" x 22" x 1/2"
U_1	8" x 18" x 1/2"
U_2	10-1/4" x 22" x 1/2"

TABLE VII

Y, θ VALUES AT WHICH THE ASYMMETRY MEASUREMENTS WERE MADE

Y"	.000	.003	.006	-.003	-.006	.500	-.500	1.000	1.006	.994	-1.006	-1.000	-.994
θ°	.000	.463	.926	-.463	-.926	.000	.000	.000	.926	-.926	- .926	.000	.926

experiment if ϵ_m, the measured asymmetry, $\bar{y}$, $\bar{\theta}$, and p for that experiment are known, provided, of course, that $\bar{y}$, $\bar{\theta}$, and p lie within the calibration range.

Least squares fits to the data were made using the functional form

$$\begin{aligned} E_j(y,\theta,p) &= A_0^j(p) + A_1^j(p)y + A_2^j(p)\theta + A_3^j(p)y\theta + A_4^j(p)y\theta^2 \\ &+ A_5^j(p)y^2\theta + A_6^j(p)y^2 + A_7^j(p)\theta^2 + A_8^j(p)y^2\theta^2 \\ &+ A_9^j(p)y^3 + A_{10}^j(p)\theta^3 \quad , \end{aligned}$$

where

$$A_\ell^j(p) = D_{\ell 1}^j + D_{\ell 2}^j p + D_{\ell 3}^j p^2 \quad .$$

No physical reason is given for expecting this form to be appropriate: its utility is that accurate interpolation between data points is obtained. The values of the D coefficients, for y in inches, θ in degrees, p in GeV/c, are given in Table VIII, and the analyzing powers determined from these fits in Table III.

There exists an uncertainty in the analyzing power due to counting statistics (see Section IV-B) and the statistical error in determining the mean beam trajectory. In all cases the contribution of this uncertainty to the determination of the polarization parameter is negligible.

Histograms of the beam distribution in the horizontal and vertical spatial coordinates, and the horizontal and vertical angular coordinates, respectively, are shown in Figs. 30-33 for the incident beam energy of 300 MeV.

Graphs of the asymmetry versus y for various values of θ are presented in Figs. 34-38 for a central energy at each of the five analyzer configurations.

TABLE VIII

EXPANSION COEFFICIENTS FOR THE ASYMMETRY

Configuration I (350-415 MeV):

ℓ ↓	$D^{I}_{\ell 1}$	$D^{I}_{\ell 2}$	$D^{I}_{\ell 3}$
0	10.2842	-21.1817	11.0158
1	- 2.7532	7.5758	- 4.6712
2	5.4611	-10.9575	5.6125
3	- .6805	1.2335	- .5550
4	.0880	- .2688	.1778
5	.8846	- 1.9223	1.0378
6	- .0455	- .2524	.2909
7	2.7214	- 5.8532	3.1433
8	- 4.4262	9.5001	- 5.0905
9	9.0864	-19.0560	10.0203
10	- 4.2901	9.2357	- 4.9721

Configuration II (260-350 MeV):

ℓ ↓	$D^{II}_{\ell 1}$	$D^{II}_{\ell 2}$	$D^{II}_{\ell 3}$
0	- .8885	3.1496	- 2.3053
1	.7482	- .7772	.0925
2	- .1898	1.0309	- .8184
3	- 1.2725	3.0438	- 1.8280
4	.8936	- 2.1747	1.3247
5	.6557	- 1.6772	1.0637
6	- 1.4150	3.2839	- 1.9205
7	- .6969	1.5899	- .9069
8	- .5984	1.5363	- .9775
9	2.0968	- 4.9734	2.9741
10	1.9549	- 4.7240	2.8361

Configuration III (120-240 MeV):

ℓ ↓	$D^{III}_{\ell 1}$	$D^{III}_{\ell 2}$	$D^{III}_{\ell 3}$
0	1.1525	- 2.9180	2.0518
1	.5764	- .5245	- .1363
2	.3362	- .1579	- .2877
3	.5184	- 1.6544	1.2892
4	- .4352	1.3427	- 1.0262
5	- .4490	1.2585	- .8703

TABLE VIII (Concluded)

Configuration III (120-240 MeV) (Continued):

ℓ ↓	$D^{III}_{\ell 1}$	$D^{III}_{\ell 2}$	$D^{III}_{\ell 3}$
6	- 1.1523	3.3750	- 2.4844
7	- .1221	.1845	- .0153
8	1.0603	- 3.0194	2.1398
9	.6123	- 1.8436	1.4189
10	.0471	- .1443	.1139

Configuration IV (120-185 MeV):

ℓ ↓	$D^{IV}_{\ell 1}$	$D^{IV}_{\ell 2}$	$D^{IV}_{\ell 3}$
0	- 1.5236	5.6529	- 4.8062
1	- 1.5827	6.6157	- 6.1350
2	1.3499	- 4.2218	3.6243
3	- .4092	1.4014	- 1.2158
4	- .0261	.1113	- .1278
5	- .1472	.4163	- .2720
6	- .6052	2.0908	- 1.8112
7	.9259	- 3.5484	3.3853
8	.4673	- 1.5257	1.1814
9	.8791	- 2.8031	2.2387
10	- 1.7074	6.4331	- 6.0385

Configuration V (103-150 MeV):

ℓ ↓	$D^{V}_{\ell 1}$	$D^{V}_{\ell 2}$	$D^{V}_{\ell 3}$
0	.7895	- 3.1312	3.5005
1	- 7.0633	28.3104	-27.6236
2	- 2.1389	9.2196	- 9.2979
3	- .1387	.6968	- .8685
4	- 2.0387	8.0550	- 7.8621
5	.2150	- .9197	1.0014
6	- .9681	3.9775	- 4.0156
7	1.0257	- 4.2290	4.3013
8	- .6278	2.5547	- 2.6069
9	6.2300	-24.8554	24.6071
10	2.4375	- 9.4953	9.1977

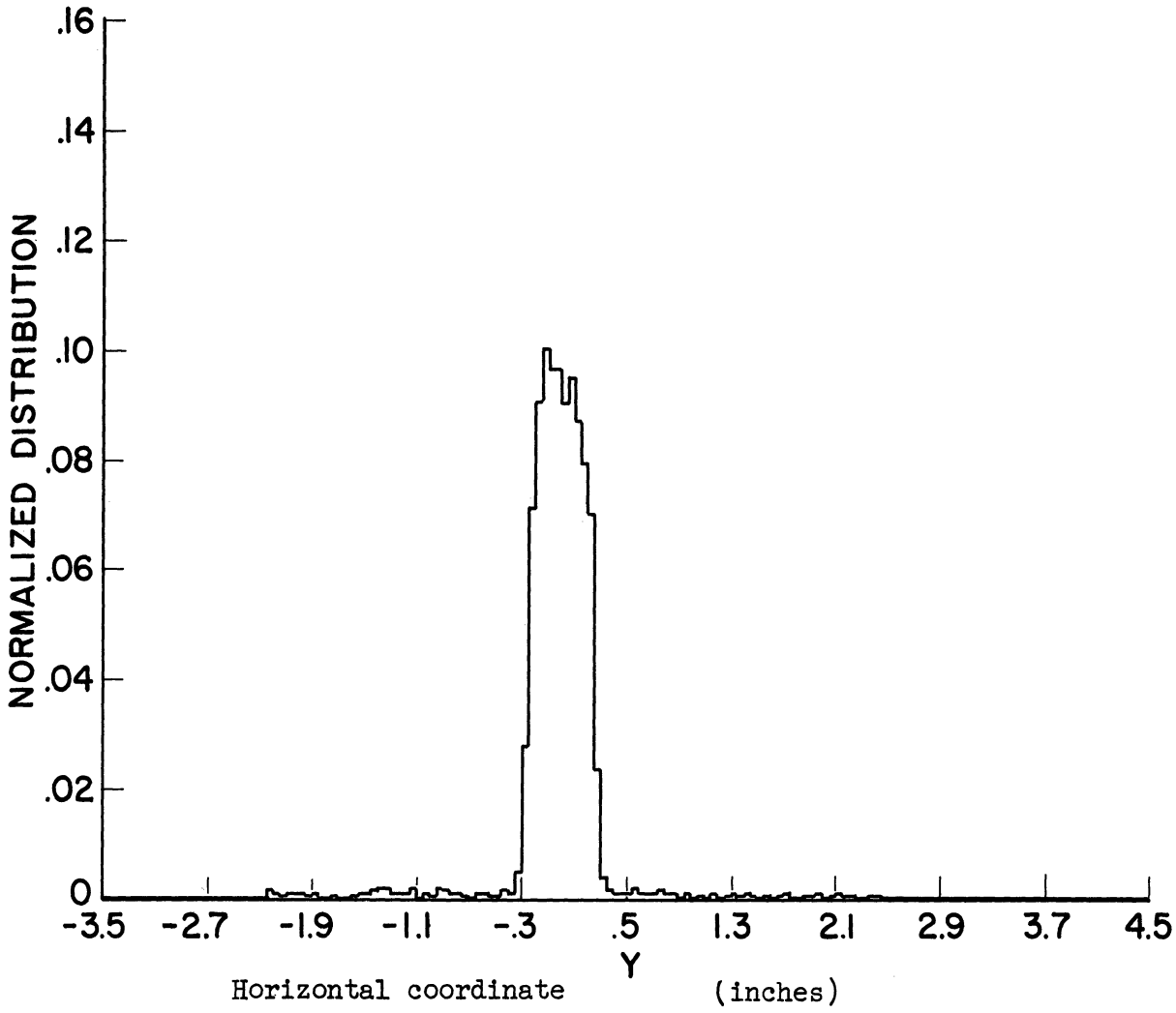

Fig. 30. Normalized distribution of the calibration beam in the horizontal coordinate at 300 MeV.

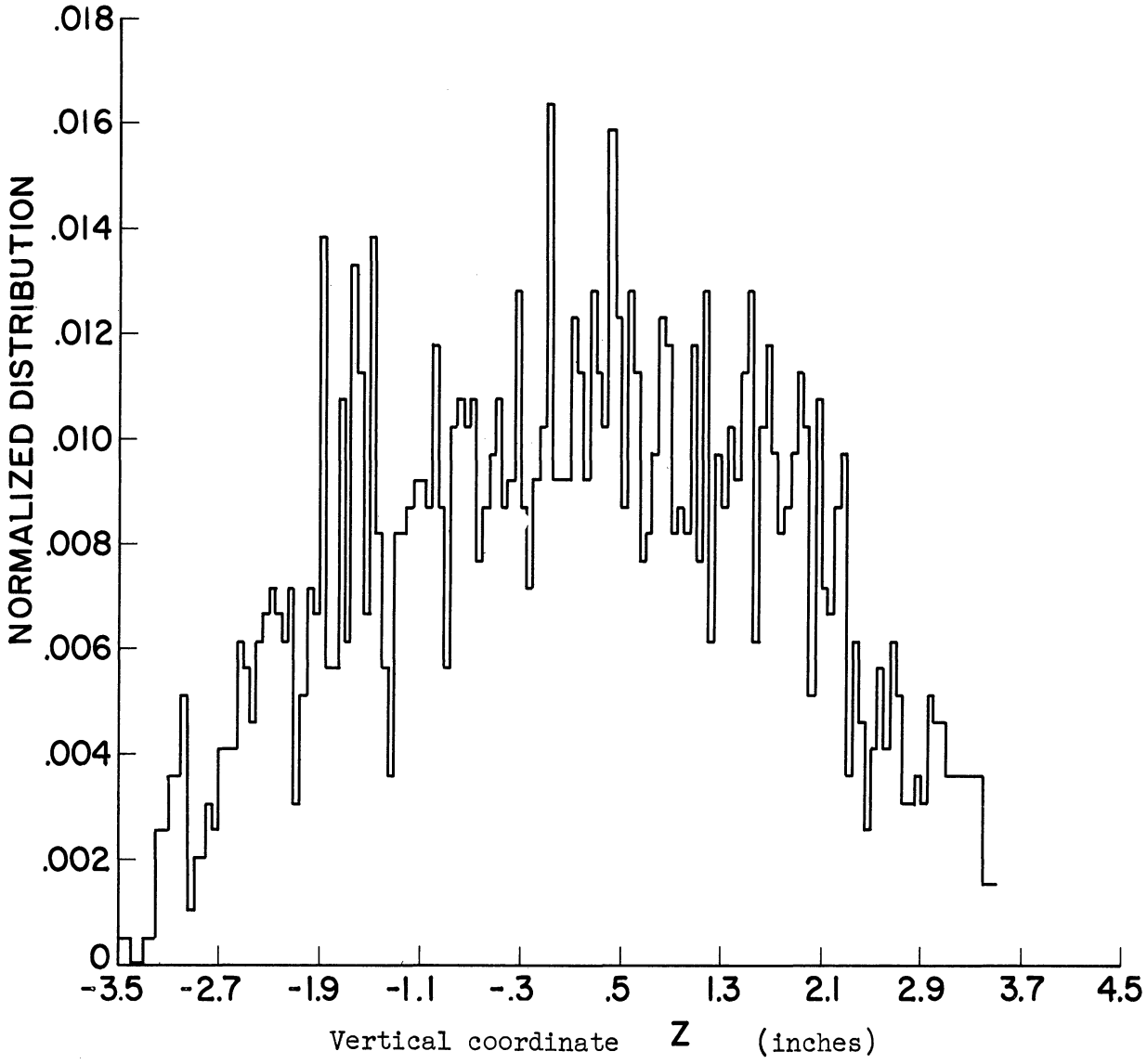

Fig. 31. Normalized distribution of the calibration beam in the vertical coordinate at 300 MeV.

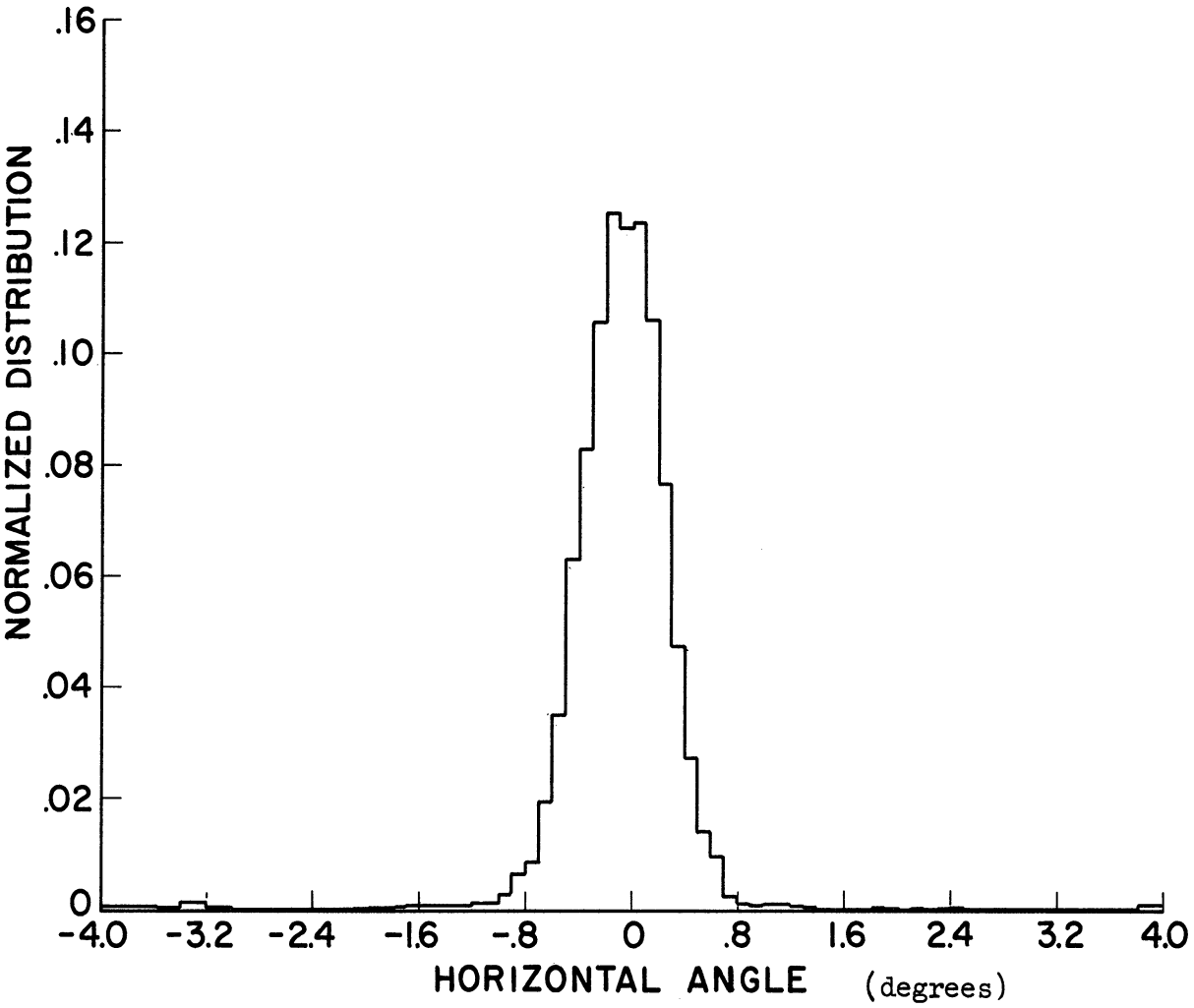

Fig. 32. Normalized distribution of the calibration beam in the horizontal angle at 300 MeV.

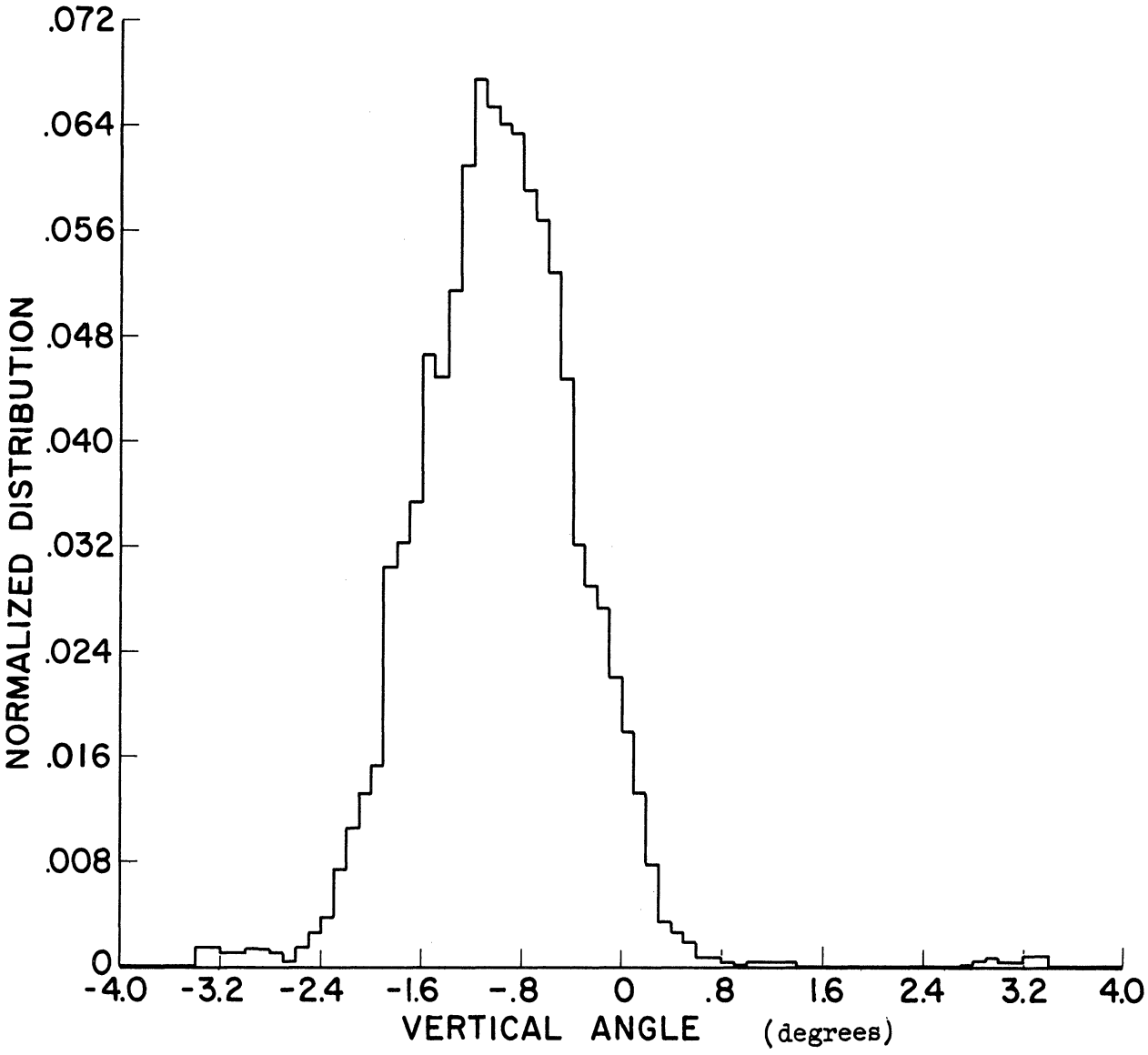

Fig. 33. Normalized distribution of the calibration beam in the vertical angle at 300 MeV. Reference angle is arbitrary.

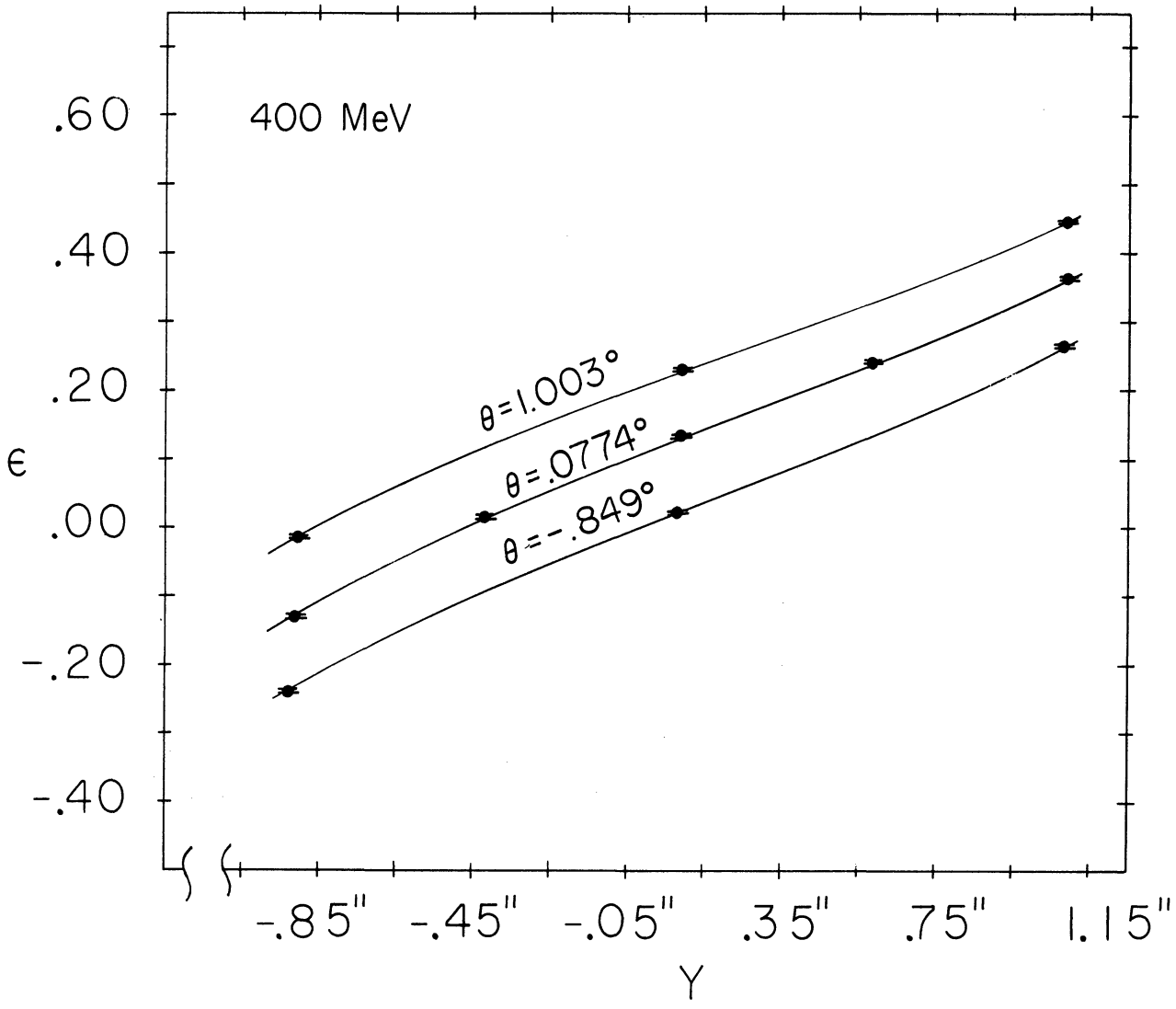

Fig. 34. Asymmetry measured in calibration experiment as a function of y for various values of θ at 400 MeV.

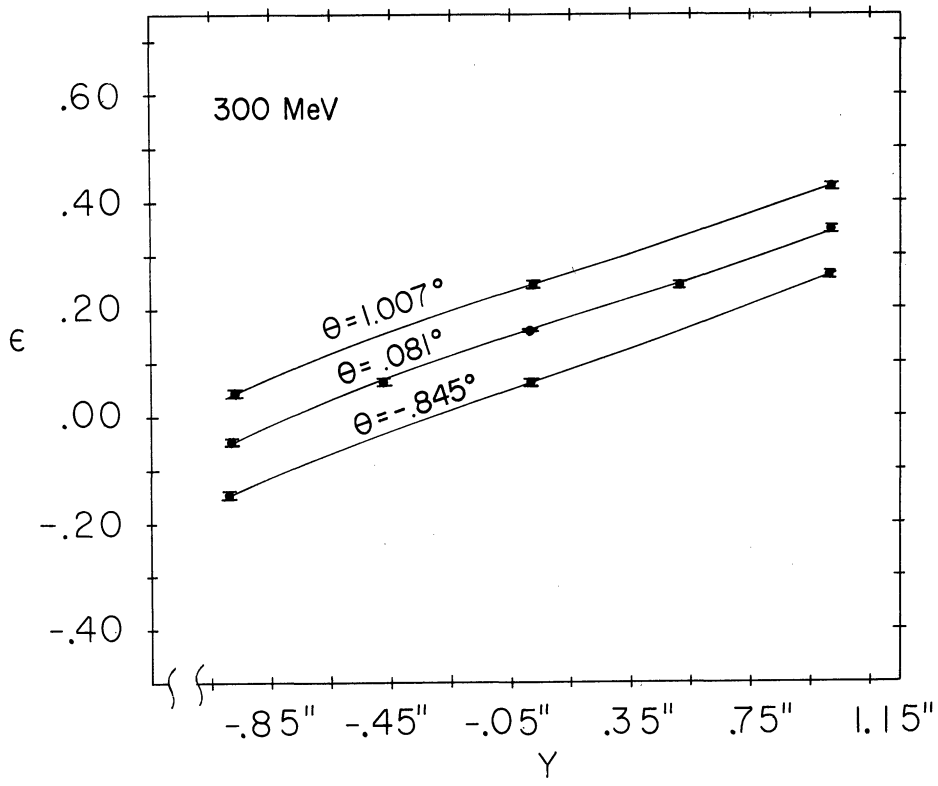

Fig. 35. Asymmetry measured in calibration experiment as a function of y for various values of θ at 300 MeV.

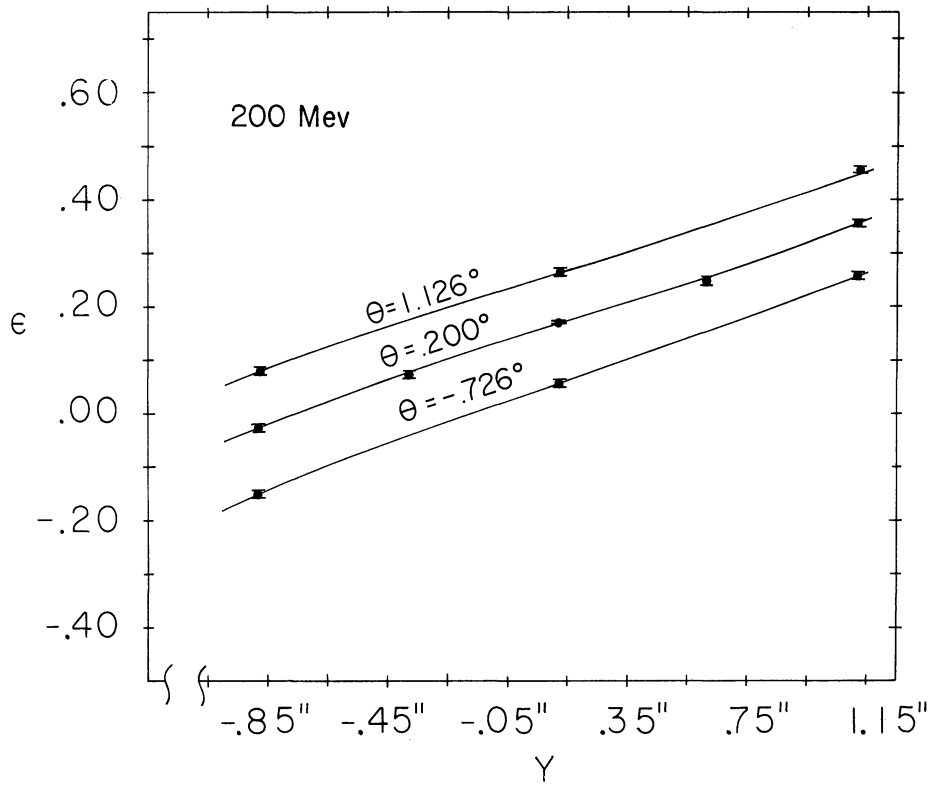

Fig. 36. Asymmetry measured in calibration experiment as a function of y for various values of θ at 200 MeV.

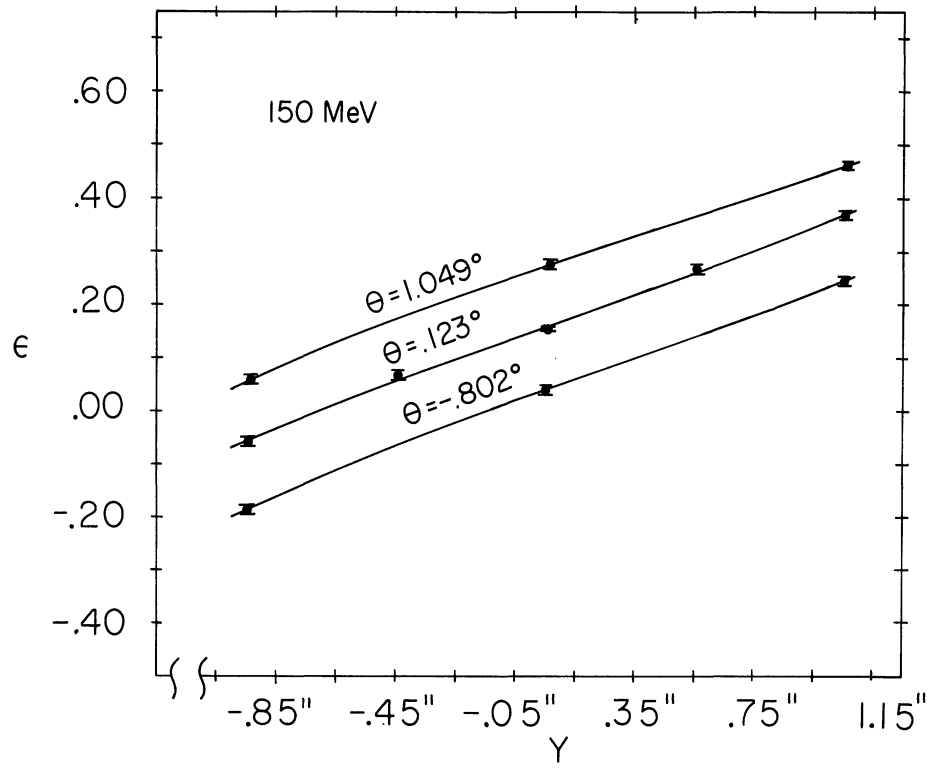

Fig. 37. Asymmetry measured in calibration experiment as a function of y for various values of θ at 150 MeV.

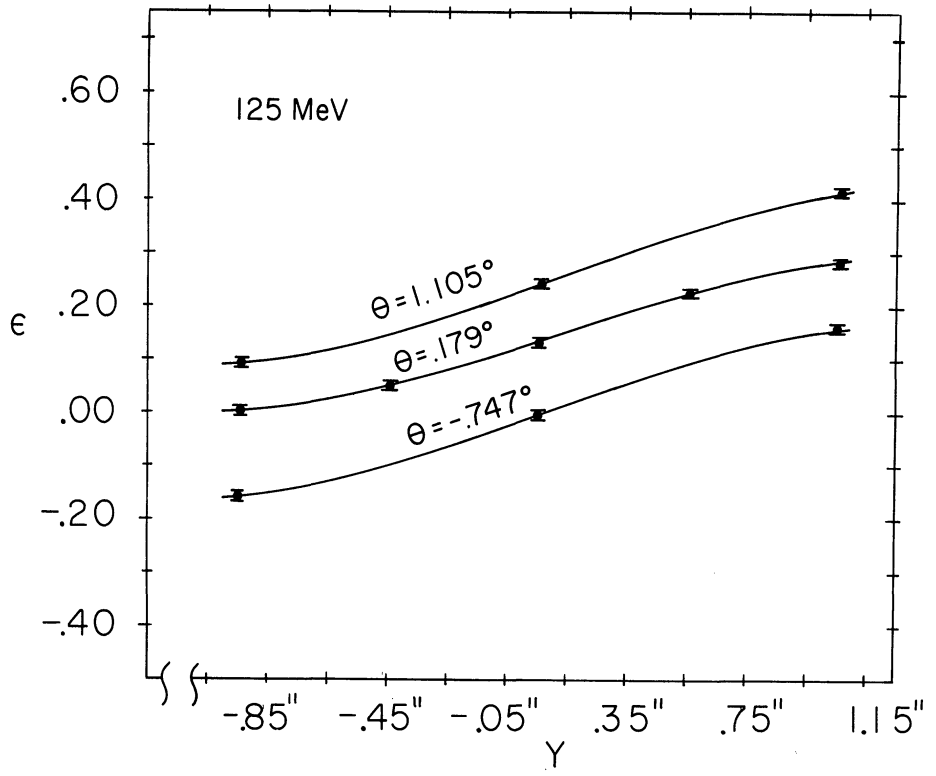

Fig. 38. Asymmetry measured in calibration experiment as a function of y for various values of θ at 125 MeV.

APPENDIX II

In this section a relationship is derived between the asymmetry measured when a proton beam with centroid specified by y and ϕ is incident on the analyzer and the asymmetry that would have been observed if the beam had entered the analyzer with both y and ϕ zero (see Fig. 39). The azimuthal asymmetry, ϵ_m, measured by the telescopes is

$$\epsilon_m = (R_M - L_M)/(R_M + L_M) \quad ,$$

where

$$R_m = nN \int_{\psi_1^R}^{\psi_2^R} S(\theta)(1+\epsilon(\theta))d\theta$$

$$L_m = nN \int_{\psi_2^L}^{\psi_1^L} S(\theta)(1+\epsilon(\theta))d\theta$$

and N is the number of incident protons, n is the number of participating target protons, $\epsilon(\theta)$ is the azimuthal asymmetry for scattering at angle $\theta(\epsilon(-\theta) = -\epsilon(\theta))$, and $S(\theta)$ is the probability for an unpolarized beam to scatter through an angle θ.

Let $\psi_2^R = \theta_2 - \delta_2 - \phi$, then to first order in ϕ and y/v_3

$$\delta_2 = y \cos \theta_2 / v_3$$

Also

$$\psi_1^R = \theta_1 - \delta_1 - \phi$$

$$\psi_2^L = -\theta_2 - \delta_2 - \phi$$

$$\psi_1^L = -\theta_1 - \delta_1 - \phi$$

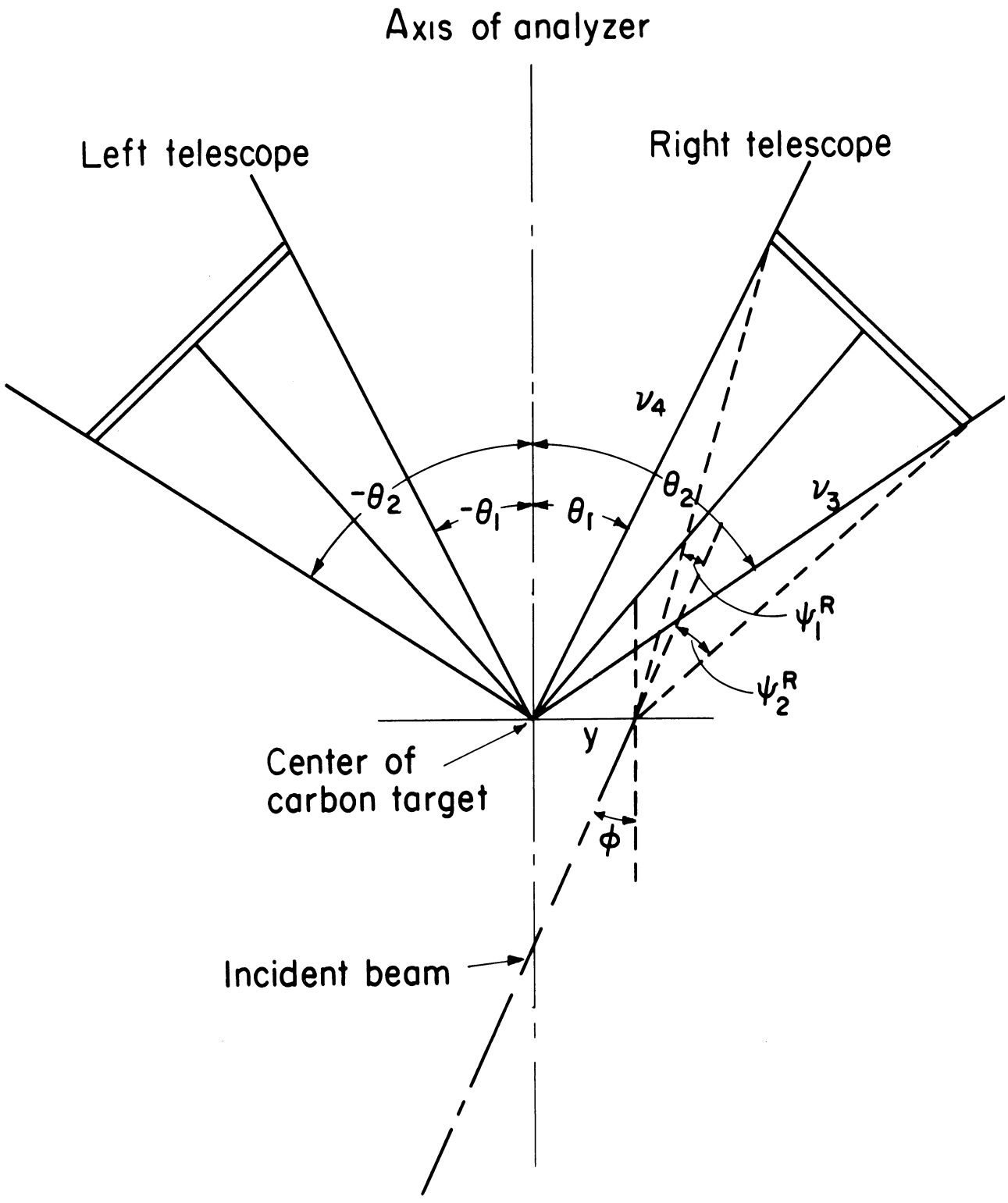

Fig. 39. Geometry of telescopes for trajectories not coincident with axis of rotation.

where

$$\delta_1 \cong \delta_2 \ ,$$

since $v_3 = v_4$ and $\cos\theta_1/\cos\theta_2 = 1.1.$

Let

$$I(A,B) = nN \int_A^B S(\theta)(1+\epsilon(\theta))d\theta \ ,$$

and note that

$$I(A+\Delta_A, B+\Delta_B) = I(A,B) + \Delta_B S(B)(1+\epsilon(B))\ Nn - \Delta_A S(A)(1+\epsilon(A))\ Nn$$

where Δ_A and Δ_B are small increments in A and B, respectively. If we set $\delta = \delta_1+\phi$, then

$$L_M = I(-\theta_2-\delta, -\theta_1-\delta)$$

$$= I(-\theta_2,-\theta_1) - \delta Nn\ S(-\theta_1)(1+\epsilon(-\theta_1)) + \delta Nn\ S(-\theta_2)(1+\epsilon(-\theta_2))$$

$$R_M = I(\theta_1-\delta, \theta_2-\delta)$$

$$= I(\theta_1,\theta_2) - \delta Nn\ S(\theta_2)(1+\epsilon(\theta_2)) + \delta Nn\ S(\theta_1)(1+\epsilon(\theta_1))$$

We may neglect the terms containing $S(\pm\theta_2)$ since for our geometry $S(\theta_1)/S(\pm\theta_2) \approx 100.$ The measured asymmetry becomes

$$\epsilon_M = \frac{R_M-L_M}{R_M+L_M} = \frac{I(\theta_1,\theta_2)-I(-\theta_2,-\theta_1)+ Nn\delta\ S(\theta_1)(2)}{I(\theta_1,\theta_2)+I(-\theta_2,-\theta_1)+ Nn\delta\ S(\theta_1)(2\epsilon(\theta_1))} \ ,$$

$$= (\epsilon_o+\alpha)/(1+\alpha\epsilon(\theta_1))$$

where

$$\alpha = 2Nn\delta\ S(\theta_1)/(I(\theta_1,\theta_2)+I(-\theta_2\ -\theta_1)) \ .$$

In all cases encountered $|\alpha\epsilon(\theta_1)| \lesssim .005$; therefore we may write $\epsilon_M = \epsilon_o+\alpha$ without introducing any significant error.

Thus α may be assumed a function of y, ϕ, and beam energy only, and is consequently a definite property of the analyzer. Data from the calibration experiment were used to evaluate $\alpha(y,\phi,p)$ in the following manner. In the calibration experiment (Appendix I) the asymmetry $\epsilon_m(y,\phi,p)$ was determined for the range of y, ϕ, and p anticipated in the primary experiment. The function $\alpha(y,\phi,p)$ over this range is merely

$$\alpha(y,\phi,p) = \epsilon_m(y,\phi,p) - \epsilon_m(0,0,p)$$

Knowledge of $\alpha(y,\phi,p)$ allows determination of the true asymmetry $E_o(0,0,p)$ from the measured asymmetry, $E_M(y,\phi,p)$, in an analysis experiment as

$$E_o(0,0,p) = E_M(y,\phi,p) - \alpha(y,\phi,p)$$

when y, ϕ and p are known.

BIBLIOGRAPHY

1. C. L. Oxley, W. F. Cartwright, and J. Rouvina, Phys. Rev. 93, 806 (1954).

2. R. S. Christian and H. P. Noyes, Phys. Rev. 70, 85 (1950).

3. K. M. Case and A. Pais, Phys. Rev. 80, 203 (1950).

4. R. Jastrow, Phys. Rev. 81, 165 (1951).

5. P. Bareyre, J. F. Detoeuf, L. W. Smith, R. D. Tripp, and L. Van Rossum, Nuovo Cimento 20, 1049 (1961).

6. H Steiner, F. Betz, O. Chamberlain, B. Dieterle, P. Grannis, C. Shultz, G. Shapiro, L. Van Rossum, and D. Weldon, Polarization in Proton-Proton Scattering Using a Polarized Target, Part II, Lawrence Radiation Laboratory Report UCRL-11440, June 1964 (unpublished).

7. V. P. Kanavets, I. I. Levintor, B. V. Morozov, M. D. Shafranov, Zh. Eksperim. i. Teor. Fiz. 45, 1272 (1963).

8. Y. Hara, Phys. Letters 2, 246 (1962).

9. L. Wolfenstein and J. Ashkin, Phys. Rev. 85, 947 (1952).

10. R. H. Dalitz, Proc. Phys. Soc. (London) A65, 175 (1952).

11. M. H. MacGregor, M. J. Moravcsik, and H. P. Stapp, Ann. Rev. Nucl. Sci. 10, 291 (1960).

12. H. P. Stapp, The Theory and Interpretation of Polarization Phenomena in Nuclear Scattering (Thesis), Lawrence Radiation Laboratory Report UCRL-3098, August 1955 (unpublished)

13. H. P. Stapp, Phys. Rev. 103, 425 (1956); K.-C. Chou and M. I. Shirokov, Soviet Phys. JETP, 7, 851 (1958); G. Breit, Phys. Rev. 106, 314 (1957). A Garren, Phys. Rev. 96, 1709 (1954); B. Steck, Z. Physik, 144, 215 (1955).

14. P. Cziffra, M. H. MacGregor, M. J. Moravcsik and H. P. Stapp, Phys. Rev. 114, 880 (1959).

15. R.J.N. Phillips, Nuclear Physics 30, 148 (1962).

16. N. Hoshizaki and S. Machida, Prog. Theor. Phys. 29, 49 (1963). Y. Hama and N. Hoshizaki, Prog. Theor. Phys. 31, 609 (1964).

17. I. J. Muzinich, Phys. Rev. Letters 9, 475 (1962).

18. Y. Hara, Prog. Theor. Phys. 28, 1048 (1962).

19. M. L. Goldberger, M. T. Grisaru, S. W. MacDowell, and D. Y. Wong, Phys. Rev. 120, 2250 (1960).

20. M. Jacob and G. C. Wick, Ann. Phys. 7, 404 (1959).

21. Y. Hara, Prog. Theor. Phys. 28, 711 (1962).

22. Thomas J. Devlin, Optik: An IBM 7090 Computer Program for the Optics of High-Energy Particle Beams, Lawrence Radiation Laboratory Report, UCRL-9727, 1961 (unpublished).

23. G. W. Bennett, Cosmotron Internal Report No. GWB-2.

24. R. Sugarman, F. C. Merritt, and W. A. Higginbotham, Nanosecond Counter Circuit Manual, Brookhaven National Laboratory Report BNL711(T-248), 1962 (unpublished).

25. P. G. Hoel, Introduction to Mathematical Statistics, (John Wiley and Sons, Inc., New York, 1958), second edition, Ch. 5, p. 67.

26. F. W. Betz, Polarization Parameter in Proton-Proton Scattering from 328 to 736 MeV (Thesis), Lawrence Radiation Laboratory Report UCRL-11565, 1964 (unpublished).

27. D. Cheng, Nucleon-Nucleon Polarization at 700, 600, 500, and 400 MeV (Thesis), Lawrence Radiation Laboratory Report UCRL-11926, July 1965 (unpublished).

28. Y. Ducros, A. de Lesquen, J. Movchet, J. C. Raoul, L. Van Rossum, J. Deregel, J. M. Fontaine, A. Boucherie, and J. F. Mougel, Determination of the Asymmetry Parameter in Proton-Proton Scattering up to 1.2 GeV, Oxford International Conference on Elementary Particles, September 1965 (unpublished).

29. J. A. Kane, R. A. Stallwood, R. B. Sutton, T. M. Fields, and J. G. Fox, Phys. Rev. 95, 1694 (1954).

30. R. J. Homer, W. K. MacFarlane, A. W. O'Dell, E. J. Sacharidis, and G. H. Eaton, Nuovo Cimento 23, 690 (1962).

31. J. Tinlot and R. E. Warner, Phys. Rev. 124, 890 (1961).

32. O. Chamberlain, E. Segre, R. D. Tripp, C. Wiegand, and T. Ypsilantis, Phys. Rev. 105, 288 (1957).

33. L. Azhgirey, Yu. Kumekin, M. Mescheryakov, S. Nurushev, V. Solovyanov and G. Stoletov, Physics Letters 18, 203 (1965).

34. R. Wilson, The Nucleon-Nucleon Interaction, Experimental and Phenomenologic Aspects (Interscience Publishers, 1963).

35. W. Galbraith, E. W. Jenkins, T. F. Kycia, B. A. Leontic, R. H. Phillips, A. L. Read, and R. Rubinstein, Total Cross-Sections of Protons, Anti-Protons, Pi-and K- Mesons on Hydrogen and Deuterium in the Momentum Range 6-22 GeV/c, Brookhaven National Laboratory Report BNL-8744 (unpublished).

36. D. W. Ritson, Techniques of High Energy Physics (Interscience Publishers, 1961).

37. E. Heiberg, U. E. Kruse, L. Marshall, J. Marshall and F. Solomitz, Phys. Rev. 97, 250 (1955); L. Wolfenstein, Phys. Rev. 75, 1964 (1949).

UNCLASSIFIED

Security Classification

DOCUMENT CONTROL DATA - R&D

(Security classification of title, body of abstract and indexing annotation must be entered when the overall report is classified)

1. ORIGINATING ACTIVITY *(Corporate author)*
University of Michigan, Department of Physics
Ann Arbor, Michigan

2a. REPORT SECURITY CLASSIFICATION
Unclassified

2b. GROUP

3. REPORT TITLE
THE POLARIZATION PARAMETER IN ELASTIC PROTON-PROTON SCATTERING FROM .75 TO 2.84 GeV

4. DESCRIPTIVE NOTES *(Type of report and inclusive dates)*
Technical Report No. 23

5. AUTHOR(S) *(Last name, first name, initial)*
Neal, Homer A., Jr.

6. REPORT DATE	7a. TOTAL NO. OF PAGES	7b. NO. OF REFS
April 1966	115	37

8a. CONTRACT OR GRANT NO.	9a. ORIGINATOR'S REPORT NUMBER(S)
Nonr-1224(23)	
b. PROJECT NO.	03106-23-T
NR-022-274	
c.	9b. OTHER REPORT NO(S) *(Any other numbers that may be assigned this report)*
d.	

10. AVAILABILITY/LIMITATION NOTICES
Distribution of this document is unlimited

11. SUPPLEMENTARY NOTES	12. SPONSORING MILITARY ACTIVITY
	Department of the Navy Office of Naval Research Washington, D. C.

13. ABSTRACT

A double-scattering technique has been employed to measure the polarization parameter in elastic proton-proton scattering at .75, 1.03, 1.32, 1.63, 2.24, and 2.84 GeV. An external proton beam from the Brookhaven Cosmotron was focussed on a three inch long liquid hydrogen target and the elastic recoil and scattered protons were detected in coincidence by scintillation counters. The polarization produced in the scattering process was inferred from the azimuthal asymmetry exhibited in the scattering of the recoil beam from a carbon target. This asymmetry was measured by a set of two scintillation counter telescopes which symmetrically viewed the carbon target. The analyzing power of this arrangement was previously determined in an independent experiment employing a 40% polarized proton beam at the Carnegie Institute of Technology synchrocyclotron. The corrected values of the polarization parameter are exhibited as a function of the center-of-mass scattering angle for each incident beam energy. The prediction of the Regge theory that the polarization parameter in elastic proton-proton scattering is related to the total p-p and p-$\bar{p}$ cross sections has been found to be consistent with the experimental results.

DD FORM 1 JAN 64 1473

UNCLASSIFIED

Security Classification

14 KEY WORDS	LINK A		LINK B		LINK C	
	ROLE	WT	ROLE	WT	ROLE	WT

INSTRUCTIONS

1. ORIGINATING ACTIVITY: Enter the name and address of the contractor, subcontractor, grantee, Department of Defense activity or other organization *(corporate author)* issuing the report.

2*a*. REPORT SECURITY CLASSIFICATION: Enter the overall security classification of the report. Indicate whether "Restricted Data" is included. Marking is to be in accordance with appropriate security regulations.

2*b*. GROUP: Automatic downgrading is specified in DoD Directive 5200.10 and Armed Forces Industrial Manual. Enter the group number. Also, when applicable, show that optional markings have been used for Group 3 and Group 4 as authorized.

3. REPORT TITLE: Enter the complete report title in all capital letters. Titles in all cases should be unclassified. If a meaningful title cannot be selected without classification, show title classification in all capitals in parenthesis immediately following the title.

4. DESCRIPTIVE NOTES: If appropriate, enter the type of report, e.g., interim, progress, summary, annual, or final. Give the inclusive dates when a specific reporting period is covered.

5. AUTHOR(S): Enter the name(s) of author(s) as shown on or in the report. Enter last name, first name, middle initial. If military, show rank and branch of service. The name of the principal author is an absolute minimum requirement.

6. REPORT DATE: Enter the date of the report as day, month, year; or month, year. If more than one date appears on the report, use date of publication.

7*a*. TOTAL NUMBER OF PAGES: The total page count should follow normal pagination procedures, i.e., enter the number of pages containing information.

7*b*. NUMBER OF REFERENCES: Enter the total number of references cited in the report.

8*a*. CONTRACT OR GRANT NUMBER: If appropriate, enter the applicable number of the contract or grant under which the report was written.

8*b*, 8*c*, & 8*d*. PROJECT NUMBER: Enter the appropriate military department identification, such as project number, subproject number, system numbers, task number, etc.

9*a*. ORIGINATOR'S REPORT NUMBER(S): Enter the official report number by which the document will be identified and controlled by the originating activity. This number must be unique to this report.

9*b*. OTHER REPORT NUMBER(S): If the report has been assigned any other report numbers *(either by the originator or by the sponsor)*, also enter this number(s).

10. AVAILABILITY/LIMITATION NOTICES: Enter any limitations on further dissemination of the report, other than those imposed by security classification, using standard statements such as:

(1) "Qualified requesters may obtain copies of this report from DDC."

(2) "Foreign announcement and dissemination of this report by DDC is not authorized."

(3) "U. S. Government agencies may obtain copies of this report directly from DDC. Other qualified DDC users shall request through _____."

(4) "U. S. military agencies may obtain copies of this report directly from DDC. Other qualified users shall request through _____."

(5) "All distribution of this report is controlled. Qualified DDC users shall request through _____."

If the report has been furnished to the Office of Technical Services, Department of Commerce, for sale to the public, indicate this fact and enter the price, if known.

11. SUPPLEMENTARY NOTES: Use for additional explanatory notes.

12. SPONSORING MILITARY ACTIVITY: Enter the name of the departmental project office or laboratory sponsoring *(paying for)* the research and development. Include address.

13. ABSTRACT: Enter an abstract giving a brief and factual summary of the document indicative of the report, even though it may also appear elsewhere in the body of the technical report. If additional space is required, a continuation sheet shall be attached.

It is highly desirable that the abstract of classified reports be unclassified. Each paragraph of the abstract shall end with an indication of the military security classification of the information in the paragraph, represented as *(TS)*, *(S)*, *(C)*, or *(U)*.

There is no limitation on the length of the abstract. However, the suggested length is from 150 to 225 words.

14. KEY WORDS: Key words are technically meaningful terms or short phrases that characterize a report and may be used as index entries for cataloging the report. Key words must be selected so that no security classification is required. Identifiers, such as equipment model designation, trade name, military project code name, geographic location, may be used as key words but will be followed by an indication of technical context. The assignment of links, rules, and weights is optional.